NUMERICAL INVESTIGATION OF THE UNSTEADY CONVECTIVE FLOW ALONG A WEDGE WITH THERMOPHORESIS

A. T. M. MAHOBUBUR RAHAMAN SHARKER

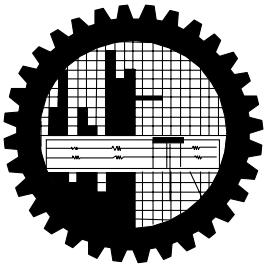

DEPARTMENT OF MATHEMATICS

BANGLADESH UNIVERSITY OF ENGINEERING AND TECHNOLOGY

DHAKA-1000, BANGLADESH

MARCH, 2015

NUMERICAL INVESTIGATION OF THE UNSTEADY CONVECTIVE FLOW ALONG A WEDGE WITH THERMOPHORESIS

A thesis submitted in partial fulfillment of the requirement for the award of the degree

of

DOCTOR OF PHILOSOPHY

in

MATHEMATICS

by

A. T. M. MAHOBUBUR RAHAMAN SHARKER

Student No.: P0409094004 P, Session: April/2009

Registration No.: 0404395

Under the supervision of

Professor Dr. Md. Mustafa Kamal Chowdhury
DEPARTMENT OF MATHEMATICS

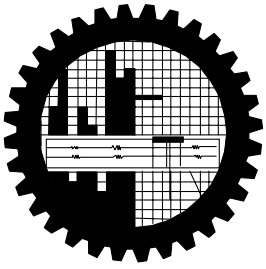

BANGLADESH UNIVERSITY OF ENGINEERING AND TECHNOLOGY

DHAKA-1000, BANGLADESH

MARCH, 2015

The thesis entitled **"Numerical Investigation of the Unsteady Convective Flow along a Wedge with Thermophoresis"** submitted by A. T. M. Mahobubur Rahaman Sharker, Roll No.: P0409094004 P, Registration No.: 0404395, Session: April/2009 has been accepted as satisfactory in partial fulfillment of the requirement for the degree of **Doctor of Philosophy in Mathematics** on March 29, 2015.

Board of Examiners

1. _____

Dr. Md. Mustafa Kamal Chowdhury — Chairman
Professor — (Supervisor)
Department of Mathematics
BUET, Dhaka-1000

2. _____

Head — Member
Department of Mathematics — (Ex-Officio)
BUET, Dhaka-1000

3. _____

Dr. Md. Abdul Maleque — Member
Professor
Department of Mathematics
BUET, Dhaka-1000

4. _____

Dr. Md. Manirul Alam Sarker — Member
Professor
Department of Mathematics
BUET, Dhaka-1000

5. _____

Dr. Md. Abdul Alim — Member
Professor
Department of Mathematics
BUET, Dhaka-1000

6. _____

Dr. Mohammad Ali Member
Professor
Department of Mechanical Engineering
BUET, Dhaka-1000

7. _____

Dr. Md. Shariful Alam Member
Associate Professor
Department of Mathematics
Jagannath University, Dhaka-1100

8. _____

Dr. Md. Shamsul Alam Sarker Member
Professor (External)
Department of Mathematics
University of Rajshahi
Rajshahi

DEDICATION

This work is dedicated

to

My dearest Parents

Certificate

This is to certify that the thesis entitled **"Numerical Investigation of the Unsteady Convective Flow along a Wedge with Thermophoresis"** submitted by A. T. M. Mahobubur Rahaman Sharker, to Bangladesh University of Engineering and Technology, Dhaka, is a record of original research work carried out by him under my supervision in the Department of Mathematics, Bangladesh University of Engineering and Technology, Dhaka. Mr. A. T. M. Mahobubur Rahaman Sharker, has worked sincerely for preparing his thesis and the thesis is, in my opinion, worthy of consideration for the award of degree of Doctor of Philosophy in Mathematics in accordance with the rules and regulations of this University. I believe that this research work is a unique one and has not been submitted elsewhere for the award of any degree.

_____

Professor Dr. Md. Mustafa Kamal Chowdhury
Supervisor

Statement of originality

I, hereby, declare that this thesis work, submitted to the Department of Mathematics, Bangladesh University of Engineering and Technology (BUET) in partial fulfillment of the requirements for the degree of Doctor of Philosophy in Mathematics has not been submitted elsewhere (Universities or Institutions) for any other degree.

A. T. M. Mahobubr Rahaman Sharker March 29, 2015

Acknowledgements

At first all Praise belongs to “The Almighty **ALLAH**”, the most merciful, munificent to men and His exploit.

I would like to express heartiest gratitude to my supervisor, Prof. Dr. Mustafa Kamal Chowdhury, Department of Mathematics, BUET, Dhaka for his good guidance, support, valuable suggestions, constant inspiration and supervision during the research work of the Ph. D Program.

My regards also due to Prof. Dr. Md. Manirul Alam Sarker, Head, Department of Mathematics, BUET, Dhaka for providing me all research facilities from the Department without any famine. I express my deep regards to Prof. Dr. Md. Abdul Maleque, Prof. Dr. Md. Abdul Hakim Khan, Prof. Dr. Md. Elias and Prof. Dr. Md. Abdul Alim, Department of Mathematics, BUET, Dhaka for their wise and liberal co-operation in providing me all necessary help from the Department during my Ph. D program. I would also like to extend my thanks to all my respectable teachers, Department of Mathematics, BUET, Dhaka for their constant encouragement.

I am also indebted to the members of the Doctoral committee, Prof. Dr. Mohammad Ali, Department of Mechanical Engineering, BUET, Dhaka and Dr. Md. Shariful Alam, Associate Professor, Department of Mathematics, Jagannath University, Dhaka for their advice and constructive comments and voluntary supports. I am also grateful to the external member Prof. Dr. Md. Shamsul Alam Sarker, Department of Applied Mathematics, University of Rajshahi for his time and cooperation.

I express my sincere thanks to the authority of Dhaka International University, Dhaka, for providing me necessary support and facilities during my research works and my special thanks to my colleagues and friends who tremendously and positively inspired me all through my journey.

I am very grateful to my parents who guided me through the entire studies and helped me morally and spiritually. It is almost impossible to express my indebtedness in words to my beloved wife for her sacrifice, cooperation and motivation during the preparation of this work.

Abstract

In this thesis titled “Numerical Investigation of the Unsteady Convective Flow along a Wedge with Thermophoresis” characteristic of an unsteady two-dimensional laminar forced convective hydrodynamic heat and mass transfer flow of a viscous incompressible fluid along a heated wedge in the presence of thermophoresis have been studied. The potential flow velocity has been taken as a function of the distance x and time t. The governing time dependent non-linear partial differential equations are reduced to a set of non-linear ordinary differential equations by introducing a new class of similarity transformations. Comparisons with published works are done, and the results are found to be in excellent agreement. The resulting local similarity equations for unsteady flow have been solved numerically by applying Nachtsheim-Swigert shooting iteration technique along with sixth order Runge-Kutta integration scheme. Depending on various flow conditions the work can be summarized as follows:

Local similarity solutions for unsteady two-dimensional forced convective heat and mass transfer flow along a wedge with thermophoresis are investigated at the outset. Numerical results for the velocity, temperature and concentration profiles as well as local skin-friction coefficient, rate of heat and mass transfer, thermophoretic velocity and thermophoretic particle deposition velocity for different values of unsteadiness parameter, wedge angle parameter, Prandtl number, Schmidt number, thermophoretic coefficient, thermophoresis parameter and concentration ratio are displayed graphically in addition to tabular form. The results show that the thermophoretic particle deposition velocity decreases as the thermophoretic coefficient increases but it increased a bit with the increase of unsteadiness parameter.

Secondly, the effects of thermophoresis particle deposition on an unsteady two dimensional forced convective heat and mass transfer flow past a wedge with respect to variable fluid viscosity due to changes in temperature and Prandtl

number has been studied. Results for the non-dimensional velocity, temperature, concentration, variable Prandtl number and thermophoretic velocity are presented graphically whereas thermophoretic particle deposition velocity is shown in the tabular form for various values of the pertinent parameters. The obtained numerical results indicate that in modeling the thermal boundary-layer flow with a temperature-dependent viscosity, the Prandtl number shall be treated as a variable rather than a constant within the boundary layer to obtain realistic results.

Thirdly, unsteady two dimensional magnetohydrodynamic (MHD) forced convective heat and mass transfer flow of a viscous, incompressible and electrically conducting fluid along a porous wedge in the presence of the temperature-dependent thermal conductivity and variable Prandtl number have been carried out numerically. The velocity, temperature, concentration, thermophoretic velocity and thermophoretic particle deposition velocity are computed and discussed in details for various parametric conditions. The numerical results show that the heat transfer rate decreases by 45% when the thermal conductivity variation parameter varies from 0 to 9 for variable Prandtl number, but decreases by 77% for constant Prandtl number in case of suction.

Finally, thermophoretic particle deposition on unsteady two dimensional convective slip flow over a wedge with temperature dependent fluid properties such as fluid viscosity and thermal conductivity have been studied numerically. The nondimensional velocity, temperature and concentration as well as thermophoretic velocity and thermophoretic particle deposition velocity for different values of the related parameters are displayed graphically and tabular form. The obtained numerical results show that both the fluid velocity and thermophoretic particle deposition velocity increase with the increasing values of the variable viscosity parameter as well as wedge angle parameter.

CONTENTS

NOMENCLATURE

Roman Symbols	Entities	Dimension
B_0	: applied magnetic field	$[ML^2T^{-1}Q^{-1}]$
C	: species concentration in the boundary layer	$[kg.m^{-2}]$
C_p	: specific heat due to constant pressure	$[L^2\theta^{-1}T^{-2}]$
C_m, C_s, C_t	: constants	[---]
C_1, C_2, C_3	: constants	[---]
C_{fx}	: local skin friction coefficient	[---]
C_w	: species concentration at the wall	[---]
C_∞	: species concentration of the ambient fluid	[---]
D	: molecular diffusivity	[---]
f	: dimensionless stream function	[---]
f_w	: dimensionless wall mass transfer coefficient	[---]
Ha	: Hartman number	[---]
Kn	: Knudsen number	[---]
L	: slip length	[---]
m	: constant	[---]
N_c	: concentration ratio	[---]
N_t	: thermophoresis parameter	[---]
Nu_x	: local Nusselt number	[---]
Pr	: Prandtl number	[---]
Pr_c	: constant Prandtl number	[---]
Pr_v	: variable Prandtl number	[---]
Pr_w	: Prandtl number at the surface of the wedge	[---]

Pr_∞	: ambient Prandtl number	[---]
q_w	: rate of heat transfer	[---]
Re	: Reynolds number	[---]
Sc	: Schmidt number	[---]
Sh_x	: local Sherwood number	[---]
T	: temperature of the fluid within the boundary layer	[θ]
T_w	: temperature at the surface of the wedge	[θ]
T_∞	: temperature of the ambient fluid	[θ]
U	: free stream velocity	[$m.s^{-1}$]
u, v	: the x and y component of the velocity field	[---]
v_w	: wall suction/ injection velocity	[---]
V_T	: thermophoretic velocity	[---]
V_{TW}	: dimensionless thermophoretic velocity	[---]
V_d^*	: dimensionless thermophoretic particle deposition velocity	[---]
x, y	: axis in direction along and normal to the wedge	[---]

Greek Symbols

β	: wedge angle parameter	[---]
γ	: thermal conductivity variation parameter	[---]
δ	: time dependent length scale	[---]
κ	: thermophoretic coefficient	[---]
κ_f	: thermal conductivity of the fluid	[$MLT^{-3}\ \theta^{-1}$]
κ_∞	: thermal conductivity of the ambient fluid	[$MLT^{-3}\ \theta^{-1}$]
λ	: unsteadiness parameter	[---]

λ_p	: thermal conductivity of diffused particles	[---]
η	: similarity variable	[---]
μ	: viscosity of the fluid inside the boundary layer	$[ML^{-1}T^{-1}]$
μ_∞	: viscosity of the ambient fluid	$[ML^{-1}T^{-1}]$
υ	: Kinematic viscosity of the fluid inside the boundary layer	$[L^2T^{-1}]$
υ_∞	: Kinematic viscosity of the ambient fluid	$[L^2T^{-1}]$
ρ	: density of the fluid	$[ML^{-3}]$
ρ_∞	: density of the ambient fluid	$[ML^{-3}]$
τ_w	: wall shear stress	[Pa]
θ	: dimensionless temperature	[---]
θ_r	: variable viscosity parameter	[---]
σ	: electrical conductivity	$[MLT^{-3}\ \theta^{-1}]$
ϕ	: dimensionless concentration	[---]
ψ	: stream function	$[\ m^2.s^{-1}]$

Subscripts

w	: condition at wall	[---]
∞	: condition at infinity	[---]

Superscripts

Prime $(')$ differentiation with respect to η

List of tables

List of figures

Chapter I

1.1 Introduction

Thermophoresis is a phenomenon, which causes small particles (such as soot particles or aerosol particles) to be driven away from a hot surface towards a cold one. Thermophoresis is important when temperature gradient is very large and particle diameter lies between 0.1 μm-1.0 μm. As the temperature of the hotter region is greater than that of the colder region, a temperature gradient will be developed between these two regions. In Figure 1.1, it has been considered two regions one is hot and other is cold. When the wall is hot, the particles tend to repel from that surface, while when the wall is cold, the small particles tend to deposit on the surface due to thermophoresis. These phenomenons depend on many factors like thermal conductivity of aerosol particles, thermophoretic coefficient, the heat capacity of the gas and the Knudsen number. Blackening of glass globe of kerosene lanterns, chimneys and industrial furnace walls by carbon particles, corrosion of heat exchanger, which reduces heat transfer coefficient, and fouling of gas turbine blades are examples of thermophoresis phenomenon. Thermophoresis plays a vital role in the mass transfer mechanism of several devices involving small micron sized particles and large temperature gradients. Thermophoresis principle is utilized to manufacture graded index silicon dioxide and germanium dioxide in the fabrication of optical fiber used in the field of communications.

The thermophoretic force is the force on particles submerged in a gas or liquid with a temperature gradient. The direction of the force is opposite to the temperature gradient. The thermophoretic force is a strong function of Knudsen number, Kn = $2\xi / d_p$, where d_p is the particle diameter and ξ is the gas mean free path. The mean free path of a gas is the average distance a gas molecule

travels between collisions with other gas molecules. The velocity acquired by the particles is called the thermophoretic velocity.

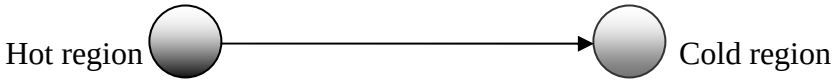

Figure 1.1: Thermophoresis phenomenon.

Heat transfer is the transfer of thermal energy from one region to another. The basic requirement for heat transfer is the presence of temperature difference. The transfer of energy as heat is always from the higher temperature medium to the lower temperature one and heat transfer stops when the two mediums reach the same temperature. Heat transfer plays an important role in many fields due to the heating and cooling processes involved. Increase of the heat transfer efficiency in macro- and nano-devices is desirable, because increasing efficiency, reduce process time of work and lengthen the working life of equipment. There are several methods to improve the heat transfer efficiency. Some methods use extended surfaces, application of vibration to the heat transfer surfaces, and usage of micro channels. Heat transfer efficiency can also be improved by increasing the thermal conductivity of the working fluid. Commonly used heat transfer fluids such as water, ethylene glycol, and engine oil, have relatively low thermal conductivities compared to the thermal conductivity of solids. High thermal conductivity of solids can be used to increase the thermal conductivity of a fluid by adding small solid particles to that fluid. Heat transfer is commonly encountered in engineering systems and other aspects of life. The human body is constantly rejecting heat to its surroundings, and human comfort is closely tied to the rate of heat rejection. Many ordinary household appliances are designed by using the principles of heat transfer. Some examples include the electric or gas range, the heating and air-conditioning system, the refrigerator and freezer, the water heater, the iron, and even the computer, the television etc. Heat transfer plays a major role in the design of many other devices, such as car radiators, solar collectors, various components of power plants, and even spacecraft. In the design of nuclear-reactor cores, a thorough heat transfer analysis of fuel elements

is important for proper sizing of fuel element to prevent burnout. In aerospace technology, heat transfer problems are crucial because of weight limitations and safely considerations. The optimal insulation thickness in the walls and roofs of the houses, on hot water or steam pipes, or on water heaters is determined on the basis of a heat transfer analysis with economic consideration.

There are three distinct modes of heat transfer, namely conduction, convection and radiation. All mode of heat transfer require the existence of temperature difference, and all modes are from the high temperature medium to a lower-temperature one. In reality, the combined effects of these three modes of heat transfer control temperature distribution in a medium.

Conduction is the transfer of energy through matter from particle to particle. For example, a spoon in a cup of hot soup becomes warmer because the heat from the soup is conducted along the spoon. Conduction is the mode of heat transfer in which energy exchange takes place from the region of higher temperature to that of lower temperature by the kinetic motion or direct impact of molecules, as in the case of fluid at rest, and by the drift of electrons, as in the case of metals. Convection is possible only in the presence of a fluid medium. When a fluid flows inside a duct or over a solid body while temperatures of the fluid and the solid surface are different, heat transfer between the fluid and the solid surface takes place as a consequence of the motion of fluid relative to the surface; this mechanism of heat transfer is called convection. The convective mode of heat transfer is divided into two basic processes. The fluid motion artificially induced with a pump or a fan forces the fluid flow over the surface. This heat transfer is termed as forced convection. Such problems are very frequently encountered in technology where the heat transfers to or from a body is often due to an imposed flow of a fluid at a different temperature from that of the body. If the fluid motion is set up by buoyancy effects resulting from density difference caused by temperature difference in the fluid, the heat transfer is said to be free or natural convection. There are essentially three factors, which govern the natural convection processes, namely the body force, the temperature variation in the flow field and the fluid density variation with temperature. Free convection is the

principal mode of heat transfer from pipes, transmission lines, refrigerating coils, hot radiators and many other practical situations in everyday life. But in many cases of practical interest, both processes are important and heat transfer is by mixed convection, in which neither mode is truly predominant. The mode of heat transfer by which this equilibrium is achieved is called thermal radiation. In fact the energy transfer by radiation is maximum when the two bodies exchanging energy are separated by a perfect vacuum. Thermal radiation depends only on the temperature and on the optical properties of the emitter.

Mass transfer is the net movement of mass from one location to another. Mass transfer occurs in many processes, such as absorption, evaporation etc. Some common examples of mass transfer processes are the evaporation of water from a pond to the atmosphere, the purification of blood in the kidney and liver, and the distillation of alcohol. On the other hand examples of mass transfer in everyday life are the diffusion of smoke through tall chimneys into the environment, the dissolution of sugar added to a cup of tea, the separation of the components of a mixture by distillation or absorption, There are some other examples of mass transfer for industrial applications such as refrigeration by the evaporation of liquid ammonia in the atmosphere of H_2 is electrolux refrigerator, humidification of air in cooling tower, evaporation of petrol in the carburetor of an I. C. engine, neutron diffusion within nuclear reactors, estimation of depth to which carbon will penetrate in a mild steel specimen during the act of carburizing etc.

The mechanism of mass transfer depends greatly on the dynamics of the system in which it occurs. Like those of heat transfer, there are three different modes of mass transfer, which are mass transfer by diffusion or molecular diffusion, mass transfer by convection and mass transfer by the change of phase. The transport of water on a microscopic level as a result of diffusion from a region of high concentration to a region of low concentration in a system/mixture of liquids or gases is called molecular diffusion. It occurs when a substance diffuses through a layer of stagnant fluid and may be due to concentration, temperature or pressure gradients. In a gaseous mixture, molecular diffusion occurs due to random motion of the molecules. Mass transfer by convection involves transfer of mass between a

moving fluid and a surface, or between two relatively immiscible moving fluids. The convective mass transfer depends on the transport properties and on the dynamic (laminar or turbulent) characteristics of the flowing fluid. As in heat convection, mass convection can also takes place under free or forced convection. The buoyancy force causing circulation in free convection, mass transfer results from the differences in density of the vapor air mixtures of varying compositions. The evaporation of alcohol and heat and mass transfer from the human body are examples where free convection mechanism dominates. The evaporation of water from an ocean when air blows over it, is a case of forced convection mass transfer. Mass transfer also occurs whenever a change from one phase to another takes place. The mass transfer in such case occurs due to simultaneous action of convection and diffusion. Hot gases escaping from the chimney rise by convection and then diffuse into the air above the chimney is an example of mass transfer by the phase change.

Magnetohydrodynamics (MHD) is that branch of science, which deals with the motion of highly conducting ionized (electric conductor) fluid in presence of magnetic field. Examples of such fluids include plasmas, liquid metals and salt water. The motion of the conducting fluid across the magnetic field generates electric currents which change the magnetic field and the action of the magnetic field on these currents give rise to mechanical forces, which modify the fluid. It is possible to attain equilibrium in a conducting fluid if the current is parallel to the magnetic field. Then the magnetic forces vanish and the equilibrium of the gas is the same as in the absence of magnetic fields. But most liquids and gases are poor conductors of electricity. In the case when the conductor is either a liquid or a gas, electromagnetic forces will be generated which may be of the same order of magnitude as the hydrodynamical and inertial forces. Thus in the equation of motion these electromagnetic forces should be taken into account. The MHD was originally applied to astrophysical and geophysical problems, where it is still very important but more recently applied to the problem of fusion power where the application is the creation and containment of hot plasmas by electromagnetic forces, since material walls would be destroyed. Astrophysical problems include solar structure, especially in the outer layers, the solar wind bathing the earth and

other planets and interstellar magnetic fields. The primary geophysical problem in planetary magnetism produced by currents deep in the planet a problem that has not been solved to any degree of satisfaction. The interaction of the magnetic field and the moving electric charge carried by the flowing fluid induces a force, which tends to oppose the fluid motion and near the leading edge, the velocity is very small, so that the magnetic force which is proportional to the magnitude of the longitudinal velocity and acts in the opposite direction is also very small. Consequently, the influence of the magnetic field on the boundary layer is exerted only through induced forces within the boundary layer itself without additional effects arising from the free stream pressure gradient. Solid matter is generally excluded from MHD effects, but it should be realized that the same principles would apply. The motion of an electrically conducting fluid, like mercury, under a magnetic field, in general, gives rise to induced electric currents on which mechanical forces are exerted by the magnetic field. On the other hand, the induced electric currents also produce induced magnetic field. Thus there is a two-way interaction between the flow field and the magnetic field, the magnetic field exerts force on the fluid by producing induced currents and the induced currents change the original magnetic field. Therefore, the magnetohydrodynamic flows (the flows of electrically conducting fluids in the presence of magnetic field) are more complex than the ordinary hydrodynamic flows.

Several methods of controlling the boundary layer have been developed experimentally and also on the basis of theoretical considerations. The suction is one of them. It is the most efficient, simple and common method of controlling the boundary layer. Hence, the effect of suction on magnetohydrodynamic boundary layer is of great interest in astrophysics. It is often necessary to prevent separation of the boundary layer to reduce the drag and attain high lift values. On the other hand, one of the important problems facing in engineering for high-speed flow is the cooling of the surface to avoid the structural failures as a result of frictional heating. In this respect the possibility of using the injection at the surface is a measure to cool the body in the high temperature fluid.

Injection of secondary fluid through porous walls is of practical importance in flim cooling of turbine blades combustion chambers. In such applications injection usually occur normal to the surface and the injected fluid may be similar to or different from the primary fluid. Due to the importance of suction or injection for the boundary layer control in the field of aerodynamics space science, many research papers along these lines have been published for both steady and unsteady flows. Moreover, the stability of the boundary layer and the transition to turbulence are also considerably influenced by continuous suction and injection. Suction always stabilizes the boundary layer growth.

Slip velocity is a function of the velocity gradient near the wall. It is known that for gaseous flow there always exists a non–zero velocity near the wall and based on a momentum balance at the wall. In certain situations, the assumption of no slip boundary condition does no longer apply. When fluid flows in micro electro mechanical systems (MEMS), the no-slip condition at the solid fluid interface is no longer applicable. A slip flow model more accurately describes the non-equilibrium near the interface. A partial slip may occur on a stationary and moving boundary when the fluid is particulate such as emulsions, suspensions, foams, and polymer solutions.

Viscosity is the “resistance to flow” of a liquid**.** Viscosity of a fluid depends on temperature. In liquids, viscosity decreases with increasing temperature (i.e. cohesion decreases with increasing temperature). In gases, viscosity increases with increasing temperature (i.e. molecular interchange between layers increases with temperature setting up strong internal shear). The viscosity of air is 1.3289 kg $m^{-1} s^{-1}$, 2.671 kg $m^{-1} s^{-1}$, and 3.625 kg $m^{-1} s^{-1}$, at 100^0C, 500^0C and 800^0C temperature, respectively. The viscosity of water is 1006.523 kg $m^{-1} s^{-1}$, 471.049 kg $m^{-1} s^{-1}$, and 282.425 kg $m^{-1} s^{-1}$, at 20^0C, 60^0C and 100^0C temperature, respectively.

Thermal conductivity is the intensive property of material that indicates its ability to conduct heat. Thermal conductivity approximately tracks electrical conductivity, as freely moving valence elections transfer not only electric current

but also heat energy. A high value for thermal conductivity indicates that the material is a good heat conductor and a low value for thermal conductivity indicates that the material is a poor heat conductor or insulator. For example the material such as copper and silver that are good electric conductors are also good heat conductors, and have high values of thermal conductivity. Materials such as rubber, wood are poor conductors of heat and have low conductivity values. For liquid, it has been found that the thermal conductivity κ varies with temperature in an approximately linear manner in the range from 0 to 400^0 F.

1.2 Literature survey

Thermophoresis is an instrument of particle deposition, moreover other ones like inertial impaction, sedimentation etc. A synthetic description of this phenomenon may be the following: submicron sized (nano) particles suspended in a moving isothermal gas are subjected to a driving force towards the wall, when this wall is cold and away from the wall when it is hot. Thermophoretic force would act upon particles of aerosol while a temperature gradient is present. The effect was first observed by Tyndall (1870), when he observed that a particle free zone around a heated surface appeared in dusty air. In Aitken (1884) proved that the microscopic explanation to the effect was due to the heavier bombardment of the particle from the gas molecules on the hot side compared to the cold side. The thermophoretic transport involved in simple one-dimensional flows for the measurement of thermophoretic velocity was studied by Goldsmith and May (1966). Hales et al. (1972) studied the thermophoretic deposition in geometry of engineering interest and they solved the laminar boundary layer equations for simultaneous aerosol and steam transport to an isothermal vertical flat surface situated adjacent to a large body of an otherwise quiescent air-steam-aerosol mixture. Derjaguin et al. (1976) performed various experiments on the thermophoresis of aerosol particles and measured the thermal slip coefficient to calculate thermophoretic velocity, and then compared it with a theoretical one. Goren (1977) analyzed thermophoresis in laminar flow over a horizontal flat plate. He found the deposition of particles on cold plate and particle free layer thickness in hot plate case. The deposition efficiency of small particles due to thermophoresis in a

laminar tube flow was calculated by Walker et al. (1979). Thermophoresis of particles in a heated boundary layer was studied by Talbot et al. (1980). They calculated the trajectory of a particle entering the boundary layer by using several available theoretical expressions for the thermophoretic force. Measurements of the thickness of the particle-free layer next to the heated plate were compared with the calculated particle trajectories. Blasius series solution for thermophoretic deposition of small particles was studied by Homsy et al. (1981). Thermophoresis in natural convection for a cold vertical flat surface has been analyzed by Epstein et al. (1985). Numerical analysis for thermophoretic deposition of a laminar slot jet on an inclined plate has been studied by Garg and Jayaraj (1988). In their analysis, they used cold, hot and adiabatic wall conditions. Garg and Jayaraj (1990) studied the thermophoretic transport of aerosol particles through a forced convection laminar boundary layer in cross flow over a cylinder. Jia et al. (1992) investigated numerically the interaction between radiation and thermophoresis in forced convection laminar boundary layer flow. Chiou and Cleaver (1996) studied the effect of thermophoresis on submicron particle deposition from a laminar forced convection boundary layer flow on to an isothermal cylinder whereas Chiou (1998) analyzed the effect of thermophoresis on submicron particle deposition from a forced convective boundary layer flow on to an isothermal moving plate through similarity solutions. Thermophoretic analysis in narural convection laminar flow over a cold vertical flat plate has been studied by Jayaraj et al. (1999). He observed that for a cold plate, the wall concentration increases with the decrease of the Prandtl number. The problem of steady, two-dimensional, laminar, hydromagnetic flow with heat and mass transfer over a semi-infinite, permeable flat surface in the presence of thermophoresis and heat generation/absorption was studied numerically by Chamkha and Issa (2000). Thermophoresis of particles in gas-particle two-phase flow with radiation effect was investigated by Sohn et al. (2002) and they observed that gas as well as particle radiation exists; the deposition of particle is mainly influenced by the gas. The effect of surface mass transfer on mixed convection flow past a heated vertical flat permeable plate with thermophoresis has been studied numerically by Selim et al. (2003). In their investigation they found that as the thermophoretic

parameter increases, the surface mass flux increases. The steady and two-dimensional free convection boundary layer flow over an isothermal vertical circular cylinder in a fluid-saturated porous medium in the presence of the thermophoresis particle deposition effect was analyzed by Chamkha et al. (2004). Wang and Chen (2006) studied numerically the thermophoretic deposition of particles from a boundary layer flow onto a continuously moving wavy surface. Their numerical results showed that the mean deposition effect of the wavy plate is greater than the flat plate. Mixed convection heat and mass transfer flow along an isothermal vertical flat plate embedded in a fluid-saturated porous medium and the effects of viscous dissipation and thermophoresis in both aiding and opposing flows have been studied numerically through similarity solutions by Seddeek (2006). Postelnicu (2007) studied the effects of thermophoresis particle deposition in free convection boundary layer from a horizontal flat plate embedded in a porous medium. Bakier and Mansour (2007) studied numerically the combined effects of magnetic field and thermophoresis particle deposition in free convection boundary layer flow along a vertical flat plate embedded in a porous medium. Their numerical results showed that the nature of variation of particle concentration profile and magnetic field with respect to buoyancy force and Prandtl number was found to be similar. Duwairi and Damesh (2008) analyzed the effects of thermophoresis particle deposition on mixed convection from vertical surfaces embedded in saturated porous medium. Alam et al. (2008 and 2009) studied the effects of thermophoresis on steady two-dimensional hydromagnetic heat and mass transfer flow over an inclined flat plate with various flow conditions. Damesh et al. (2009) studied non-similar solutions of magnetohydrodynamic and thermophoresis particle deposition on mixed convection problem in porous media along a vertical surface with variable wall temperature. Rahman and Postelnicu (2010) studied the effects of thermophoresis on the forced convective laminar flow of a viscous incompressible fluid over a rotating disk. Postelnicu (2012) studied the thermophersis particle deposition in natural convection over inclined surfaces in porous media.

The unsteady mixed convection flow past an infinite vertical isothermal plate of an incompressible fluid is a physical situation, which is often experienced, in the

industrial applications. Some important contributions in this aspect have been given by Schneider (1979). Jha (1991) investigated the MHD unsteady mixed convection flow through a porous medium. He, however, obtained the solutions by employing Laplace transform technique and taking the value of the Prandtl number to be equal to one. Sattar et al. (1997) obtained an analytical solution of an unsteady MHD forced convective flow through a porous medium taking a constant heat source and a variable suction velocity. The phenomenon of natural convection heat and mass transfer is carried on MHD flow by many investigators. The effects of mass transfer on free convective flow of an electrically conducting, viscous fluid past an infinite porous plate with constant suction and transversely applied magnetic field studied by Haldavneker and Soundalgeker (1977). Raptis and Kafoussias (1982) considered the free convection and mass transfer steady hydromagnetic flow of an electrically conducting viscous incompressible fluid through a porous medium, occupying a semi-infinite region of the space bounded by an infinite vertical and porous plate under the action of a transverse magnetic field. The solution of velocity, temperature, concentration field and rate of heat transfer are obtained for the effects of different parameters. An analytical study is performed showing the effects of magnetic field on the free convection and mass transfer flow through porous medium by Jha and Prasad (1989). The solutions to the problem are obtained by Laplace transform technique. Later, the same method is employed by Jha et al. (1994) for the study of unsteady free convection and mass transfer flow past an exponentially accelerated infinite non-conducting vertical plate through a porous medium in the presence of uniform transverse magnetic field. Hossain et al. (2006) studied the unsteady mixed-convection boundary layer flow along a symmetric wedge with variable surface temperature. Singh et al. (2009) analyzed the unsteady mixed convection flow over a vertical wedge. Sparrow and Cess (1961) considered the case of a constant magnetic field, and have used a perturbation scheme, taking the non-magnetic case as the first approximation. Their results are applicable in the immediate neighborhood of the leading edge and for weak magnetic fields. Cramer (1963) studied the influence of magnetic field on the laminar free convection flow of liquid metals over a vertical flat plate and between two parallel plates. He obtained an analytical

solution for liquid metals. MHD mixed convection flow investigated by many researchers such as Yu (1965), Gardner and Lo (1975), Hossain and Ahmed (1990) and Al-Khawaja (1999). Yu (1965) showed the stabilizing effect of magnetohydrodynamic on combined forced and free convection channel flows similar to the case of horizontal layer heated from below. Grardner and Lo (1975) investigated the combined free and forced convection problem using a perturbation method, which produced some details of the secondary flow but his result, were limited to small values of the Hartman number. Hossain and Ahmed (1990) studied the combined forced and free convection of an electrically conducting fluid past a vertical flat plate at which the surface heat flux was uniform and a magnetic field was applied parallel to the direction normal to the plate. Recently, Vajravelu et al. (2013) analyzed unsteady convective boundary layer flow of a viscous fluid at a vertical surface with variable fluid properties.

Hasimoto (1957) studied the boundary layer growth on an infinite flat plate with uniform suction or injection. Exact solutions of the Navier-Stokes equations of motion were derived for the case of uniform suction and injection. Nanbu (1971) studied the vortex flow over a flat surface for large suction. He obtained the solutions by using perturbation method. The conditions under which similarity solutions exist to the hydromagnetic flow over a semi-infinite flat plate in the presence of a magnetic field and a pressure gradient with or without suction and injection are obtained by Cobble (1977). Following this, Soundalgeker and Ramanamurthy (1980) analyzed the thermal boundary layer and they solved the similarity equations taking into account the effects of suction or injection and pressure gradient. Gupta et al. (2003) studied the effects of suctrced coion or blowing (injection) on the velocity and temperature distribution in the flow past a porous flat plate of a power-law fluid. Alam and Rahman (2006) studied the combined free-forced convection and mass transfer flow past a vertical porous plate in a porous medium with heat generation and thermal diffusion. Recently, Noor et al. (2013) analyzed heat and mass transfer of thermophoretic MHD flow over an inclined radiate isothermal permeable surface in the presence of heat source/sink.

The slip flows under various flow configurations for Newtonian and non-Newtonian fluids have been studied widely in the literature on a stationary flat plate, moving plate as well as on a stretching surface (see for examples, Hasimoto (1958), Martin and Boyd (2000, 2006, 2010), Vedantam (2006), Andersson (2002), Wang (2006, 2009) and Aziz (2010). The general conclusion is as the slip parameter increases, the slip velocity increases and the wall shear stress decreases. Very recently, Rahman et al. (2014) analyzed the boundary layer flow of a nanofluid past a permeable exponentially shrinking/stretching surface with second order slip using Buongiorno's model.

All the above studies were confined to a fluid with constant viscosity. However, it is known that this physical property may change significantly with temperature. The effect of variable viscosity on hydrodynamic flow and heat transfer past a continuously moving porous boundary with radiation has been investigated by Seddeek (2000). Ali (2006) analyzed the effect of variable viscosity on mixed convection heat transfer along a vertical moving surface. Alam et al. (2009) studied transient magnetohydrodynamic free convective heat and mass transfer flow with thermophoresis past a radiative inclined permeable plate in the presence of variable chemical reaction and temperature-dependent viscosity. Pantokratoras (2005) obtained some new results on forced and mixed convection boundary layer flow along a flat plate with variable viscosity and variable Prandtl number while Pantokratoras (2007) further studied non-Darcian forced convection heat transfer over a flat plate in a porous medium with variable viscosity and variable Prandtl number. Rahman and his co-workers (2009 and 2011) analyzed several thermal boundary-layer problems taking into account the variability of viscosity for both Newtonian and Non-Newtonian fluids in different geometry with various flow conditions. All of these studies confirmed that for the accurate prediction of the thermal characteristics of variable viscosity and thermal conductivity, the Prandtl number must be treated as a variable rather than a constant. One of the main focuses behind this study is also to investigate how the Prandtl number varies within the boundary layer when fluid properties are depended on temperature.

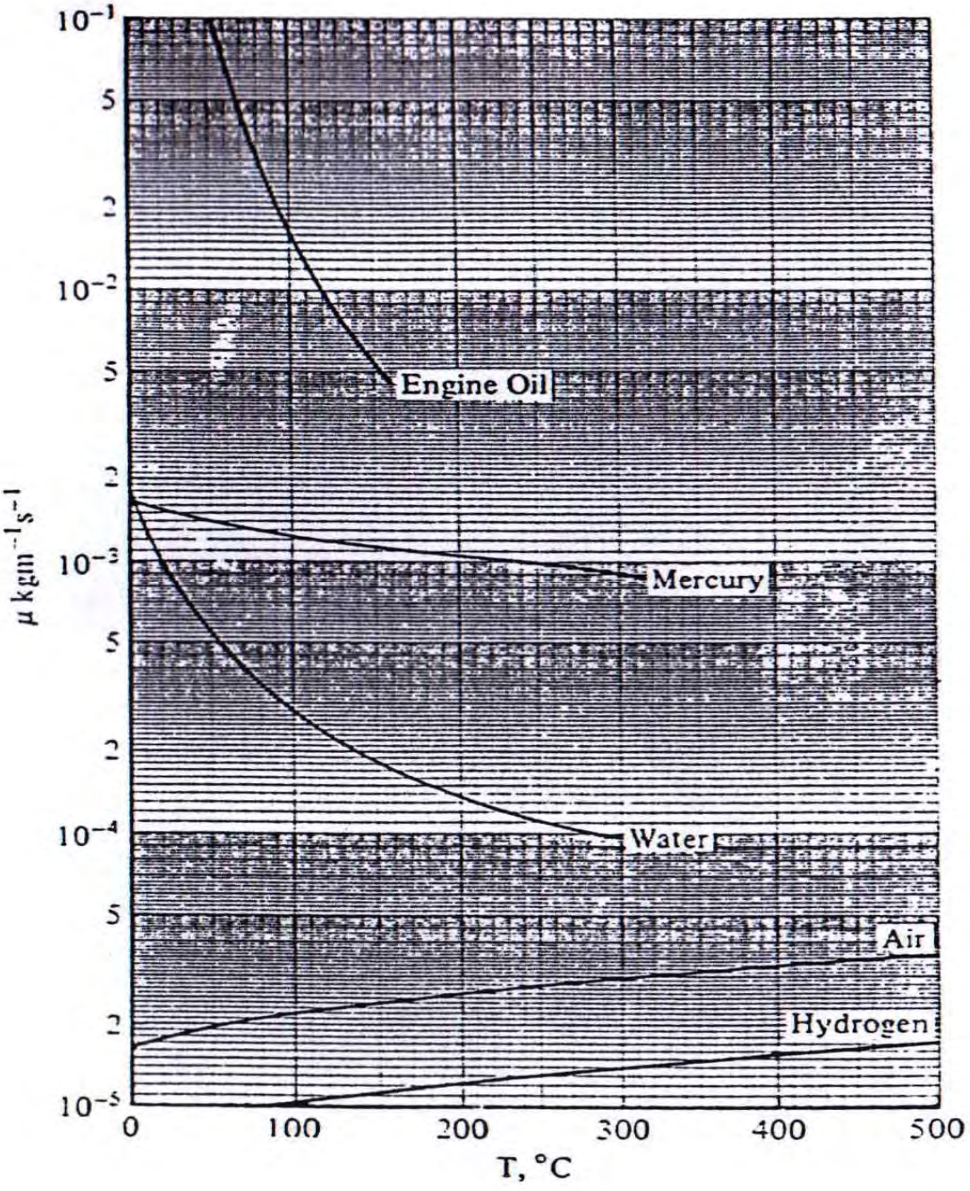

Figure 1.2: Variation of dynamic viscosity of several fluids with temperature (Cebeci and Bradshaw, 1984)

1. 3 Objectives of the present study

The objective of the present research is to investigate numerically the effect of unsteady convective flow along a wedge with thermophoresis. Then it is extended considering temperature dependent viscosity and thermal conductivity with variable Prandtl number, magnetohydrodynamic, slip flow, suction and injection on the flow field. The potential flow velocity has been taken as a function of the distance x and time t. The governing time dependent non-linear partial differential equations are reduced to a set of non-linear ordinary differential equations by introducing similarity transformations. Numerical results for the velocity, temperature and concentration profiles as well as local skin-friction coefficient, rate of heat and mass transfer, thermophoretic velocity and thermophoretic deposition velocity for different values of unsteadiness parameter, wedge angle parameter, Prandtl number, Schmidt number, thermophoretic coefficient, thermophoresis parameter and concentration ratio are displayed in graphically and tabulated form.

The major objectives of this study are:

i. To develop a mathematical model regarding the unsteady convective flow along a wedge with thermophoresis using Nachtsheim-Swigert shooting iteration technique along with sixth order Runge-Kutta integration scheme.
ii. To analyze heat and mass transfer characteristics of the unsteady convective flow along a wedge with thermophoresis from the obtained solution.
iii. To investigate the effects of unsteadiness parameter, wedge angle parameter, Prandtl number, Schmidt number, thermophoretic coefficient, thermophoresis parameter, concentration ratio and variable viscosity parameter on the velocity, temperature and concentration profiles as well as local skin-friction coefficient, rate of heat and mass transfer, thermophoretic velocity and thermophoretic particle deposition velocity.
iv. To compare the results with previously published results.

1. 4 Applications

Thermophoresis phenomenon has many engineering applications in removing small particles from gas streams, in determining exhaust gas particle trajectories from combustion devices, and in studying the particulate material deposition on turbine blades. Thermophoresis is also important in thermal precipitators, which are sometimes more effective than electrostatic precipitators in removing submicron-sized particles from gas streams. Since industrial air pollution is of great concern in the world, this phenomenon can be utilized to control air pollution by removing small particles from gas streams and other flue gases. This phenomenon commonly contributes significantly to the atmospheric and environmental sciences, aerosol science and technology. This phenomenon can also be used for the production of fine ceramic powders like aluminum nitride in the high temperature aerosol flow reactors. In aerosol flow reactors, the thermophoretic depositions are important since it is desired to decrease the deposition during the process in order to increase product yield. Thermophoretic deposition of radioactive particles is one of the major factors causing accidents in nuclear reactors. Thermophoresis is considered to be the dominant mass transfer mechanism in the modified chemical vapour deposition (MCVD) processes as currently used in the manufacturing of graded index optical fiber performs (i. e. the production of optical fiber performs by using MCVD). In optical fiber process, high deposition levels are desired since the goal is to coat the interior of the tube with particles. The fabrication of high yield processors is highly dependant on thermophoresis because of the repulsion and or deposition of impurities on the wafer as it heats up during fabrication.

1. 5 Outline of the thesis

The chapter 1 is an introductory chapter which includes physical phenomena of thermophoresis, heat and mass transfer, magnetohydrodynamics, suction/ injection, slip flow and temperature dependent viscosity and thermal conductivity with applications. An extensive literature review of the past studies on the above physical facts is included with the aim of the present studies.

The basic governing equations for the flow field heat and mass transfer from standard vector form to the case by case form are discussed elaborately in chapter 2. The dimensionless form of the governing equations is presented with careful discussion. At the end of this chapter, a comprehensive discussion regarding the method of solution of the non-linear dimensionless governing equations is introduced.

Local similarity solution for unsteady two dimensional forced convective heat and mass transfer flow along a wedge with thermophoresis is investigated in chapter 3. Numerical solutions have been obtained for wedge angle parameter, unsteadiness parameter, Prandtl number, Schmidt number, thermophoresis parameter and concentration ratio.

In chapter 4, thermophoresis particle deposition on unsteady two-dimensional forced convective heat and mass transfer flow along a wedge with variable viscosity and variable Prandtl number has been considered. The main focuses of this study is to investigate how the Prandtl number varies within the boundary layer when the viscosity is dependent on temperature.

Unsteady MHD forced convective flow along a porous wedge with variable fluid properties and thermophoresis is considered in chapter 5. Three new parameters are present in this chapter, namely Hartman number, suction parameter and thermal conductivity variation parameters. The characteristics of these new parameters are presented graphically and discussed elaborately.

In chapter 6, thermophoretic particle deposition on unsteady convective slip flow over a wedge with variable fluid properties and variable prandtl number has been analyzed. New parameters are added with the parameters introduced in chapter 3, namely viscosity variation parameter, thermal conductivity variation parameter and slip parameter. The properties of this parameter on the fluid flow, heat and mass transfer are widely explained in chapter 6.

Finally, a final clarification and possible future work on this thesis has been discussed in chapter 7.

Chapter 2

Mathematical modeling of the problem

The convective heat and mass transfer occur due to temperature difference and concentration difference. The starting point of any numerical method is the mathematical model, i.e. the set of partial differential equation and boundary conditions. A solution method is usually designed for a particular set of equations. The generalized governing equations are used based on the conservation laws of mass, momentum, energy and concentration. As the heat and mass transfer depend upon a number of factors, a dimensional analysis is presented to show the important non-dimensional parameters which influence the dimensionless heat and mass transfer, i.e. local Nusselt number and local Sherwood number.

2.1 Basic equations

2.1.1 Equation of continuity

The principle of conservation of mass (i. e equation of continuity) states that the rate at which mass increases with the control volume = the rate at which mass enters the control volume through its boundaries.

The MHD continuity equation for viscous incompressible electrically conduction fluid remains as that of usual continuity equation:

$$\vec{\nabla}.\vec{q} = 0. \qquad (2.1)$$

2.1.2 Equation of Navier-Stokes

The motion of conducting fluid across the magnetic field generates electric currents, which change the magnetic field and the action of the magnetic field on these current give rises to mechanical forces, which modify the flow of the fluid. Thus, the fundamental equation of the magneto-fluid combines the equations of

the motion from the fluid mechanics with Maxwell's equations from electrodynamics.

Then the Navier-Stokes equation for an unsteady laminar viscous incompressible fluid with constant viscosity may be written in the following form:

$$\rho\left(\frac{\partial}{\partial t}+\vec{q}.\vec{\nabla}\right)\vec{q}=-\vec{\nabla}P+\mu\vec{\nabla}^{2}\vec{q}+\vec{F}+\vec{J}\times\vec{B} \tag{2.2}$$

where ρ is the density, μ is the viscosity of the fluid and *P* is the pressure. The Navier-Stokes equation for an unsteady laminar viscous incompressible fluid with variable viscosity may be written in the following form:

$$\rho\left[\frac{\partial\vec{q}}{\partial t}+\left(\vec{q}.\vec{\nabla}\right)\vec{q}\right]=-\vec{\nabla}P+\vec{\nabla}.\tau+\vec{F}+\vec{J}\times\vec{B} \tag{2.3}$$

$\tau=2\mu\dot{\varepsilon}$

and

$$\dot{\varepsilon}=\begin{pmatrix}\dot{\varepsilon}_x & \dot{\varepsilon}_{xy} & \dot{\varepsilon}_{xz}\\ \dot{\varepsilon}_{yx} & \dot{\varepsilon}_y & \dot{\varepsilon}_{yz}\\ \dot{\varepsilon}_{zx} & \dot{\varepsilon}_{zy} & \dot{\varepsilon}_z\end{pmatrix}$$

$$=\begin{pmatrix}\frac{\partial u}{\partial x} & \frac{1}{2}\left(\frac{\partial v}{\partial x}+\frac{\partial u}{\partial y}\right) & \frac{1}{2}\left(\frac{\partial w}{\partial x}+\frac{\partial u}{\partial z}\right)\\ \frac{1}{2}\left(\frac{\partial u}{\partial y}+\frac{\partial v}{\partial x}\right) & \frac{\partial u}{\partial y} & \frac{1}{2}\left(\frac{\partial w}{\partial y}+\frac{\partial v}{\partial z}\right)\\ \frac{1}{2}\left(\frac{\partial u}{\partial z}+\frac{\partial w}{\partial x}\right) & \frac{1}{2}\left(\frac{\partial v}{\partial z}+\frac{\partial w}{\partial y}\right) & \frac{\partial u}{\partial z}\end{pmatrix}$$

The left side of the equation (2.2) is the mass time acceleration; the first term on the right hand side is the pressure gradient, second term is the viscous force, third term is the body force per unit volume and the last term is the electromagnetic force due to motion of the fluid.

2.1.3 Equation of energy

The energy equation for a viscous incompressible fluid is obtained by adding the electromagnetic energy term into the classical gas dynamic energy equation. This equation can be written as:

$$\rho c_p \left[\frac{\partial T}{\partial t} + \left(\vec{q}.\vec{\nabla}\right)T \right] = \vec{\nabla}.\left(\kappa_f \vec{\nabla} T\right) \tag{2.4}$$

where κ_f is the thermal conductivity of the fluid, c_p is the specific heat at constant pressure.

The left side of the equation (2.4) represents the net energy transfer due to mass transfer. The right hand side represents conductive heat transfer.

In the above equations, $\vec{\nabla}$ is the vector differential operator and for two dimensional case it is defined as:

$$\vec{\nabla} = \hat{i}\frac{\partial}{\partial x} + \hat{j}\frac{\partial}{\partial y}$$

where $\hat{i}$ and $\hat{j}$ are the unit vectors along $\bar{x}$ and $\bar{y}$ axes, respectively. If it is considered that the external electric field is zero and induced magnetic field is negligible, then the current density is related to the velocity by Ohm's law as follows:

$$\vec{J} = \sigma\left(\vec{q} \wedge \vec{B}\right) \tag{2.5}$$

where $\vec{q} \wedge \vec{B}$ is the electrical fluid vector and σ denotes the electrical conductivity of the fluid. This condition is usually well satisfied in terrestrial applications, especially so in (low-velocity) free convection flows. So, we can write $\vec{B} = \hat{j}B_0$ (2.6)

using equations (2.5) and (2.6) the force per unit volume $\vec{J} \times \vec{B}$ acting along the $\bar{x}$ axis takes the following form:

$$\vec{J} \times \vec{B} = -\sigma {B_0}^2 \bar{u}\,. \tag{2.7}$$

2.1.4 Equation of concentration

The concentration equation can be written as:

$$\frac{\partial C}{\partial t} + \left(\vec{q}.\vec{\nabla}\right)C = D\vec{\nabla}^2 C - \vec{\nabla} V_T C \tag{2.8}$$

where D is the molecular diffusivity and V_T is the thermophoretic velocity, which is defined as $V_T = -\kappa\upsilon\frac{\vec{\nabla}T}{T}$.

The left side of the equation (2.8) represents the net concentration due to mass transfer; the first term of the right hand side represents diffusive mass transfer and the second term of the right hand side represents thermophoretic velocity term.

2.2 Physical configuration

Consider, an unsteady two-dimensional laminar forced convective hydrodynamic heat and mass transfer flow of a viscous incompressible fluid along a heated wedge. The angle of the wedge is given by $\Omega = \beta\pi$. The flow is assumed to be in the *x*-direction which is taken along a direction of the wedge and the *y*-axis is normal to it. The surface of the wedge is maintained at a uniform constant temperature T_w and a uniform constant concentration C_w which are higher than the ambient temperature T_∞ and ambient concentration C_∞, respectively. In addition, a uniform transverse magnetic field of strength B_0 is applied parallel to the *y*-axis. Besides, fluid suction or injection is imposed on the wedge surface as shown in Figure 2.1.

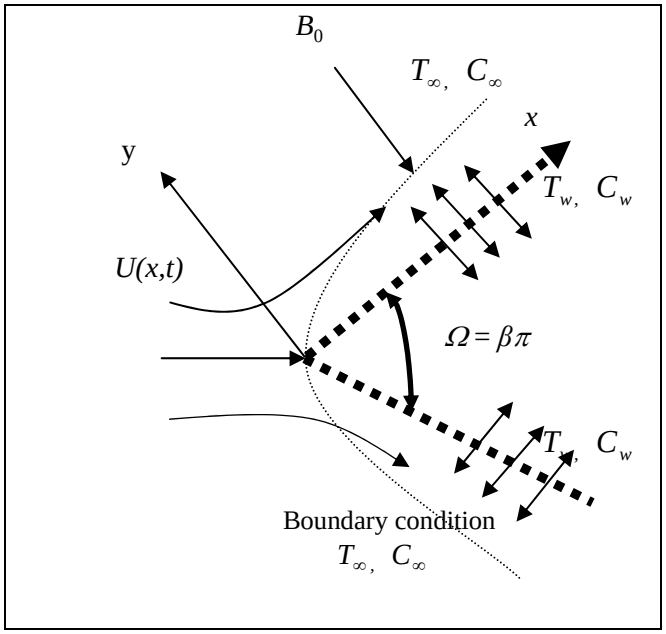

Figure 2.1: The physical model of 2-D wedge flow

2. 3 Assumptions of the study

The present work is based on the following assumptions.

i. The flow is unsteady, laminar, two-dimensional, viscous and incompressible.
ii. The fluid may be treated as continuous and is describable in terms of local properties.
iii. The wedge surface is heated.
iv. The temperature gradient in the *y*-direction is much larger than that in the *x*-direction and hence, only the thermophoretic velocity component, which is normal to the surface, is of importance.

2.4 Mathematical formulation

The mathematical analysis of the present problem has been discussed in this section. There are four cases considered in the current study, therefore, the case by case mathematical formulations of the analysis are presented in the following sub-sections.

2.4.1 Case I: Unsteady forced convective flow

Consider an unsteady two-dimensional laminar forced convective hydrodynamic heat and mass transfer flow of a viscous incompressible fluid along a heated impermeable wedge in the presence of thermophoresis. The governing boundary-layer equations (2.1), (2.2), (2.4) and (2.8) are:

Continuity equation:

$$\frac{\partial u}{\partial x}+\frac{\partial v}{\partial y}=0, \tag{2.9}$$

Momentum equation:

$$\frac{\partial u}{\partial t}+u\frac{\partial u}{\partial x}+v\frac{\partial u}{\partial y}=-\frac{1}{\rho}\frac{\partial p}{\partial x}+\upsilon\frac{\partial^2 u}{\partial y^2}, \tag{2.10}$$

Energy equation:

$$\frac{\partial T}{\partial t}+u\frac{\partial T}{\partial x}+v\frac{\partial T}{\partial y}=\frac{\kappa_f}{\rho c_p}\frac{\partial^2 T}{\partial y^2}, \tag{2.11}$$

Concentration equation:

$$\frac{\partial C}{\partial t}+u\frac{\partial C}{\partial x}+v\frac{\partial C}{\partial y}=D\frac{\partial^2 C}{\partial y^2}-\frac{\partial}{\partial y}(V_T C), \tag{2.12}$$

where u, v are the velocity components in the x and y directions respectively, t is the time, p is the pressure ,υ is the kinematic viscosity, ρ is the density of the fluid. T, T_w and T_∞ are the temperature of the fluid inside the thermal boundary layer, the wedge surface temperature and the fluid temperature in the free stream, respectively, while C, C_w and C_∞ are the corresponding concentration, κ_f is the thermal conductivity of the fluid, c_p is the specific heat at constant pressure, D is the molecular diffusivity of the species concentration and V_T is the thermophoretic velocity.

In boundary-layer flow, the temperature gradient in the y-direction is much larger than that in the x-direction and hence only the thermophoretic velocity in y-direction is considered. As a consequence, in equation (2.12), the thermophoretic velocity V_T, was recommended by Talbot et al. (1980) as

$$V_T=-\frac{\kappa\upsilon}{T}\frac{\partial T}{\partial y}, \tag{2.13}$$

The negative sign in equation (2.13) means that the particles move down the temperature gradient, i.e., from hot to cold. Here, $\kappa\upsilon$ represents the thermophoretic diffusivity and κ is the thermophoretic coefficient which ranges in value from 0.2 to 1.2 as indicated by Batchelor and Shen (1985) and is defined by

$$\kappa = \frac{2C_s(k_f / \lambda_p + C_t Kn)C_c}{(1+3C_m Kn)(1+2k_f / \lambda_p + 2C_t Kn)}, \tag{2.14}$$

where κ_f and λ_p are the thermal conductivities of the fluid and diffused particles, respectively. C_m = 1.146, C_s = 1.147, C_t = 2.20 are constants obtained from the experimental data. $C_c = [1 + Kn(C_1 + C_2 e^{-C_3/Kn})]$ is the Stokes-Cunningham correction factor and $Kn = \left(\frac{2\xi}{d_p}\right)$ is the Knudsen number of the particle, where C_1 = 1.2, C_2 = 0.41, C_3 = 0.88, d_p is the particle diameter and ξ is the mean free path of molecule.

2.4.1.1 Boundary conditions

The applicable boundary conditions for the present model are:

i. On the wedge surface $(y = 0)$:

$u = 0$, v = 0, $T = T_w$, $C = C_w$, (2.15a)

(no-slip and impermeable wall condition)

ii. Matching with quiescent free stream $(y \to \infty)$:

$u = U(x,t)$, $T = T_\infty$, $C = C_\infty$. (2.15b)

It has been established (Schlichting:1958) long ago that similar solutions of the steady 2-D boundary layer equations exist when the velocity of the potential flow is proportional to a power of the length coordinate along the boundary. Following this phenomenon, it can also be established that similar solutions of the unsteady 2-D boundary layer equations exist when the velocity of the potential flow is inversely proportional to the power of a length scale which is a function of time. Thus for the present unsteady case we consider the potential flow velocity *U(x, t)* for the wedge flow as [see Sattar (2011)]

$$U(x,t) = \frac{\upsilon x^m}{\delta^{m+1}}, \tag{2.16}$$

where m is an arbitrary constant and is related to the wedge angle and δ is the time dependent length scale, which is taken to be [see Sattar (2011) and Mia et al. (2011)] as

$$\delta = \delta(t) \tag{2.17}$$

Since the potential flow velocity is defined as a function of *(x, t)*, we have from (2.16) and (2.17)

$$-\frac{1}{\rho}\frac{\partial p}{\partial x} = \frac{\partial U}{\partial t} + U\frac{\partial U}{\partial x} = -\frac{\upsilon(m+1)x^m}{\delta^{m+1}}\frac{d\delta}{dt} + \frac{\upsilon^2 m x^{2m-1}}{\delta^{2m+2}} \tag{2.18}$$

2.4.1.2 Solution for unsteady case

In order to obtain similarity solution of the problem we introduce the following non-dimensional variables:

$$\left.\begin{aligned} \eta &= y\sqrt{\frac{(m+1)}{2}}\sqrt{\frac{x^{m-1}}{\delta^{m+1}}}, \\ \psi &= \sqrt{\frac{2}{m+1}}\,\frac{\upsilon\, x^{(m+1)/2}}{\delta^{(m+1)/2}} f(\eta), \\ \theta(\eta) &= \frac{T - T_\infty}{T_w - T_\infty}, \\ \phi(\eta) &= \frac{C - C_\infty}{C_w - C_\infty}, \end{aligned}\right\} \tag{2.19}$$

where η is the similarity variable, ψ is the stream function that satisfies the continuity equation (2.9) and is defined by

$$u = \frac{\partial \psi}{\partial y} \text{ and } v = -\frac{\partial \psi}{\partial x},$$

we have from (2.19)

$$u = U(x,t)\,f' \text{ and } v = -\sqrt{\frac{2}{m+1}}\,\frac{\upsilon}{\delta^{\frac{m+1}{2}}}\,x^{\frac{m-1}{2}}\left(\frac{m+1}{2}\right)\left[\,f + \frac{m-1}{m+1}\eta f'\,\right], \tag{2.20}$$

where f is non dimensional stream function and prime denotes differentiation with respect to η.

Now using equations (2.17)-(2.20) into equations (2.10)-(2.12) we obtain the following non linear ordinary differential equations:

$$f''' + ff'' + \beta(1 - f'^2) - \frac{\delta^m}{\upsilon x^{m-1}}\frac{d\delta}{dt}(2 - 2f' - \eta f'') = 0, \tag{2.21}$$

$$\theta'' + \Pr\, f\theta' + \frac{\delta^m}{\upsilon x^{m-1}}\frac{d\delta}{dt}\Pr\eta\theta' = 0, \tag{2.22}$$

$$\phi'' + Scf\phi' + \frac{\delta^m}{\upsilon x^{m-1}}\frac{d\delta}{dt}Sc\,\eta\phi' + \frac{\kappa\, Sc}{N_t + \theta}[(N_c + \phi)\theta'' + \theta'\phi' - (\frac{N_c + \phi}{N_t + \theta})\theta'^2] = 0, \tag{2.23}$$

with the transformed boundary conditions:

$$f = 0,\ f' = 0, \theta = 1, \phi = 1 \quad \text{at} \quad \eta = 0, \tag{2.24a}$$

$$f' = 1, \theta = 0, \phi = 0 \qquad \text{as} \quad \eta \to \infty, \tag{2.24b}$$

where $\beta = \frac{2m}{m+1}$ is the Hartree pressure gradient or wedge angle that corresponds to $\Omega = \beta\pi$ for a total angle Ω of the wedge, $\Pr = \frac{\mu c_p}{\kappa_f}$ is the Prandtl number, $Sc = \frac{\upsilon}{D}$ is the Schmidt number, $N_t = \frac{T_\infty}{T_w - T_\infty}$ is the thermophoresis parameter, $N_c = \frac{C_\infty}{C_w - C_\infty}$ is the concentration ratio.

Now in order to make the equations (2.21)-(2.23) locally similar,

$$\text{let } \frac{\delta^m}{\upsilon x^{m-1}}\frac{d\delta}{dt} = \lambda, \tag{2.25}$$

where λ is taken to be a constant and thus can be treated as a dimensionless measure of the unsteadiness.

Hence equations (2.21)-(2.23) becomes

$$f''' + ff'' + \beta(1 - f'^2) - \lambda(2 - 2f' - \eta f'') = 0, \tag{2.26}$$

$$\theta'' + \Pr\, f\theta' + \lambda \Pr \eta\theta' = 0, \tag{2.27}$$

$$\phi'' + Scf\phi' + \lambda Sc\,\eta\phi' + \frac{\kappa\, Sc}{N_t + \theta}[(N_c + \phi)\theta'' + \theta'\phi' - (\frac{N_c + \phi}{N_t + \theta})\theta'^2] = 0, \tag{2.28}$$

Further, we suppose that $\lambda = \frac{c}{x^{m-1}}$, so that

$$c = \frac{\delta^m}{\upsilon}\frac{d\delta}{dt}. \tag{2.29}$$

Thus integrating (2.29) we obtain

$$\delta = \left[c(m+1)\upsilon t\right]^{1/m+1} . \tag{2.30}$$

Now taking $c = 2$ and $m = 1$ in equation (2.30) we obtain

$$\delta = 2\sqrt{\upsilon t}\,. \tag{2.31}$$

The length scales $2\sqrt{\upsilon t}$ for the ordinate similar to one seen in (2.31) was initially used by Stokes (1856) for an unsteady parallel flow, but $\delta(t)$ form of the length scale was initially developed by Sattar and Hossain (1992) in case of a solution of an unsteady one-dimensional boundary-layer problem. The characteristics length scale $\delta(t)$ defined particularly in (2.31) physically related to the boundary-layer thickness which can be viewed in Schlichting (2000).

2.4.1.3 Parameters of engineering interest

The local skin friction coefficient (wall shear stress), wall heat transfer rate (local Nusselt number), mass transfer rate (local Sherwood number) and thermophoretic particle deposition velocity are important physical parameters which are defined respectively by the following relations:

$$C_{fx} = \frac{\tau_w}{\frac{1}{2}\rho U^2}, \tag{2.32}$$

$$Nu_x = \frac{q_w x}{\kappa_f (T_w - T_\infty)}, \tag{2.33}$$

$$Sh_x = \frac{M_w x}{D(C_w - C_\infty)}, \tag{2.34}$$

and $V_d = \left[\frac{M_w}{(C_w - C_\infty)}\right]_{y=0}$. (2.35)

Now the wall shear stress on the surface τ_w, rate of heat transfer q_w and rate of mass transfer M_w are given by

$$\tau_w = \mu\left(\frac{\partial u}{\partial y}\right)_{y=0}, \tag{2.36}$$

$$q_w = -\kappa_f \left(\frac{\partial T}{\partial y}\right)_{y=0}, \tag{2.37}$$

$$M_w = -D\left(\frac{\partial C}{\partial y}\right)_{y=0}, \tag{2.38}$$

using (2.19) and (2.36)-(2.38) the quantities of (2.32)-(2.35) can be written as follows:

Local skin-friction coefficient:

$$\frac{1}{2} C_{fx} \sqrt{2-\beta} = \mathrm{Re}^{-\frac{1}{2}} f''(0), \tag{2.39}$$

Local Nusselt number:

$$Nu_x \sqrt{2-\beta} = -\mathrm{Re}^{\frac{1}{2}} \theta'(0), \tag{2.40}$$

Local Sherwood number:

$$Sh_x \sqrt{2-\beta} = -\mathrm{Re}^{\frac{1}{2}} \phi'(0). \tag{2.41}$$

Non-dimensional thermophoretic velocity are evaluated as

$$V_{Tw} = \left(\frac{V_T x}{\upsilon}\right)_{y=0} = -\sqrt{\frac{1}{2-\beta}}\, \mathrm{Re}^{\frac{1}{2}} \frac{\kappa}{1+N_t} \theta'(0). \tag{2.42}$$

Thermophoretic particle deposition velocity at the surface of the wedge is evaluated as

$$V_d = \left[\frac{M_w}{(C_w - C_\infty)}\right]_{y=0} = -\sqrt{\frac{1}{2-\beta}}\, \frac{1}{Sc}\, \mathrm{Re}^{\frac{1}{2}} \frac{\upsilon}{x} \phi'(0). \tag{2.43}$$

Therefore non-dimensional thermophoretic particle deposition velocity is obtained as

$$V_d^* = \frac{V_d x}{\upsilon} = -\sqrt{\frac{1}{2-\beta}}\,\frac{1}{Sc}\,\mathrm{Re}^{\frac{1}{2}}\,\phi'(0), \tag{2.44}$$

where $\mathrm{Re} = \dfrac{Ux}{\upsilon}$ is the Reynolds number.

Thus from equations (2.42) and (2.44) we observe that the non-dimensional thermophoretic velocity is proportional to the numerical values of $-\theta'(0)$ whereas the non-dimensional particle deposition velocity is proportional to the numerical values of $-\phi'(0)$ which are evaluated when the corresponding differential equations are solved satisfying the convergence criterion.

2.4.2 Case II: Temperature dependent viscosity and Prandtl number

In this case, temperature dependent viscosity and variable Prandtl number in the momentum equation (2.2) are taking into account. The momentum equation for this case is

$$\frac{\partial u}{\partial t} + u\frac{\partial u}{\partial x} + v\frac{\partial u}{\partial y} = -\frac{1}{\rho}\frac{\partial p}{\partial x} + \frac{1}{\rho}\frac{\partial}{\partial y}\left(\mu\frac{\partial u}{\partial x}\right), \tag{2.45}$$

The fluid viscosity in the momentum boundary layer decreases with the increase of temperature, which in turn affects the heat transfer rate at the surface of the wedge. Thus in order to predict the flow and heat transfer rate accurately, Ling and Dybbs (1987) suggested a temperature-dependent viscosity of the form:

$$\mu = \frac{\mu_\infty}{\left[1+\tau(T-T_\infty)\right]} \tag{2.46}$$

Where τ is the thermal property of the fluid. Equation (2.46) can be rewritten as

$$\frac{1}{\mu} = A(T - T_r), \quad \text{where } A = \tau/\mu_\infty \text{ and } T_r = T_\infty - 1/\tau. \tag{2.47}$$

In the relation (2.47), both A and T_r are constants and their values depend on the reference state and τ. It is mentioned that for liquids, $A > 0$ and for gases, $A < 0$. Typical values of τ and A for air are τ = 0.026240 and A = -123.2 [see Weast (1990)].

The dimensionless temperature θ can also be written as

$$\theta = \frac{T - T_r}{T_w - T_\infty} + \theta_r, \tag{2.48}$$

where $\theta_r = (T_r - T_\infty)/(T_w - T_\infty) = -1/\tau\,(T_w - T_\infty)$ and its value is determined by the viscosity/temperature characteristics of the fluid under consideration and the temperature difference $T_w - T_\infty$. It is to be mentioned that for $T_w - T_\infty > 0$, θ_r must physically be greater than 1 for gases and $\theta_r < 0$ for liquids. On the other hands, opposite is true if $T_w - T_\infty < 0$, where θ_r must physically be greater than 1 for liquids and $\theta_r < 0$ for gases [for detailed discussion of the values of θ_r, see also Elbashbeshy and Bazid (2000) and Ali (2006)]. Using equations (2.46)-(2.48) becomes

$$\mu = \mu_\infty \left(\frac{\theta_r}{\theta_r - \theta} \right). \tag{2.49}$$

The energy equation, concentration equation and the boundary conditions remain same as equations (2.27), (2.28) and (2.24), respectively.

Now introducing the equations (2.19), (2.20), (2.25) and (2.49) into equation (2.45), we obtain the following non linear ordinary differential equation:

$$f''' + (1 - \frac{\theta}{\theta_r}) ff'' + \frac{1}{\theta_r - \theta} f''\theta' + \beta(1 - \frac{\theta}{\theta_r})(1 - f'^2) - \lambda(2 - 2f' - \eta f'') = 0, \tag{2.50}$$

The local skin friction coefficient (wall shear stress), is important physical parameters which is defined by the following relations:

$$C_{fx} = \frac{\tau_w}{\frac{1}{2}\rho U^2}. \tag{2.51}$$

Now the wall shear stress on the surface τ_w is given by

$$\tau_w = \mu \left(\frac{\partial u}{\partial y} \right)_{y=0}. \tag{2.52}$$

Using equations (2.19) and (2.52) the quantities of equation (2.51) can be written as follows:

$$\frac{1}{2} C_{fx} \sqrt{2 - \beta} = \mathrm{Re}^{-\frac{1}{2}} \left(\frac{\theta_r}{\theta_r - \theta} \right) f''(0). \tag{2.53}$$

2.4.2.1 Variable Prandtl number

From the definition of Prandtl number, we see that it is a function of viscosity, and as the viscosity varies across the boundary layer, the Prandtl number also varies. The assumption of constant Prandtl number inside the boundary layer may produce unrealistic results [more detailed in Rahman and Eltayeb (2011) and Pantokratoras (2005, 2007)]. Therefore, the Prandtl number related to the variable viscosity is defined as

$$\mathrm{Pr}_v = \frac{\mu c_p}{\kappa_f} = \frac{\mu_\infty \left(\frac{\theta_r}{\theta_r - \theta} \right) c_p}{\kappa_f} = \left(\frac{\theta_r}{\theta_r - \theta} \right) \mathrm{Pr}_\infty . \tag{2.54}$$

At the surface ($\eta = 0$) of the wedge, this can be written as

$$\mathrm{Pr}_w = \left(\frac{\theta_r}{\theta_r - 1} \right) \mathrm{Pr}_\infty . \tag{2.55}$$

From equation (2.54), it can be seen that for $\theta_r \to \infty$, the variable Prandtl number Pr_v is equal to the ambient Prandtl number Pr_∞. For $\eta \to \infty$, i.e. outside the boundary layer, $\theta(\eta)$ becomes zero; therefore, Pr_v equals Pr_∞ regardless of the values of θ_r.

In the light of the above discussion and using equation (2.54), the non-dimensional temperature equation (2.27) can be expressed as

$$\theta'' + \left(1 - \frac{\theta}{\theta_r} \right) \mathrm{Pr}_v \, f\theta' + \left(1 - \frac{\theta}{\theta_r} \right) \mathrm{Pr}_v \, \lambda \eta \theta' = 0 . \tag{2.56}$$

Equation (2.56) is the corrected non-dimensional form of the energy equation in which Prandtl number is treated as variable.

2.4.3 Case III: The study of MHD and temperature dependent thermal conductivity

In the above cases, the studies are confined with constant thermal conductivity but it is observed from definition that thermal conductivity is a function of temperature. For some liquids like engine oil, mercury and water it is inversely proportional to temperature and for air and hydrogen it is directly proportional to temperature. The momentum equation (2.2) and energy equation (2.4) for the unsteady, two dimensional forced convective flow of an electrically conducting, viscous and incompressible fluid with variable thermal conductivity along a wedge after simplifying can be written as

$$\frac{\partial u}{\partial t}+u\frac{\partial u}{\partial x}+v\frac{\partial u}{\partial y}=-\frac{1}{\rho}\frac{\partial P}{\partial x}+\upsilon\frac{\partial^2 u}{\partial y^2}-\frac{\sigma B_0^2}{\rho}(u-U), \tag{2. 57}$$

$$\frac{\partial T}{\partial t}+u\frac{\partial T}{\partial x}+v\frac{\partial T}{\partial y}=\frac{1}{\rho c_p}\frac{\partial}{\partial y}\left(\kappa_f\frac{\partial T}{\partial y}\right). \tag{2. 58}$$

The applicable boundary conditions for the present model are:

i. On the wedge surface $(y=0)$:

$$u=0,\ v=\pm v_w(x,t),\ T=T_w,\ C=C_w \tag{2.59a}$$

(no-slip and permeable wall condition)

ii. Matching with quiescent free stream $(y\to\infty)$:

$$u=U(x,t),\ T=T_\infty,\ C=C_\infty, \tag{2.59b}$$

where v_w(x, t) represents the suction/ injection velocity at the porous surface where its sign indicates suction (< 0) or injection (> 0) and $U(x, t)$ is the potential velocity generated by the wedge.

Following Chiam (1996, 1998) the model for a variable thermal conductivity is considered as:

$$\kappa_f=\kappa_\infty\left(1+\gamma\frac{T-T_\infty}{T_w-T_\infty}\right), \tag{2.60}$$

where κ_∞ is the thermal conductivity of the ambient fluid and γ is the thermal conductivity variation parameter.

The concentration equation remains same as equations (2.28).

Now employing the equations (2.18)-(2.20), (2.25) and (2.59) into equations (2.57) and (2.58), we obtain the following non linear ordinary differential equations:

$$f''' + ff'' + \beta(1 - f'^2) - \lambda(2 - 2f' - \eta f'') - \frac{2}{m+1} Ha^2 (f' - 1) = 0, \tag{2.61}$$

$$\theta'' + \frac{\gamma}{1+\gamma\theta}\theta'^2 + \frac{\Pr_\infty}{1+\gamma\theta} f\theta' + \frac{\Pr_\infty}{1+\gamma\theta}\lambda\eta\theta' = 0, \tag{2.62}$$

with the transformed boundary conditions:

$$f = f_w, f' = 0, \theta = 1, \phi = 1 \quad at \quad \eta = 0, \tag{2.63a}$$

$$f' = 1, \quad \theta = 0, \quad \phi = 0 \quad as \quad \eta \to \infty. \tag{2.63b}$$

The dimensionless parameters appear in the above equations are $\Pr_\infty = \frac{\mu c_p}{\kappa_\infty}$ is the ambient Prandtl number, $Ha = B_0\sqrt{\frac{\sigma x}{\rho U}}$ is the Hartmann number, $f_w = -v_w(x,t)\left(\frac{2}{m+1}\right)^{\frac{1}{2}} \frac{\delta^{\frac{m+1}{2}}}{\upsilon x^{\frac{m-1}{2}}}$ is the wall mass transfer coefficient which is positive ($f_w > 0$) for suction and negative ($f_w < 0$) for injection, β, λ, N_t, N_c, and *Sc* are defined earlier in case I.

The local Nusselt number within the boundary-layer can be calculated by the relations (2.37) the quantity (2.33) can be written as

$$Nu_x\sqrt{2-\beta} = -\mathrm{Re}^{\frac{1}{2}}\left(\frac{1}{1+\gamma\theta}\right)\theta'(0). \tag{2.64}$$

2.4.3.1 Variable Prandtl number

Prandtl number is a function of thermal conductivity and specific heat. However, since the thermal conductivity varies across the boundary layer, the Prandtl number also varies. The assumption of constant Prandtl number inside the boundary layer when thermal conductivities are temperature-dependent leads to

unrealistic results. Therefore, in the present work, the Prandtl number related to the variable thermal conductivity is defined as:

$$\mathrm{Pr}_v = \frac{\mu c_p}{\kappa_f} = \frac{\mu c_p}{\kappa_\infty (1+\gamma\theta)} = \left(\frac{1}{1+\gamma\theta}\right)\mathrm{Pr}_\infty . \tag{2.65}$$

At the surface ($\eta = 0$) of the wedge, this can be written as

$$\mathrm{Pr}_w = \frac{\mathrm{Pr}_\infty}{(1+\gamma)} . \tag{2.66}$$

From equation (2.65), it can be seen that for $\gamma \to 0$, the variable Prandtl number Pr_v is equal to the ambient Prandtl number Pr_∞ .

In light of the above discussion and using equation (2.65), the non-dimensional temperature equation (2.62) can be expressed as:

$$\theta'' + \frac{\gamma}{1+\gamma\theta}\theta'^2 + \mathrm{Pr}_v\ f\theta' + \mathrm{Pr}_v\ \lambda\eta\theta' = 0 . \tag{2.67}$$

2.4.4 Case IV: Temperature dependent viscosity and thermal conductivity with slip flow

The mathematical statement of the basic conservation lows of momentum equation (2.2) and energy equation (2.4) for the unsteady, two dimensional forced convective flow of a viscous incompressible fluid with combined effect of temperature dependent fluid properties like as viscosity and thermal conductivity along a wedge after simplifying can be written as

$$\frac{\partial u}{\partial t} + u\frac{\partial u}{\partial x} + v\frac{\partial u}{\partial y} = \frac{\partial U}{\partial t} + U\frac{\partial U}{\partial x} + \frac{1}{\rho_\infty}\frac{\partial}{\partial y}\left(\mu\frac{\partial u}{\partial y}\right), \tag{2.68}$$

$$\frac{\partial T}{\partial t} + u\frac{\partial T}{\partial x} + v\frac{\partial T}{\partial y} = \frac{1}{\rho_\infty c_p}\frac{\partial}{\partial y}\left(\kappa_f\frac{\partial T}{\partial y}\right), \tag{2.69}$$

The applicable boundary conditions for the present model are:

$$u = L\left(\frac{\partial u}{\partial y}\right),\ v = 0,\ T = T_w,\ C = C_w,\ \text{at}\quad y = 0, \tag{2.70a}$$

$$u = U(x,t),\ T = T_\infty,\ C = C_\infty\ ,\ \text{as}\quad y \to \infty, \tag{2.70b}$$

where L is the slip length and $U(x,t)$ is the potential flow velocity for the wedge flow which is taken as follows [see Rahman and Eltayeb (2011)].

The fluid viscosity in the momentum boundary layer decreases with the increase of temperature, which in turn affects the heat transfer rate at the surface of the wedge. Thus in order to predict the flow and heat transfer rate accurately, Ling and Dybbs (1987) suggested a temperature-dependent viscosity of the form:

$$\mu = \frac{\mu_\infty}{\left[1 + \tau(T - T_\infty)\right]}, \tag{2.71}$$

where τ is the thermal property of the fluid. For liquid metals, the thermal conductivity varies linearly with temperature in the range 0-400 ^{0}F studied by Savvas et al. (1994). Chiam (1998) considered a temperature dependent thermal conductivity as

$$\kappa_f = \kappa_\infty\left(1 + \gamma\frac{T - T_\infty}{T_w - T_\infty}\right), \tag{2.72}$$

where κ_∞ is the thermal conductivity of the ambient fluid and γ is the thermal conductivity variation parameter.

Now introducing the equations (2.18)-(2.20), (2.71), (2.72) and (2.70) into equations (2.68) and (2.69), we get the following non linear ordinary differential equations:

$$f''' + (1 - \frac{\theta}{\theta_r})ff'' + \frac{1}{\theta_r - \theta}f''\theta' + \beta(1 - \frac{\theta}{\theta_r})(1 - f'^2) - \lambda(2 - 2f' - \eta f'') = 0, \tag{2.73}$$

$$\theta'' + \frac{\gamma}{1 + \gamma\theta}\theta'^2 + \frac{\mathrm{Pr}_\infty}{1 + \gamma\theta}f\theta' + \frac{\mathrm{Pr}_\infty}{1 + \gamma\theta}\lambda\eta\theta' = 0, \tag{2.74}$$

with the transformed boundary conditions:

$$f(0) = 0,\ f'(0) = \frac{\varepsilon}{\sqrt{(2 - \beta)}}f''(0),\ \theta(0) = 1,\ \phi(0) = 1, \tag{2.75a}$$

$$f'(\infty) = 1,\quad \theta(\infty) = 0,\quad \phi(\infty) = 0, \tag{2.75b}$$

where $\mathrm{Pr}_\infty = \frac{\mu_\infty c_p}{\kappa_\infty}$ is the Prandtl number, $Sc = \frac{\upsilon_\infty}{D}$ is the Schmidt number, $\theta_r = -\frac{1}{\tau(T_w - T_\infty)}$ is the variable viscosity parameter, $\varepsilon = \frac{2-\sigma}{\sigma} Kn_{x,\tau}\, \mathrm{Re}_x^{1/2}$ is slip parameter and β, λ, N_t and N_c are defined earlier in case I.

2.4.4.1 Variable Prandtl number

The definition of Prandtl number shows that it is a function of viscosity, thermal conductivity and specific heat. Because both viscosity and thermal conductivity vary across the boundary layer, the Prandtl number also varies. The assumption of constant Prandtl number inside the boundary layer when the viscosity and thermal conductivity are temperature dependent, leads to unrealistic results. Therefore, the Prandtl number related to the variable viscosity and variable thermal conductivity is defined as:

$$\mathrm{Pr}_v = \frac{\mu c_p}{\kappa_f} = \frac{\mu_\infty \left(\frac{\theta_r}{(\theta_r - \theta)}\right) c_p}{\kappa_\infty (1+\gamma\theta)} = \frac{\mathrm{Pr}_\infty}{\left(1 - \frac{\theta}{\theta_r}\right)(1+\gamma\theta)} \,. \tag{2.76}$$

At the surface ($\eta = 0$) of the wedge, this can be written as

$$\mathrm{Pr}_w = \frac{\mathrm{Pr}_\infty}{\left(1 - \frac{1}{\theta_r}\right)(1+\gamma)} .$$

From equation (2.76), it can be seen that for $\theta_r \to \infty$ and $\gamma = 0$, the variable Prandtl number Pr_v is equal to the ambient Prandtl number Pr_∞. In light of the above discussion and using equation (2.76), the non-dimensional temperature equation (2.74) can be expressed as:

$$\theta'' + \frac{\gamma}{1+\gamma\theta}\theta'^2 + \left(1 - \frac{\theta}{\theta_r}\right)\mathrm{Pr}_v\, f\theta' + \left(1 - \frac{\theta}{\theta_r}\right)\mathrm{Pr}_v\, \lambda\eta\theta' = 0 \,. \tag{2.77}$$

Equation (2.77) is the corrected non- dimensional form of the energy equation in which Prandtl number is treated as variable.

2.5 Method of numerical solutions

In all cases of this thesis, the author has applied sixth order Runge-Kutta integration scheme together with Nachtsheim-Swigert (1965) shooting iteration technique to get the numerical solution for the velocity, temperature and concentration within boundary-layer and the skin friction coefficient, heat and mass transfer rate along the surface of the wedge, A complete discussion on the development of vector form of Nachtsheim-Swigert shooting iteration technique for case I of this thesis is given below.

2.5.1 Numerical experiment

The set of non-linear ordinary differential equations (2.26)-(2.28) together with the boundary conditions (2.24) have been solved numerically by applying Nachtsheim-Swigert (1965) iteration technique (for detailed discussion see Appendix). In equation (2.24) there are three asymptotic boundary conditions and hence three unknown surface conditions $f''(0)$, $\theta'(0)$ and $\phi'(0)$.

Within the context of the initial-value method and Nachtsheim-Swigert iteration technique the outer boundary conditions may be functionally represented as

$$\Phi_j(\eta_{\max}) = \Phi_j\left(f''(0), \theta'(0), \phi'(0)\right) = \delta_j,\ j = 1, 2\cdots 6, \tag{2.78}$$

where $\Phi_1 = f'$, $\Phi_2 = \theta$, $\Phi_3 = \phi$, $\Phi_4 = f''$, $\Phi_5 = \theta'$, $\Phi_6 = \phi'$. The last three of these represent asymptotic convergence criteria. Choosing $f''(0) = g_1, \theta'(0) = g_2$ and $\phi'(0) = g_3$ and expanding in a first-order Taylor's series after using equations (2.78) yield

$$\Phi_j(\eta_{\max}) = \Phi_{j,c}(\eta_{\max}) + \sum_{i=1}^{3} \frac{\partial \Phi_j}{\partial g_i} \Delta g_i = \delta_j, \quad j = 1, 2\cdots 6 \tag{2.79}$$

where subscript '*c*' indicates the value of the function at $\eta_{\max}$ determined from the trial integration. Solution of these equations in a least-square sense require determining the minimum value of

$$E = \sum_{j=1}^{6} \delta_j^2 \tag{2.80}$$

with respect to g_i ($i = 1, 2, 3$).

Now differentiating *E* with respect to g_i we obtain

$$\sum_{j=1}^{6} \delta_j \frac{\partial \delta_j}{\partial g_i} = 0 . \tag{2.81}$$

Substituting equations (2.79) into (2.81) after some algebra we obtain

$$\sum_{k=1}^{3} a_{ik} \Delta g_k = b_i , \; i = 1, 2, 3. \tag{2.82}$$

where $a_{ik} = \sum_{j=1}^{6} \frac{\partial \Phi_j}{\partial g_i} . \frac{\partial \Phi_j}{\partial g_k}, \;\; b_i = -\sum_{j=1}^{6} \Phi_{j,c} \frac{\partial \Phi_j}{\partial g_i}; \quad i, k = 1, 2, 3.$ (2.83)

Now solving the system of linear equations (2.82) using Cramer's rule we obtain the missing (unspecified) values of g_i as

$$g_i \approx g_i + \Delta g_i . \tag{2.84}$$

Thus adopting this numerical technique, a computer program was set up for the solutions of the governing non-linear partial differential equations of our problem where the integration technique was adopted as a sixth-order Runge-Kutta method of integration. A step size of $\Delta\eta = 0.01$ was selected to be satisfactory for a convergence criterion of 10^{-6} in all cases. The value of η_∞ was found to each iteration loop by the statement $\eta_\infty = \eta_\infty + \Delta\eta$. The maximum value of η_∞ for each group of parameters β, λ, κ, *Pr*, *Sc* and N_t is determined when the value of the unknown boundary conditions at $\eta = 0$ does not change in the successful loop with an error less than 10^{-6}.

Chapter 3

Local Similarity Solutions for Unsteady Two-Dimensional Forced Convective Heat and Mass Transfer Flow along a Wedge with Thermophoresis

3.1 Introduction

Similar solutions to a boundary layer flow are important with respect to the mathematical character of the solution. The present work is to investigate the effects of thermophoresis on an unsteady laminar two-dimensional hydrodynamic forced convective heat and mass transfer flow of a viscous incompressible fluid along a heated impermeable wedge. Mathematical analysis of this problem is discussed in section 2.4.1 as case I of chapter 2. The equations (2.26), (2.27) and (2.28) are the dimensionless form of the momentum equation, energy equation and concentration equation. The final form of the momentum, energy and concentration equations are solved numerically by applying shooting method based on the boundary condition defined in equation (2.24).

3.2 Mathematical analysis

The numerical results obtained from the governing equations (2.26), (2.27) and (2.28) based on the boundary conditions in equation (2.24) are presented and some of the numerical results are tabulated in the following sub-sections. A comparison of the stream function, velocity and the local skin friction coefficient obtained in the present work and obtained by White (2006) is shown in section 3.2.1 and the graphical presentation of the numerical results for the dimensionless velocity, temperature and concentration within the boundary layer and the local skin friction coefficient, the local rate of heat and mass transfer, thermophoretic

velocity and thermophoretic particle deposition velocity along the surface with an elaborate discussion are presented in section 3.2.2.

In order to see the effects of step size ($\Delta\eta$) we ran the code for our model with three different step sizes as $\Delta\eta$ = 0.01, $\Delta\eta$ = 0.004, $\Delta\eta$ = 0.001 and in each case we found excellent agreement among them. Figure 3.1 depicts the dimensionless velocity, temperature and concentration profiles, respectively for different step sizes. These Figures show that step size $\Delta\eta$ = 0.01 is sufficient to getting a convergent solution.

3.2.1 Testing of the code

Since the experimental results are not available in literature so the present results have been compared with the previous studies, which are shown in Table 3.1. The comparison of the dimensionless stream function $f(0)$, velocity $f'(0)$ and the local skin friction coefficient $f''(0)$ obtained in the present work with $\beta = 0,\ \lambda = 0$ and obtained by White (2006) are made available in Table 3.1. Thus from Table-3.1, it is observed that the data produced by the present code and those of White (2006) are in excellent agreement, hence an encouragement for the use of the present numerical code.

3.2.2 Results and discussion

The numerical simulations are carried out for different values of the physical parameters such as wedge angle parameter β, unsteadiness parameter λ, Prandtl number *Pr*, thermophoresis parameter N_t, thermophoretic coefficient κ, Schmidt number *Sc* and concentration ratio N_c. The values of Prandtl number *Pr* are taken to be 0.71, 1.0, 4.34 and 7.0 which correspond physically to air, electrolyte solution and water at two different temperatures 40^0C and 20^0C, respectively. The values of Schmidt number *Sc* are taken for hydrogen $(Sc = 0.22)$, helium $(Sc = 0.30)$, water-vapor $(Sc = 0.60)$ and Carbon-Dioxide $(Sc = 0.94)$. The default values of the parameters are chosen as β = 1/6 (i. e. Ω = 30^0),

Pr = 0.71, Sc = 0.94, λ = 0.50, κ = 0.50, N_t = 2.0 and N_c = 0.50, unless otherwise specified.

The effect of changes in the wedge angle parameter β on the dimensionless velocity f' against η is displayed in Figure 3.2 (a) for the values 0, 1/6, 1/2, 1 and 1.6. The value of $\beta = 0$ corresponds to wedge angle of zero degree i. e. flat plate, $\beta = 1/2$ corresponds to the wedge angle of 90 degrees i. e. the vertical plate and $\beta = 1$ corresponds to the wedge angle of 180 degrees i. e. stagnation point flow. From this Figure it is clear that velocity of the fluid within the boundary layer increases with the increasing values of wedge angle parameter β. This is due to fact that fluid always flows along the direction of the negative pressure gradient, i.e. high pressure to low pressure. Negative pressure gradient means accelerates flow. So a positive value of β indicates a negative (or favorable) pressure gradient. For accelerated flows, i.e. positive values of β, velocity profiles squeeze closer and closer to the surface of the wedge. It is also mentionable here that separation is found to occur for very small non-negative values of β. This is due to the fact that for unsteadiness. Figures 3.2 (b)-(c) shows non-dimensional temperature and concentration profiles within the boundary layer for different values of the wedge angle parameter. From these Figures we see that both the temperature and concentration of the fluid within the boundary layer decrease with the increasing values of the wedge angle parameter β. This is due to accelerate flow.

The effects of the unsteadiness parameter λ on the dimensionless velocity profiles within the boundary layer are shown in Figure 3.3 (a) when wedge angle parameter β takes the value 1/6 (i. e. $\Omega = 30^0$). From this Figure we observe that for large values of the parameter λ that is for higher unsteadiness, separation occurs even in the case of accelerated flow or of adverse pressure gradient $(m > 0, \beta > 0)$. Furthermore, from Figure 3.3 (a) for sufficiently strong unsteadiness for $\lambda > \lambda_{\text{critical}}$ (not precisely determined) it is observed that back flow occurs close to the wall indicating that unsteadiness may gives rise to turbulence close to the wall. Velocity here is also found to decrease with the

increase of the parameter λ within some domain $\eta \le \eta_{critical}$ and then for $\eta > \eta_{critical}$ the tendency is reversed in the upper portion of the boundary layer. This is due to the fact that as λ influence the kinematic viscosity of the fluid decreases to its ambient value therefore back flow occurs very close to the surface of the body. But far away from the surface of the body $\eta > \eta_{critical}$ this situation breaks down and fluid viscosity becomes stronger and reaches to its ambient value as a consequence velocity profile increases. This is an interesting phenomenon of unsteadiness. The effects of the unsteadiness parameter on the non-dimensional temperature and concentration profiles are displayed in Figures 3.3 (b)-(c), respectively. From these Figures it is observed that both the temperature and concentration decrease with the increasing values of the unsteadiness parameter λ.

The influence of Prandtl number *Pr* on the temperature profiles within the boundary layer is depicted in Figure 3.4 (a). It is well known that Prandtl number is the ratio of viscous force and thermal force. So increasing values of *Pr* decrease thermal action of the fluid, for this reason it can be observed from Figure 3.4 (a) that the temperature of the fluid decreases with the increasing Prandtl number *Pr*. In order to examine the effect of thermophoresis on particle deposition onto a wedge surface, the concentration profiles are displayed in Figure 3.4 (b), for thermophoresis parameter N_t. From this Figure it is clear that the concentration of the fluid particles decreases for the increasing values of N_t. This is due to the fact that from definition of thermophoresis parameter increasing values of N_t reduces temperature at the surface of the wedge. For this reason, the particles tend to deposit on the surface from the fluid. The effect of the thermophoretic coefficient κ on the concentration profiles are shown in Figure 3.4 (c). This Figure shows that the concentration of the fluid particles within the boundary layer increases with the increasing values of thermophoretic coefficient; this is due to favorable temperature gradients.

Figure 3.5 (a) shows the effect of the Schmidt number *Sc* on the dimensionless concentration profiles. It can be noted that the Schmidt number embodies the ratio of the momentum to the mass diffusivity. Schmidt number therefore quantities the

relative effectiveness of the momentum and mass transport by diffusion in the hydrodynamic (velocity) and concentration (species) boundary layers. From this Figure it is seen that the concentration of the fluid particles within the boundary layer decreases with the increasing values of *Sc* and this is the analogous to the effect of increasing the Prandtl number on the thickness of the thermal boundary layer. From Figure 3.5 (b) it is observed that the concentration of the fluid particles within the boundary layer increases with the increasing values of N_c and this is due to the favorable concentration difference between the wedge surface and the free stream conditions.

The combined effects of wedge angle parameter β and unsteadiness parameter λ on the local skin-friction coefficient, local Nusselt number and the local Sherwood number are shown in Figures 3.6 (a)-(c), respectively. From these Figures, it is clear that the local skin-friction coefficient, the local Nusselt number and local Sherwood number increase with increasing values of wedge angle parameter β. It is also evident from these Figures that both the local Nusselt number and local Sherwood number increase whereas the local skin-friction coefficient decreases with increasing values of the unsteadiness parameter for all values of wedge angle parameter. These behaviors depict the nature of the profiles shown in Figures 3.2 (a)-(c) and Figures 3.3 (a)-(c).

The combined effects of β and λ, κ and λ, N_t and λ on thermophoretic velocity V_{Tw} are shown in Figures 3.7 (a)-(c), respectively. From definition of thermophoretic velocity, N_t is inversely proportional to thermophoretic velocity and κ is directly proportional to thermophoretic velocity. For this reason from these Figures it is seen that the thermophoretic velocity decreases with the increasing values of thermophoresis parameter N_t whereas thermophoretic velocity increases for the increasing values of κ and β. These Figures, also confirm that unsteadiness parameter enhance the thermophoretic velocity.

Finally, Table 3.2 and Table 3.3 show the variations of the thermophoretic particle deposition velocity ($V_d^* \, \mathrm{Re}^{-1/2}$) at the wedge surface for different values of thermophoretic coefficient κ, wedge angle parameter β and unsteadiness

parameter λ. These Tables show that the thermophoretic particle deposition velocity decreases with the increase of the thermophoretic coefficient κ while it increases with the increase of the unsteadiness parameter λ. From Table 3.3 it is also clear that as the wedge angle parameter increases the thermophoretic particle deposition velocity also increases for fixed values of the unsteadiness parameter. This is because for increasing non negative values of β the driving force of the fluid motion intensifies which then accelerates the fluid flow and carries more heat from the surface of the wedge to the fluid. So the temperature at the surface of the wedge decreases.

Table 3.1: Comparison of the present numerical results of stream function $f(\eta)$, velocity $f'(\eta)$ and local skin friction coefficient $f''(\eta)$ with White (2006) for different values of η when wedge angle parameter β = 0 and unsteadiness parameter $\lambda = 0$.

η	$f(\eta)$		$f'(\eta)$		$f''(\eta)$	
	Present work	White (2006)	Present work	White (2006)	Present work	White (2006)
0.0	0.00000000	0.00000	0.00000000	0.00000	0.47027089	0.46960
0.5	0.05872926	0.05864	0.23456114	0.23423	0.46568757	0.46503
1.0	0.23332581	0.23299	0.46127690	0.46063	0.43494906	0.43438
1.5	0.51575598	0.51503	0.66235843	0.66147	0.36218408	0.36180
2.0	0.88800281	0.88680	0.81770859	0.81669	0.25581418	0.25567
3.0	1.79780496	1.79557	0.97006212	0.96905	0.06763291	0.06771
4.0	2.78709815	2.78388	0.99872084	0.99777	0.00684790	0.00687
5.0	3.78738993	3.78323	1.00087632	0.99994	0.00025589	0.00026

Table 3.2: Variations of thermophoretic particle deposition velocity at the wedge surface for different values of κ while β = 1/6 (i. e. Ω = 30^0), Pr = 0.71, Sc = 0.94, λ = 0.50, N_t = 2.0 and N_c = 3.0.

κ	0.2	0.5	0.8	1.0	1.2
$V_d^* \, \mathrm{Re}^{-\frac{1}{2}}$	0.4650164	0.4060784	0.3495130	0.3134839	0.2780497

Table 3.3: Variations of thermophoretic particle deposition velocity at the wedge surface for different values of β and λ while Pr = 0.71, Sc = 0.94, κ = 0.50, N_t =2.0 and N_c = 3.0.

β	λ	$V_d^* \, \mathrm{Re}^{-\frac{1}{2}}$
0.5 (vertical plate)	0.0	0.275058
	0.5	0.354816
	1.0	0.415233
	1.2	0.428337
1.0 (stagnation point flow)	0.0	0.485798
	0.5	0.627626
	1.0	0.742530
	1.2	0.782386
1.6 (wedge flow)	0.0	0.796992
	0.5	1.021776
	1.0	1.210440
	1.2	1.277976

(a)

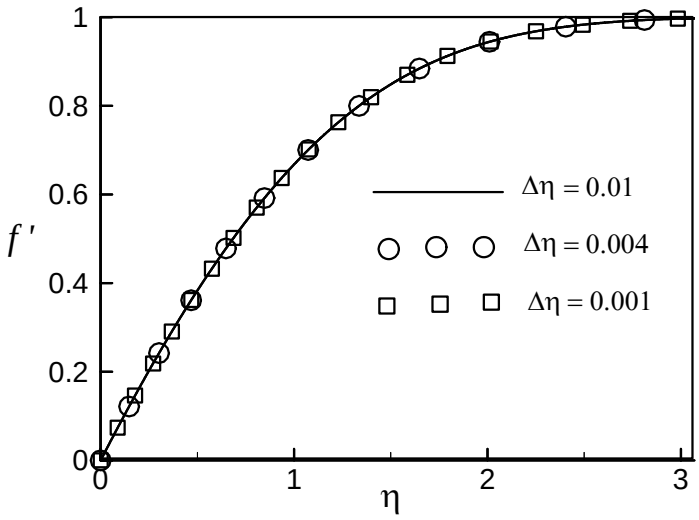

(b)

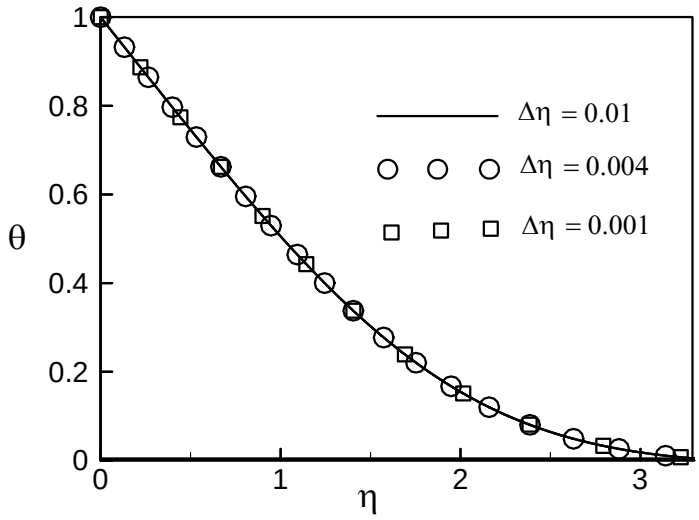

(c)

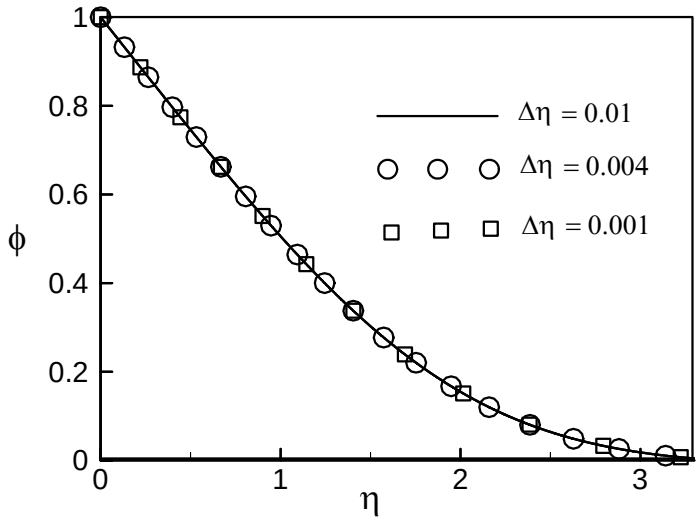

Figure 3.1: Dimensionless (a) velocity, (b) temperature and (c) concentration for different step sizes

(a)

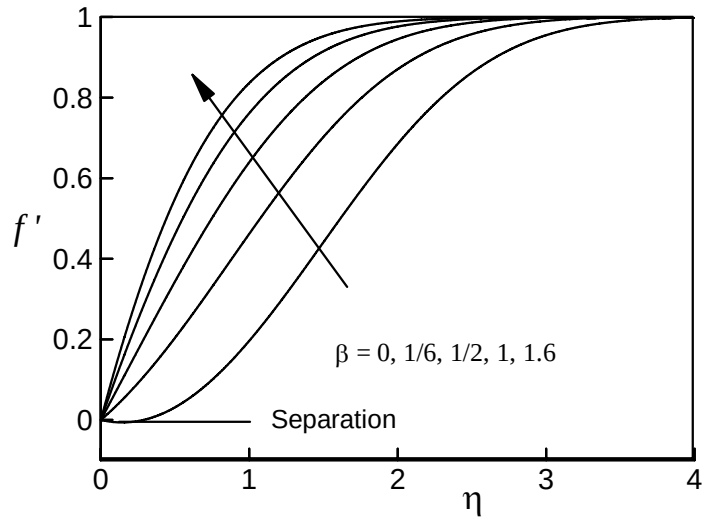

(b)

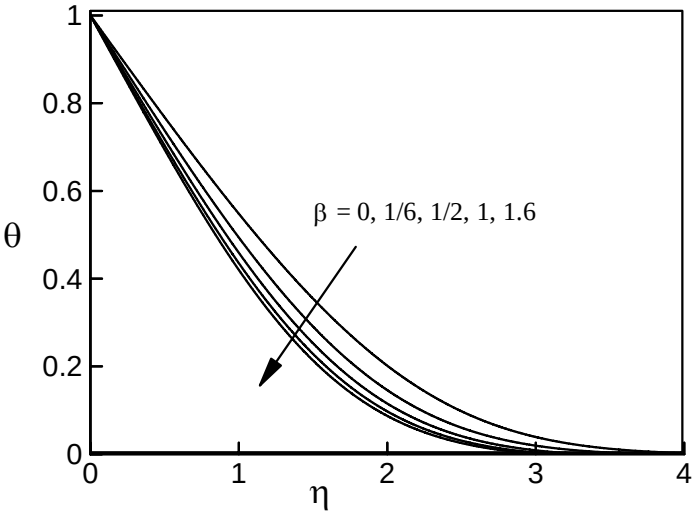

(c)

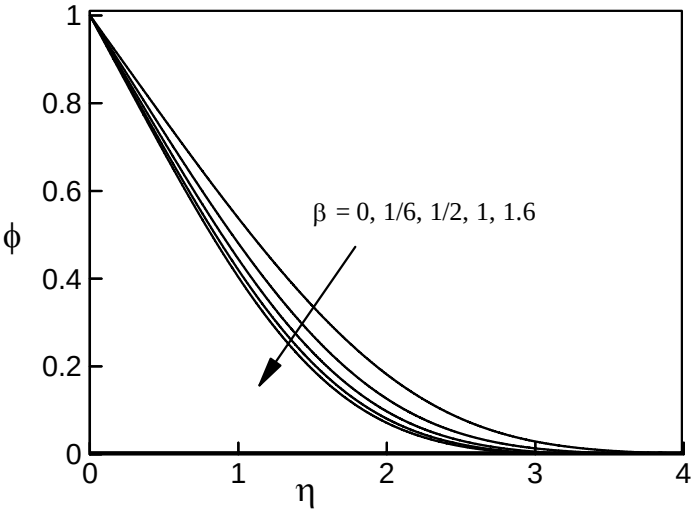

Figure 3.2: Dimensionless (a) velocity, (b) temperature and (c) concentration for different values of β

(a)

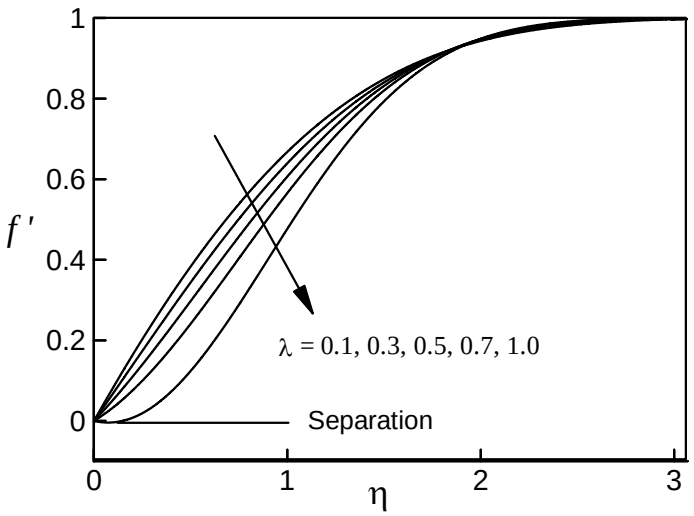

(b)

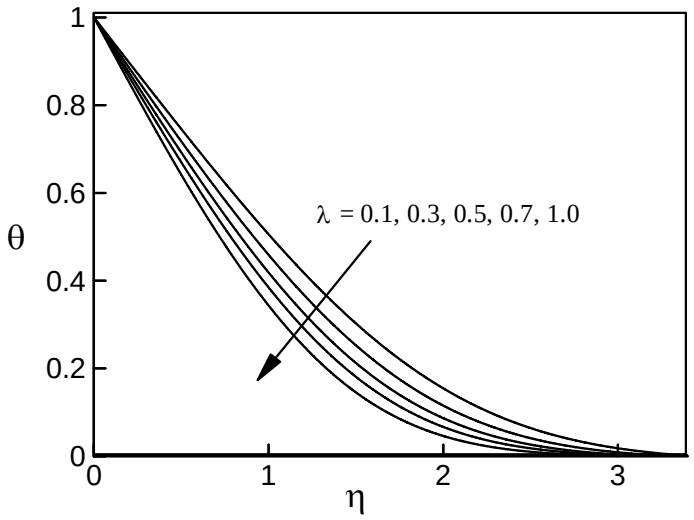

(c)

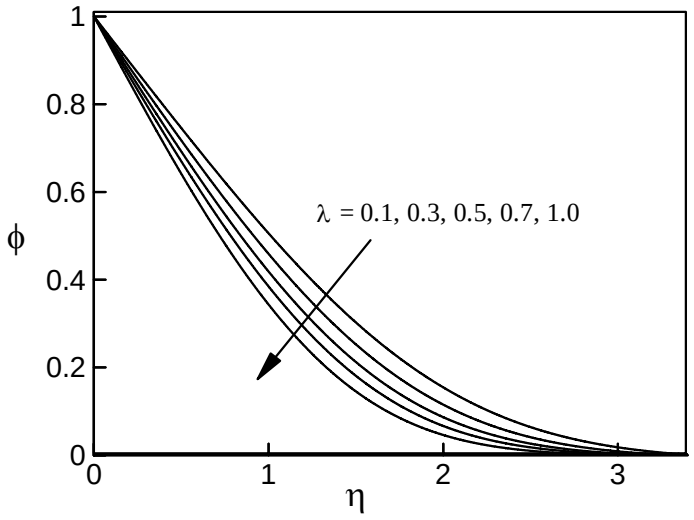

Figure 3.3: Dimensionless (a) velocity, (b) temperature and (c) concentration for different values of λ

(a)

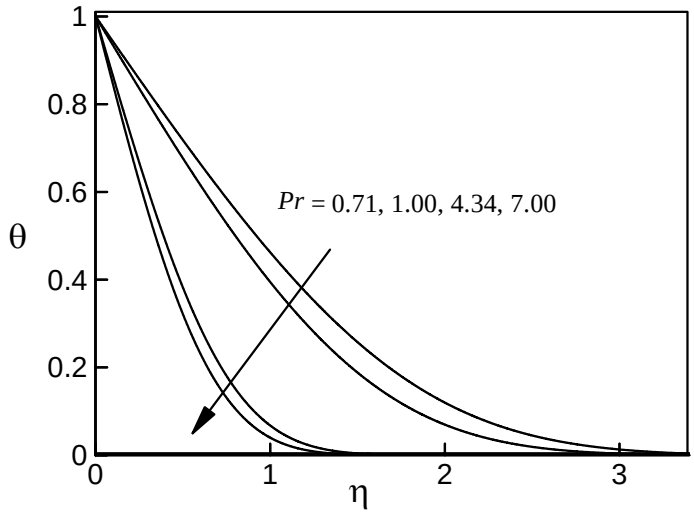

(b)

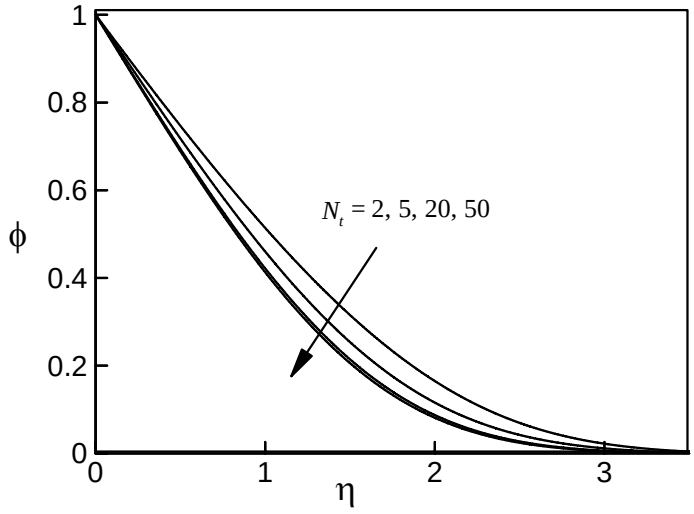

(c)

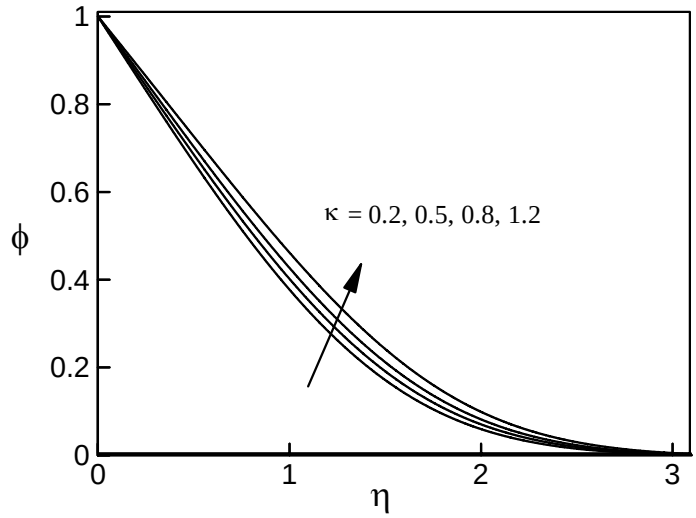

Figure 3.4: Dimensionless (a) temperature for different values of *Pr* and concentration for different values of (b) N_t ($\kappa = 0.50$) and (c) κ ($N_t = 2.00$)

(a)

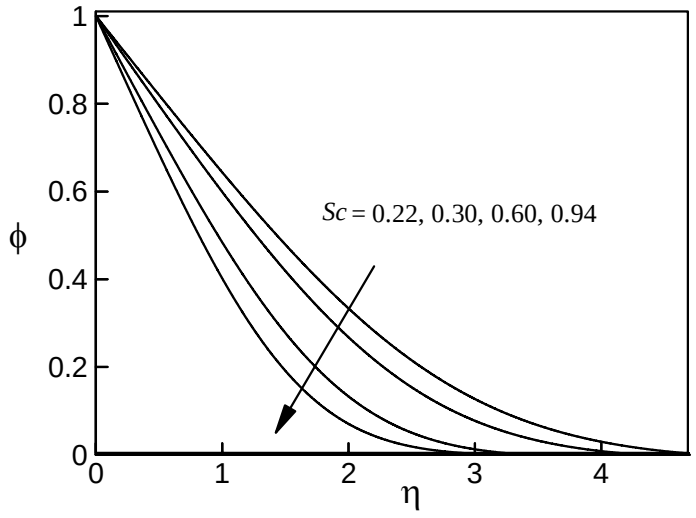

(b)

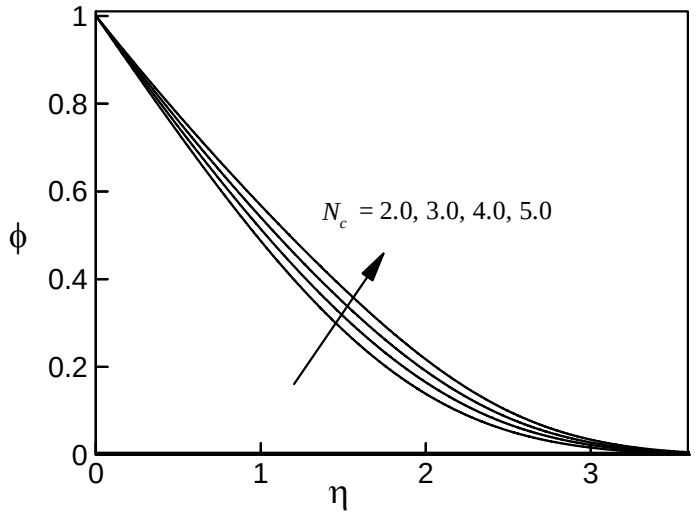

Figure 3.5: Dimensionless concentration for different values of (a) *Sc* (N_c = 3.00) and (b) *Nc* (*Sc* = 0.94)

(a)

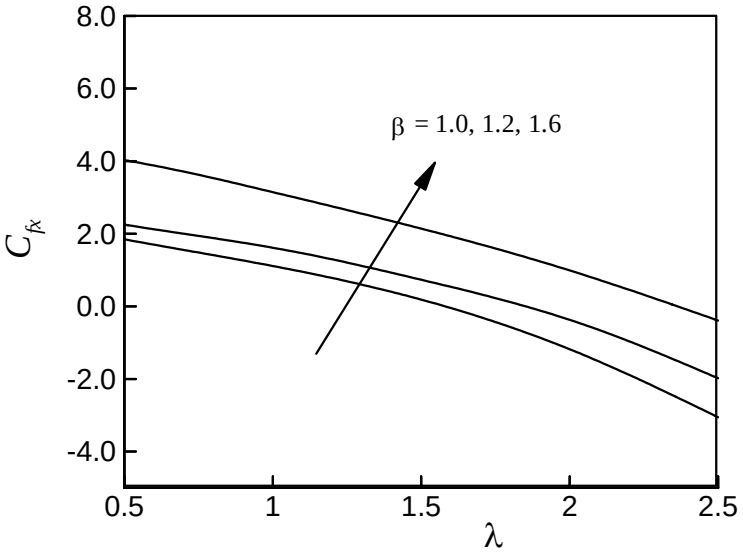

(b)

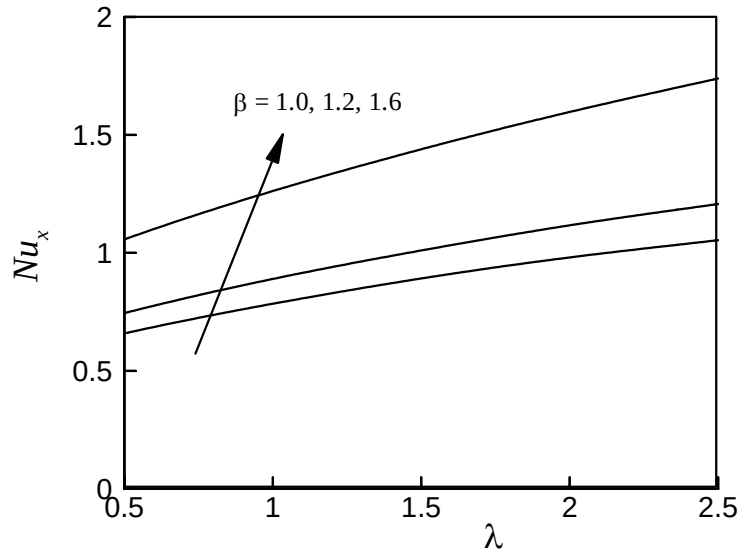

(c)

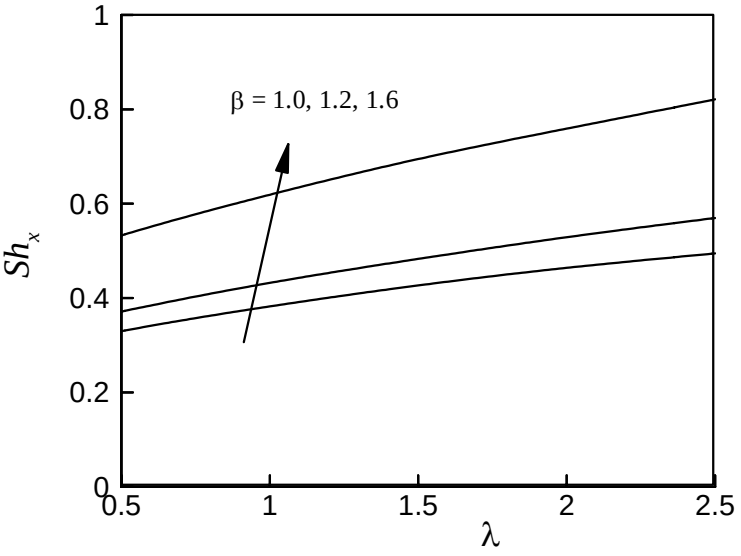

Figure 3.6: Effects of λ and β on (a) local skin-friction coefficient, (b) local Nusselt number and (c) local Sherwood number

(a)

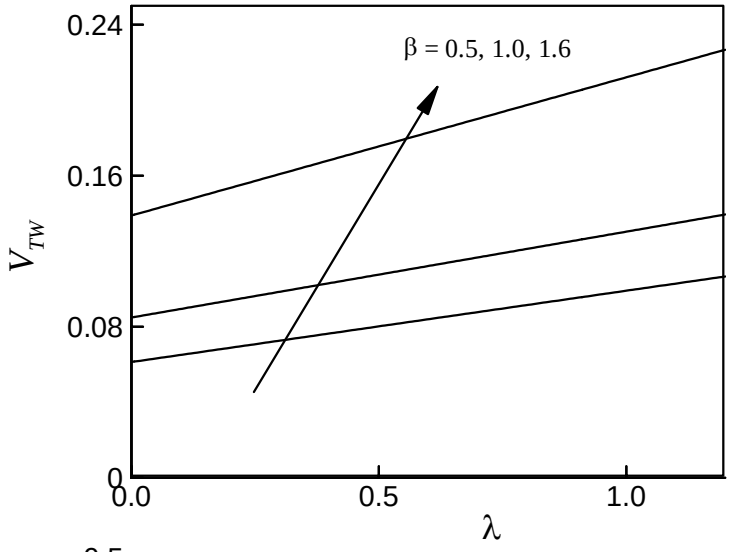

(b)

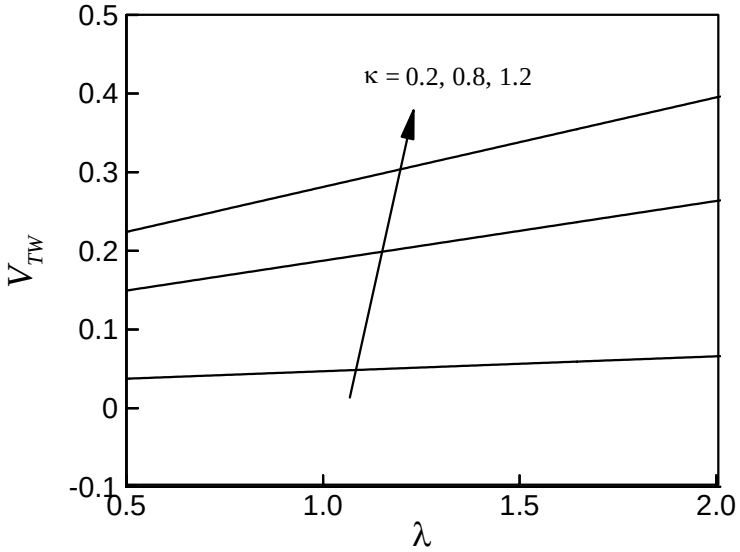

(c)

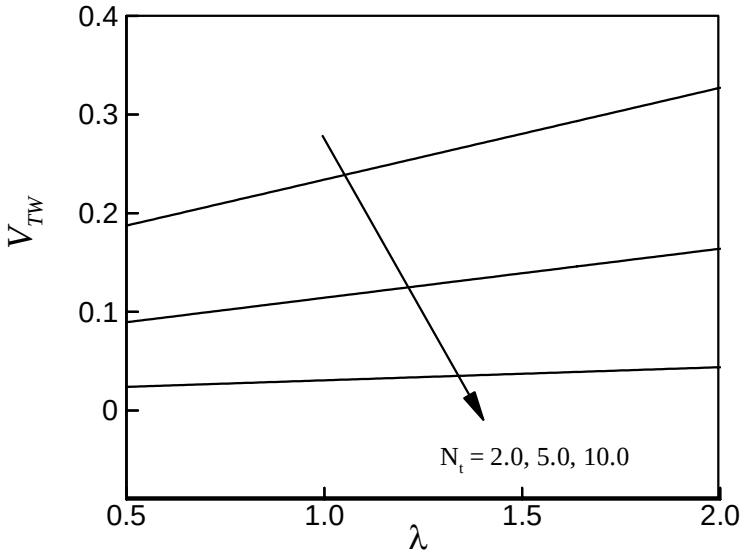

Figure 3.7: Effect of (a) λ and β, (b) λ and κ, (c) λ and N_t on thermophoretic velocity

3.3 Conclusions

In this model, we have discussed the effects of thermophoresis on an unsteady two-dimensional forced convective heat and mass transfer flow over a heated impermeable wedge. The governing non-linear partial differential equations are transformed into locally similar boundary layer equations which are solved numerically by applying shooting method. Comparisons with previously published work were performed and the results were found to be in excellent agreement. The numerical results have been presented in the form of graphs and tables. From the present numerical investigations the following major conclusions may be drawn:

i. Velocity of the fluid within the boundary layer increases with the increasing values of wedge angle parameter β. For accelerated flows, the velocity profiles squeeze closer and closer to the surface of the wedge. Separation may occur for non-negative small values of $\beta \geq 0$.

ii. Temperature and concentration of the fluid within the boundary layer decrease with the increasing values of the wedge angle parameter β.

iii. Concentration of the fluid particles decreases for the increasing values of thermophoresis parameter N_t. This is due to the fact that increasing values of thermophoresis parameter N_t, reduces temperature at the surface of the wedge. For this reason, the particles tend to deposit on the surface from the fluid.

iv. Concentration of the fluid particles within the boundary layer increases with the increasing values of N_c and this is due to the favorable concentration difference between the wedge surface and the free stream conditions.

v. Both the local Nusselt number and local Sherwood number increase whereas the local skin-friction coefficient decreases with increasing values of the unsteadiness parameter λ for all values of wedge angle parameter β.

vi. Thermophoretic velocity decreases for increasing thermophoresis parameter N_t whereas it increases with the increasing values of thermophoretic coefficient κ and wedge angle parameter β.

vii. Thermophoretic particle deposition velocity decreases with the increase of the thermophoretic coefficient κ while it increases with the increase of the unsteadiness parameter λ.

Chapter 4

Thermophoresis Particle Deposition on Unsteady Two-Dimensional Forced Convective Heat and Mass Transfer Flow along a Wedge with Temperature Dependent Viscosity and Prandtl Number

4.1 Introduction

In the classical treatment of thermal boundary layers, the kinematic viscosity is assumed to be constant; however, experimental studies indicate that this assumption is valid only if the temperature variation during the flow is not large. But when the variation of temperature within the boundary layer is large, then the variation of viscosity in thermal boundary layers is significant in many applications such as wire drawing, hot rolling, glass fiber production, paper production, gluing of labels on hot bodies, drawing of plastic films, etc. In view of this importance, Kafoussias and Williams (1995) studied the thermal diffusion and diffusion thermo effects on mixed free-forced convective heat and mass transfer flow with temperature-dependent viscosity. The effect of variable viscosity on hydrodynamic flow and heat transfer past a continuously moving porous boundary with radiation has been investigated by Seddeek (2000). Flow of viscous incompressible fluid with temperature dependent viscosity and thermal conductivity past a permeable wedge with uniform surface heat flux has been studied by Hossain et al. (2000). Ali (2006) analyzed the effect of variable viscosity on mixed convection heat transfer along a vertical moving surface. Alam et al. (2009) studied transient magnetohydrodynamic free convective heat and mass transfer flow with thermophoresis past a radiative inclined permeable plate

in the presence of variable chemical reaction and temperature-dependent viscosity.

The thickness of the thermal boundary layer relative to the velocity boundary layer depends on the Prandtl number which by its definition varies directly with the fluid viscosity and inversely with the thermal conductivity of the fluid. As the viscosity varies with temperature so does the Prandtl number. Despite this fact is all the afore-mentioned studies treated, the Prandtl number is considered as a constant. The use of a constant Prandtl number within the boundary layer when the fluid properties are temperature dependent, introduces errors in the computed results. Pantokratoras (2005) investigated some new results on forced and mixed convection boundary layer flow along a flat plate with variable viscosity and variable Prandtl number while Pantokratoras (2007) further studied non-Darcian forced convection heat transfer over a flat plate in a porous medium with variable viscosity and variable Prandtl number. Rahman and his co-workers (2010 and 2011) analyzed several thermal boundary-layer problems taking into account the variability of viscosity for both Newtonian and Non-Newtonian fluids in different geometry with various flow conditions. All of these studies confirmed that for the accurate prediction of the thermal characteristics of variable viscosity, the Prandtl number must be treated as a variable rather than a constant.

The objective of the present study is to investigate the effects of thermophoresis particle deposition on an unsteady two-dimensional forced convective heat and mass transfer flow of a viscous incompressible fluid along a heated wedge with variable viscosity and variable Prandtl number.

4.2 Governing equations

Mathematical formulation of the present investigation has been discussed elaborately in section 2.4.2 as case II of chapter 2. The dimensionless concentration equation and boundary conditions are same as equation (2.28) and (2.24), however there are some modifications in the momentum equation and energy equation due to temperature dependent viscosity and variable Prandtl number. The modified dimensionless momentum equation and energy equation

are given in equations (2.50) and (2.56). The resulting local similarity equations for unsteady flow have been solved numerically by applying Nachtsheim-Swigert shooting iteration technique along with sixth order Runge-Kutta integration scheme based on the boundary condition defined in equation (2.24). The shearing stress, the local rate of heat and mass transfer in terms of local skin friction coefficient, local Nusselt number and local Sherwood number, respectively and the velocity, temperature and concentration within the boundary-layer can be calculated by the relations (2.53), (2.40) and (2.41), respectively. A comparison will be provided in section 4.3 with a complete discussion.

4.3 Code verification

The comparison of the dimensionless stream function, velocity and the local skin friction coefficient obtained in the present work with $\beta = 0$, $\lambda = 0$, $\theta_r \to \infty$ and obtained by White (2006) has been shown in Table 4.1. From this Table it has been observed that there is an excellent agreement between these results.

4.4 Results and discussion

For the purpose of discussing the effects of various parameters namely viscosity variation parameter θ_r, wedge angle parameter β, unsteadiness parameter λ, Schmidt number *Sc*, thermophoretic coefficient κ, thermophoresis parameter N_t, and variable Prandtl number Pr_v on the flow behavior near the wedge surface, the numerical calculations are presented in the form of non-dimensional velocity, temperature and concentration profiles. The default values of the pertinent parameters considered in the numerical simulation are $\beta = 1/3$ (i. e. $\Omega = 60^0$), κ = 0.50, *Sc* = 0.94, *Nc* = 2.00, λ = 0.10, N_t = 2.00 and θ_r = 2.00, unless otherwise stated. When viscosity does not depend on the temperature, the values of the ambient Prandtl number, $\mathrm{Pr}_\infty = 0.71$, $\mathrm{Pr}_\infty = 2.97$ and $\mathrm{Pr}_\infty = 7.00$ correspond to air, methylchloride and water, respectively. As viscosity depends on the temperature, then these values at the surface of the wedge $(\eta = 0)$ and for

θ_r = 2.00 correspond to 1.42, 5.94 and 14, respectively. Therefore, in the simulation the value of the variable Prandtl number Pr_v is chosen as 1.42.

The effect of the variable viscosity parameter θ_r on the dimensionless velocity is displayed in Figures 4.1 (a) and 4.2 (a) for $\theta_r > 0$ and $\theta_r < 0$, respectively. From Figure 4.1(a) we see that the velocity within the boundary-layer increases with the increase of θ_r when it is positive. The opposite effect is observed for $\theta_r < 0$ on the velocity from Figure 4.2 (a). It is also mentionable from these both Figures that for very large θ_r change in $f'(\eta)$ are negligible. This is because for $|\theta_r| \to \infty$, the viscosity of the fluid (μ) equals the viscosity of the fluid (μ_∞) at the ambient temperatures and corresponds to the constant viscosity case. The effects of the variable viscosity parameter θ_r on the temperature fields within the boundary-layer are shown in Figures 4.1 (b) and 4.2 (b) for $\theta_r > 0$ and $\theta_r < 0$, respectively. From Figure 4.1 (b), it is observed that the temperature within the boundary layer decrease with the increase of θ_r and asymptote to zero as $\eta \to \infty$. This Figure also confirms that when θ_r is very large, variations in the temperature profiles become less pronounced, since equation (2.49) implies that $\mu \to \mu_\infty$ as $\theta_r \to \infty$. On the other hand, from Figure 4.2 (b), it is seen that for $\theta_r < 0$, the temperature within the boundary-layer increases with the increasing negative values of θ_r. The effects of θ_r on the concentration fields within the boundary-layer are shown in Figures 4.1 (c), and 4.2 (c) for $\theta_r > 0$ and $\theta_r < 0$, respectively. Figure 4.1 (c), shows that the concentration of the fluid particles within the boundary-layer decrease with the increase of θ_r. On the other hand, from Figure 4.2 (c), it is seen that the concentration of the fluid increases with the increasing negative values of θ_r.

The effect of the wedge angle parameter β on the dimensionless velocity is displayed in Figure 4.3 (a) for the values 0, 1/6, 1/3, 1/4 and 1/2. The value of $\beta = 0$ corresponds to wedge angle of zero degree i. e. flat plate whereas $\beta = 1/2$ corresponds to the wedge angle of 90 degrees i. e. the vertical plate. From this

Figure, it is clear that as the wedge angle parameter β increases the fluid velocity also increases. The wedge angle parameter is a measure of the pressure gradient and so positive values of β indicates a negative (or favorable) pressure gradient. For accelerated flows, i. e. positive values of β, velocity profiles squeeze closer and closer to the surface of the wedge, and overshoot or backflow phenomenon does not occur. From Figure 4.3 (b) and Figure 4.3 (c), we see that both the temperature and concentration of fluid decrease with the increasing non-negative values of wedge angle parameter β. It is also clear from these two Figures that the maximum temperature and concentration can be found for the flow over a wedge.

The effects of unsteadiness parameter λ on the dimensionless velocity, temperature and concentration profiles within the boundary-layer have been displayed in Figures 4.4 (a)-(c), respectively. Figure 4.4 (a), shows that the velocity reduces with the increasing values of unsteadiness parameter λ. This is due to the fact that λ influences the kinematic viscosity of the fluid. From Figure 4.4 (b) and Figure 4.4 (c), it can be observed that both the temperature and concentration of the fluid increase with the increasing values of the unsteadiness parameter λ.

The variation of dimensionless concentration profiles for various values of Schmidt number Sc, thermophoresis parameter N_t and thermophoretic coefficient κ are shown in Figures 4.5 (a)-(c), respectively. From these Figures, it is shown that concentration of the fluid particles within the boundary-layer increases with the increasing values of the thermophoretic coefficient κ whereas it decreases with the increasing values of both Sc and N_t.

The combined effects of variable viscosity parameter θ_r and unsteadiness parameter λ on the local skin-friction coefficient, local Nusselt number and the local Sherwood number are shown in Figures 4.6 (a)-(c), respectively. From these Figures it is seen that local skin-friction coefficient, the local Nusselt number and local Sherwood number increases with the increasing values of the variable viscosity parameter θ_r. It is also evident from these Figures that as the

unsteadiness parameter increases, the local skin-friction coefficient, local Nusselt number and the local Sherwood number also decrease for a fixed value of the variable viscosity parameter θ_r. These behaviors depict the nature of the profiles shown in Figures 4.1(a)-(c) and Figures 4.4 (a)-(c), respectively.

The combined effects of Pr_v and N_t, κ and N_t, θ_r and N_t on thermophoretic velocity V_{Tw} are shown in Figures 4.7 (a)-(c), respectively. From definition of thermophoretic velocity, N_t is inversely proportional to thermophoretic velocity and κ is proportional to thermophoretic velocity. For this reason from these Figures we see that the thermophoretic velocity decreases with the increasing values of thermophoresis parameter N_t, whereas thermophoretic velocity increases for the increasing values of Pr_v, κ and θ_r.

Figure 4.8 (a) and Figure 4.8 (b) depict the variable Prandtl number Pr_v within the boundary-layer for various values of the variable viscosity parameter $\theta_r > 0$ and $\theta_r < 0$, respectively at an ambient Prandtl number $\mathrm{Pr}_\infty = 0.71$. From both these Figures, it is seen that variable Prandtl number Pr_v asymptotically converges to the value of ambient Prandtl number Pr_∞ as $\eta \to \infty$. It is noticeable that at the surface of the wedge variable Prandtl number Pr_v approaches ambient Prandtl number Pr_∞ for large values of θ_r. From these two Figures, it is also seen that Pr_v decreases with the increase of θ_r when it is positive while an opposite effect is observed for $\theta_r < 0$. The variation of the variable Prandtl number within the boundary layer for different values of the wedge angle parameter is shown in Figure 4.8 (c). This Figure reveals that variable Prandtl number Pr_v decreases with the increase of the wedge angle parameter β.

The variations of the thermophoretic particle deposition velocity ($V_d^* \mathrm{Re}^{-1/2}$) at the wedge surface for different values of thermophoretic coefficient κ has been displayed in Table 4.2. This Table shows that the thermophoretic particle deposition velocity decreases with the increase of the thermophoretic

coefficient κ. Table 4.3 shows the variation of the Prandtl number at the surface of the wedge for several values of θ_r for a fixed value of the ambient Prandtl number $\Pr_\infty = 0.71$. From this Table, it is observed that for a positive value of θ_r, Prandtl number at the surface of the wedge $\Pr_w$ decreases as θ_r increases. On the other hand, the opposite effect is observed for $\theta_r < 0$.

Finally, the significance of the variable viscosity parameter θ_r within the boundary layer on the local Nusselt number for both constant Prandtl number and variable Prandtl number are shown in Table 4.4. This Table shows that the local rate of heat transfer in a fluid of constant Prandtl number is lower than in a fluid of variable Prandtl number when θ_r is negative while the opposite result is found for positive values of θ_r. The most interesting feature of this table is the variation among the results produced by considering Prandtl number as variable and constant within the boundary layer. From this Table, it also can be seen that the variation between the produced results differs by less than 1% when the values of θ_r (whether positive or negative) are very large. The variation between the produced results is more than 4% when $\theta_r = 2$, but these difference become 20.51% at $\theta_r = -0.5$.

Table 4.1: Comparison of the present numerical results of stream function $f(\eta)$, velocity $f'(\eta)$ and local skin friction coefficient $f''(\eta)$ with White (2006) for different values of η when wedge angle parameter $\beta = 0$, unsteadiness parameter $\lambda = 0$ and $\theta_r \to \infty$.

η	$f(\eta)$		$f'(\eta)$		$f''(\eta)$	
	Present work	White (2006)	Present work	White (2006)	Present work	White (2006)
0.0	0.00000000	0.00000	0.00000000	0.00000	0.47027089	0.46960
0.5	0.05872926	0.05864	0.23456114	0.23423	0.46568757	0.46503
1.0	0.23332581	0.23299	0.46127690	0.46063	0.43494906	0.43438
1.5	0.51575598	0.51503	0.66235843	0.66147	0.36218408	0.36180
2.0	0.88800281	0.88680	0.81770859	0.81669	0.25581418	0.25567
3.0	1.79780496	1.79557	0.97006212	0.96905	0.06763291	0.06771
4.0	2.78709815	2.78388	0.99872084	0.99777	0.00684790	0.00687
5.0	3.78738993	3.78323	1.00087632	0.99994	0.00025589	0.00026

Table 4.2: Variations of thermophoretic particle deposition velocity at the surface of the wedge for different values of thermophoretic coefficient κ.

κ	0.2	0.5	0.8	1.0	1.2
$V_d^* \, \mathrm{Re}^{-\frac{1}{2}}$	0.358873	0.317314	0.287061	0.253014	0.231675

Table 4.3: Values of Prandtl number at the wedge Pr_w versus variable viscosity parameter θ_r for ambient Prandtl number $\mathrm{Pr}_\infty = 0.71$ at $\eta = 0$.

θ_r	-1.0	-0.5	-0.1	2.0	3.0	5.0	10.0
Pr_w	0.355	0.236	0.065	1.42	1.06	0.887	0.788

Table 4.4: Values of local Nusselt number ($Nu_x \, \mathrm{Re}^{-\frac{1}{2}}$) for different values of variable viscosity parameter θ_r .

$Nu_x \, \mathrm{Re}^{-\frac{1}{2}}$			
θ_r	(i) For constant Prandtl number	(i) For variable Prandtl number	Variation in %
-100	0.3600719	0.3618878	< 1
-10	0.3646713	0.3680900	< 1
-5	0.3683388	0.3758403	2.036
-2	0.3784811	0.3980864	5.18
-1	0.3901856	0.4311427	10.49
-0.5	0.4059519	0.4891995	20.51
2	0.3324099	0.3181646	4.29
2.5	0.3395494	0.3254091	4.16
3	0.3437905	0.332639	3.24
4	0.3490905	0.3393183	2.79
5	0.3512969	0.3437517	2.14
10	0.3562204	0.3517553	1.25
100	0.3602290	0.3592557	< 1

(a)

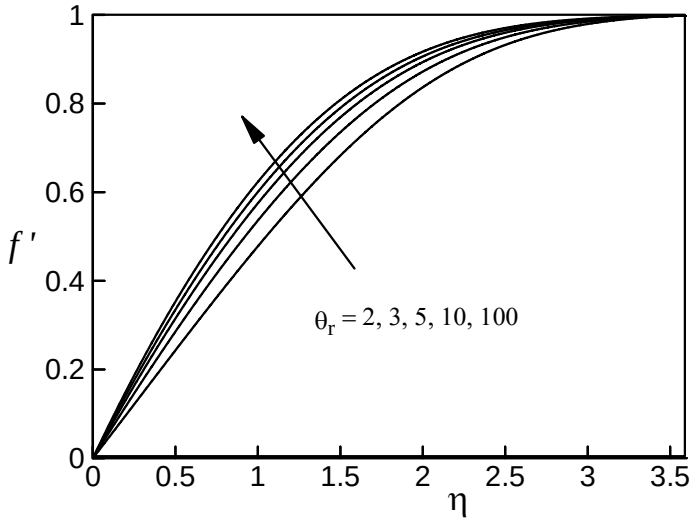

(b)

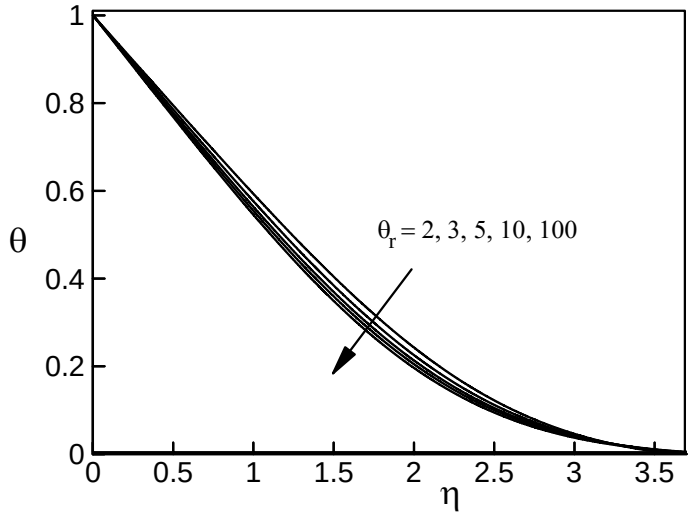

(c)

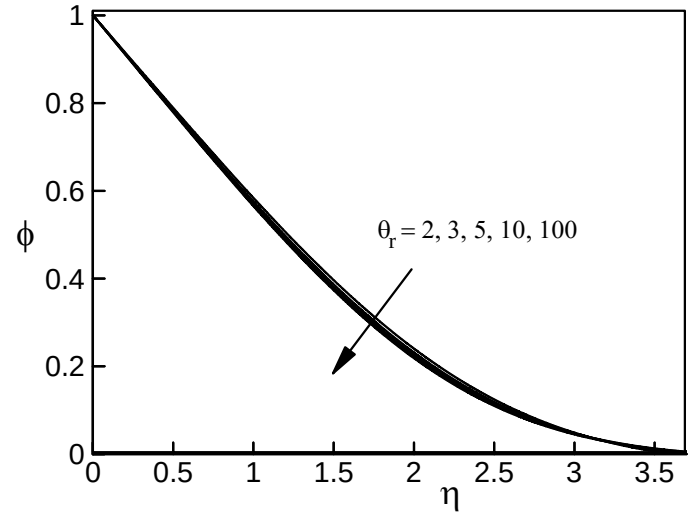

Figure 4.1: Variation of dimensionless (a) velocity, (b) temperature and (c) concentration for several values of $\theta_r > 0$

(a)

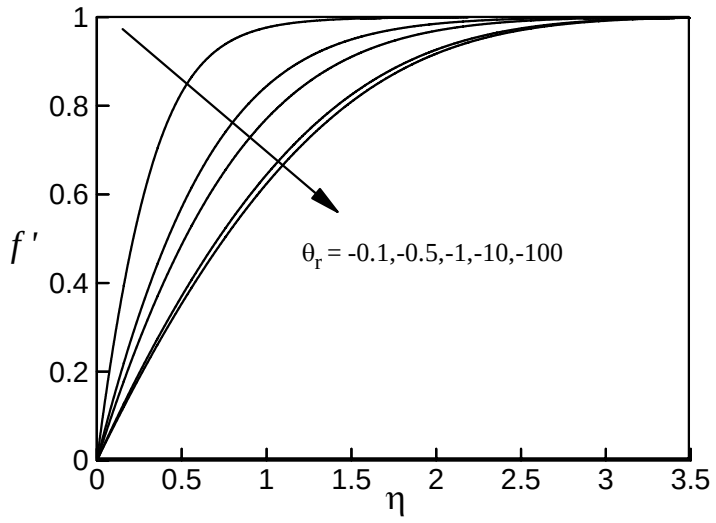

(b)

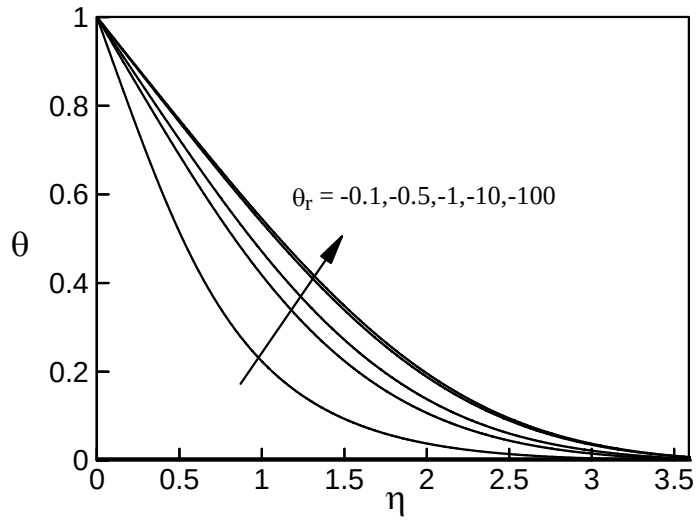

(c)

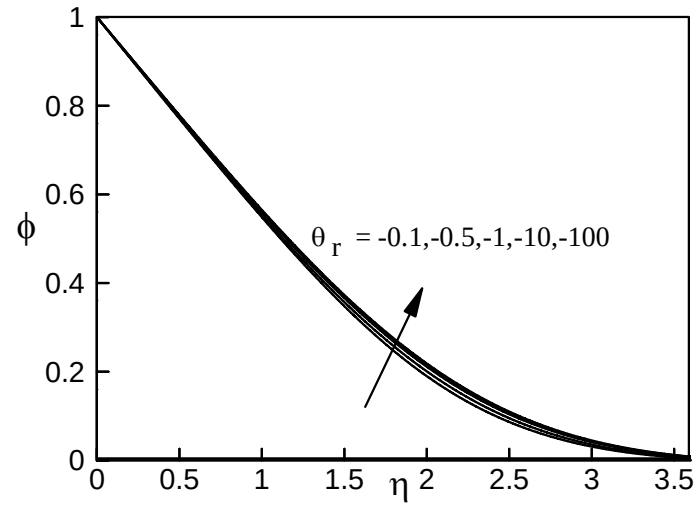

Figure 4.2: Variation of dimensionless (a) velocity, (b) temperature and (c) concentration for several values of $\theta_r < 0$

(a)

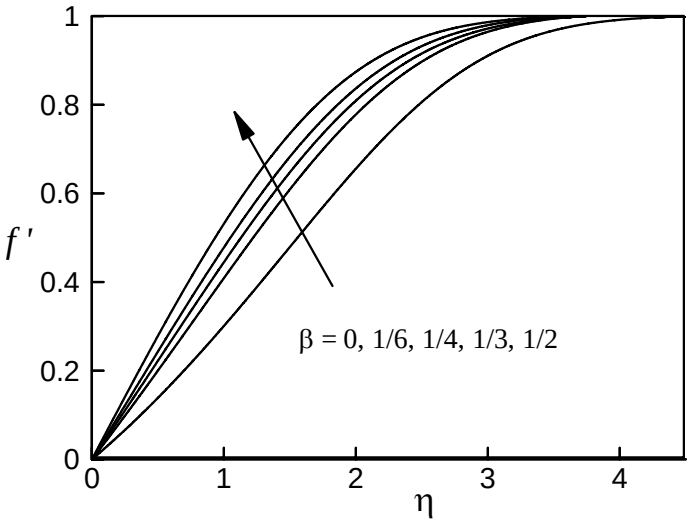

(b)

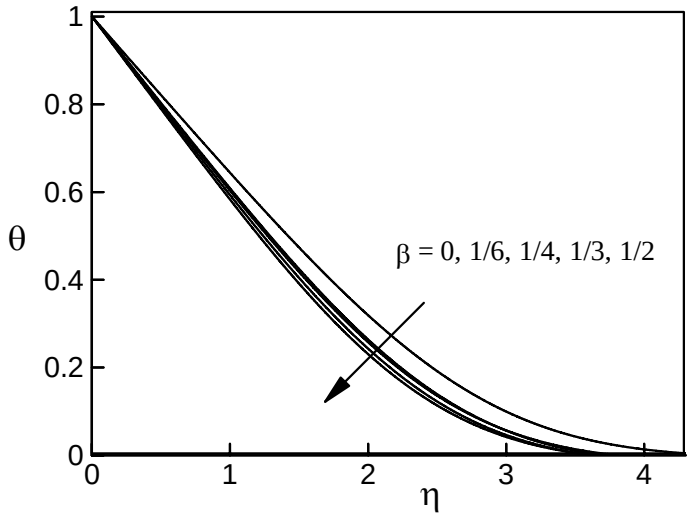

(c)

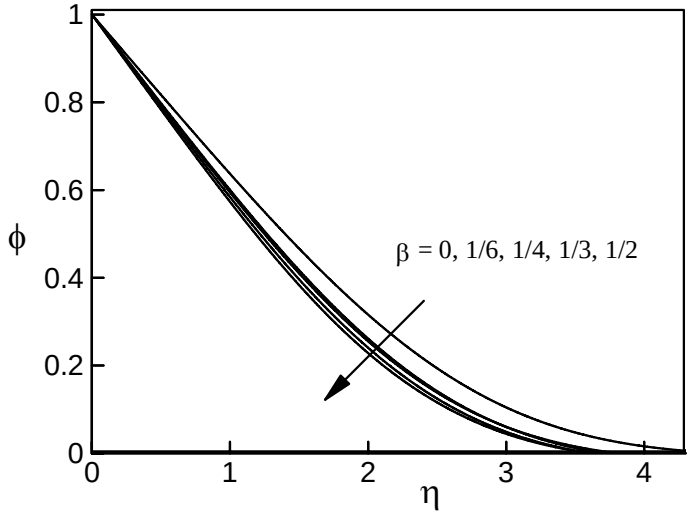

Figure 4.3: Variation of dimensionless (a) velocity, (b) temperature and (c) concentration for several values of β

(a)

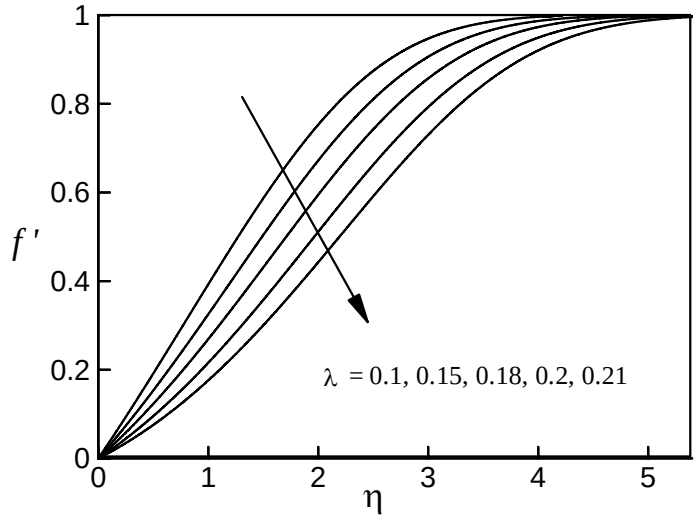

(b)

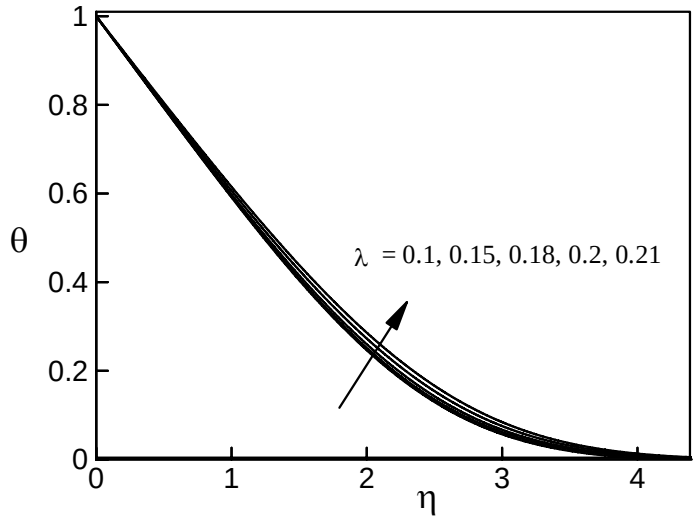

(c)

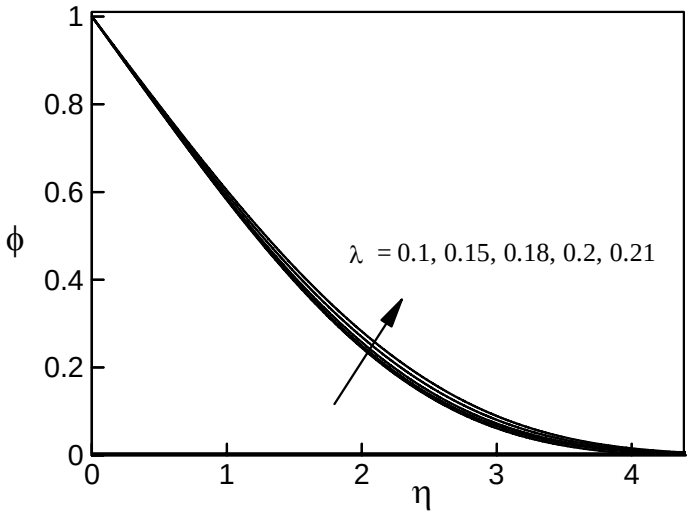

Figure 4.4: Variation of dimensionless (a) velocity, (b) temperature and (c) concentration for several values of λ

(a)

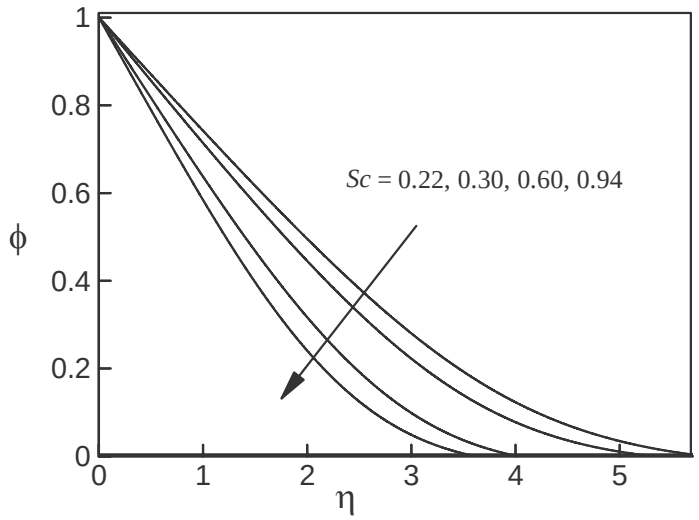

(b)

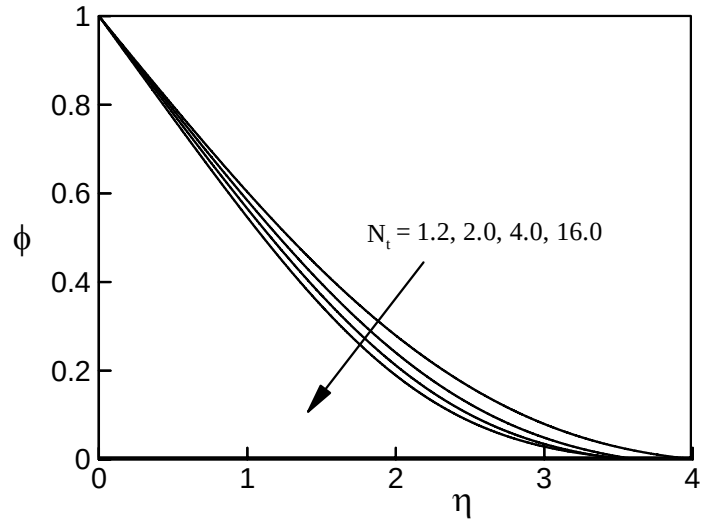

(c)

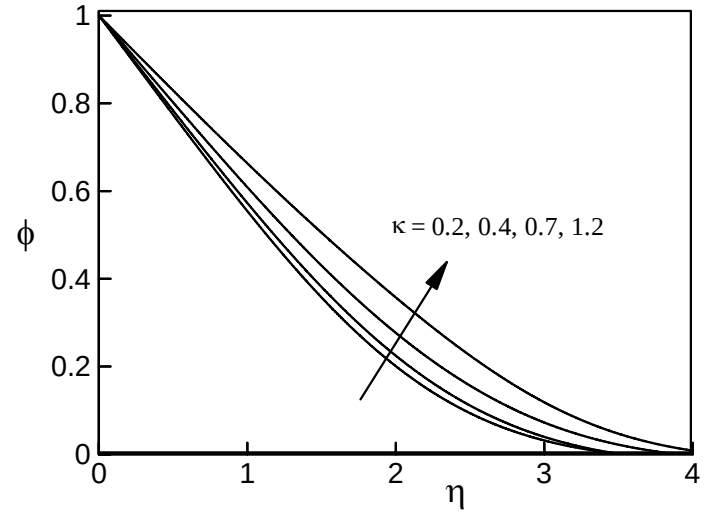

Figure 4.5: Variation of dimensionless concentration profiles for various values of (a) Sc, (b) N_t and (c) κ

(a)

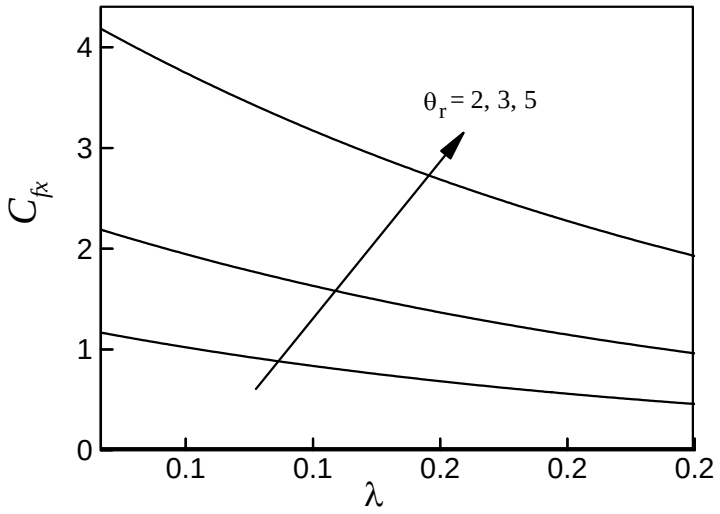

(b)

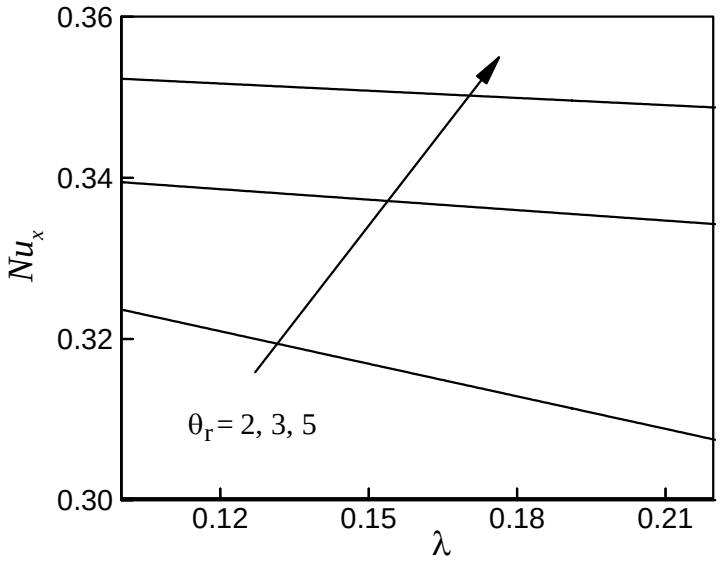

(c)

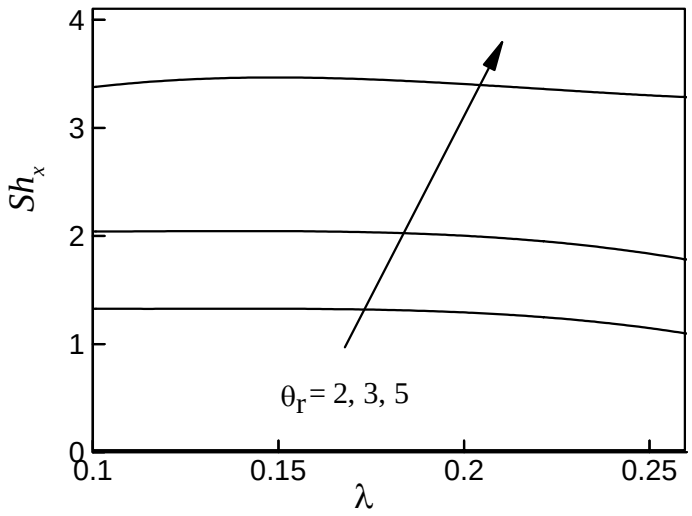

Figure 4.6: Effects of λ and θ_r on (a) local skin-friction coefficient, (b) local Nusselt number and (c) local Sherwood number

(a)

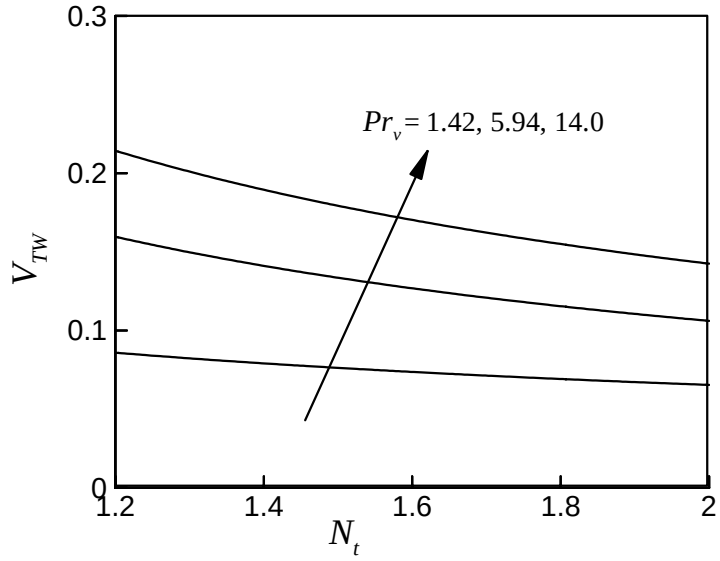

(b)

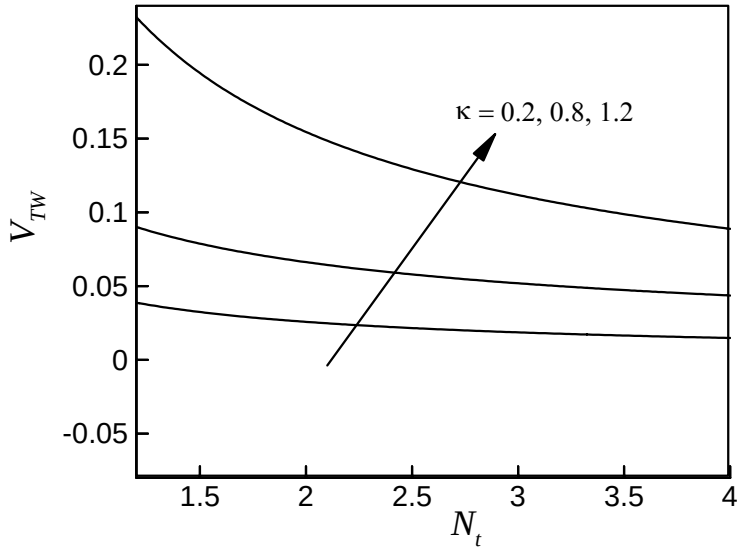

(c)

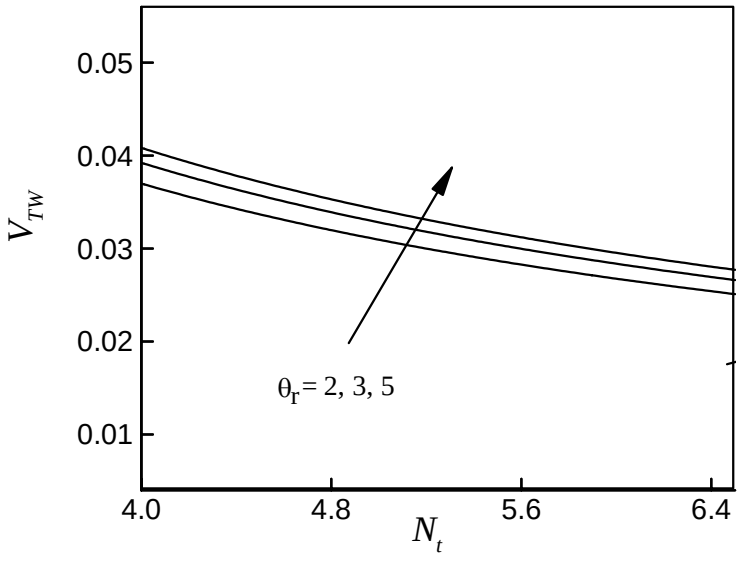

Figure 4.7: Effect of (a) Pr_v and N_t, (b) κ and N_t, (c) θ_r and N_t on thermophoretic velocity

(a)

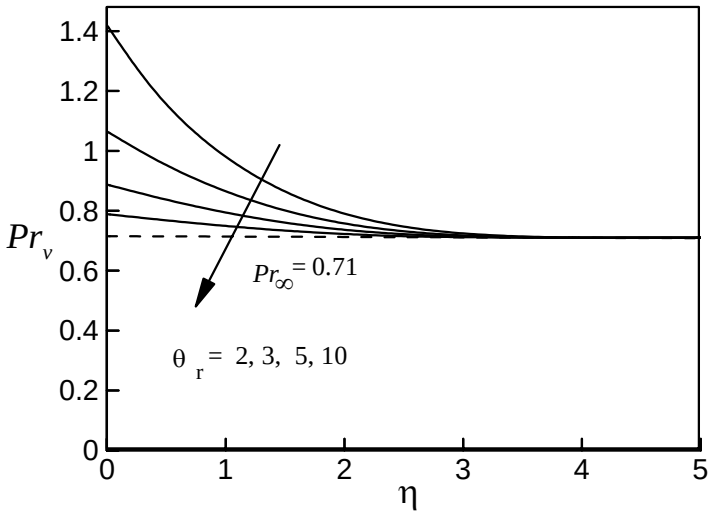

(b)

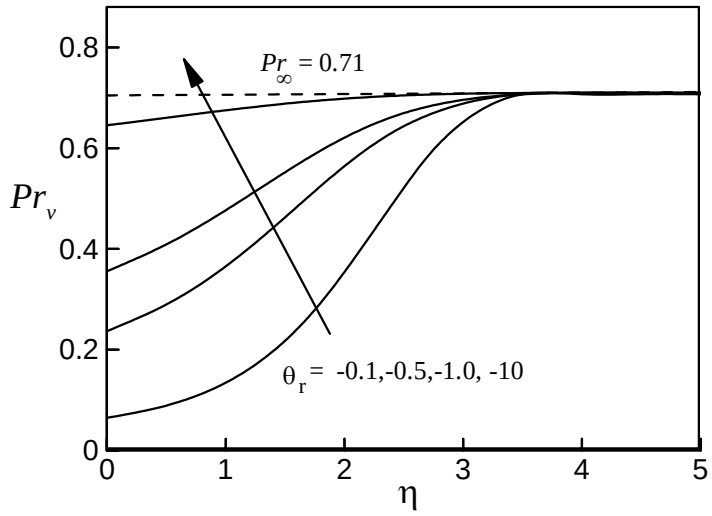

(c)

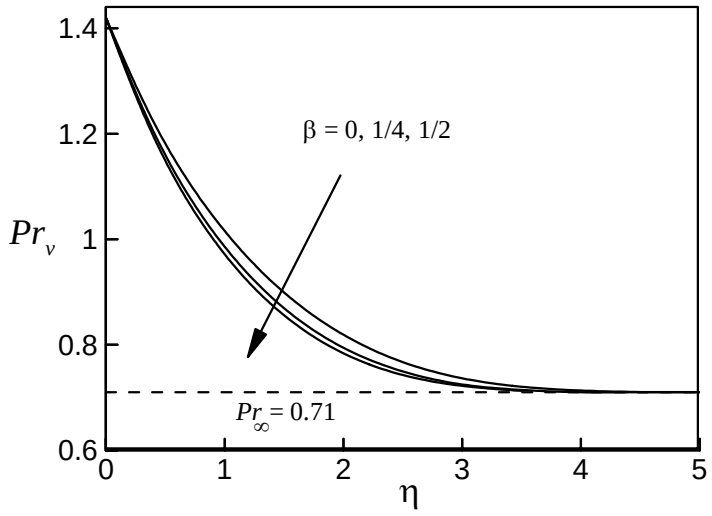

Figure 4.8: Variation of dimensionless variable Prandtl number Pr_v for different values of (a) $\theta_r > 0$, (b) $\theta_r < 0$ and (c) β

4.5 Conclusions

In this work, the effects of thermophoresis on an unsteady two-dimensional forced convective heat and mass transfer flow along a wedge with variation of fluid viscosity and fluid Prandtl number have been analyzed. Comparisons with previously published work were performed, and the results were found to be in excellent agreement. From the present numerical investigations, the following major conclusions can be drawn:

i. Velocity within the boundary-layer increases with the increasing values of variable viscosity parameter θ_r when it is positive. The opposite effect is observed for $\theta_r < 0$.

ii. Temperature and concentration of fluid within the boundary layer decrease with the increasing positive values of θ_r and asymptote to zero as $\eta \to \infty$. On the other hand, the opposite effect is observed for negative values of θ_r.

iii. Velocity boundary-layer thickness reduces with the increasing values of variable viscosity parameter θ_r when it is positive while it increases for increasing values of variable viscosity parameter θ_r when it is negative. Furthermore, as the wedge angle parameter β increases, the growth of the velocity boundary-layer thickness decreases.

iv. Local skin-friction coefficient, local Nusselt number and local Sherwood number decrease with the increasing values of unsteadiness parameter λ.

v. Thermophoretic velocity V_{Tw} increases with the increasing values of variable Prandtl number Pr_v.

vi. Thermophoretic particle deposition velocity ($V_d^* \, \mathrm{Re}^{-1/2}$) at the wedge surface decreases with the increase of the thermophoretic coefficient κ.

Chapter 5

Unsteady MHD Forced Convective Flow along a Porous Wedge with Temperature Dependent Thermal Conductivity and Thermophoresis

5.1 Introduction

The study of magnetohydrodynamic (in short MHD) flow of an electrically conducting fluid is of considerable interest in modern metallurgical and metal-working processes. Heat transfer flow is deemed as of great interest due to the effect of the magnetic field on the boundary-layer flow control and on the performance of many systems using electrically conducting fluids. Some of the engineering applications are in MHD generators, plasma studies, nuclear reactor, geothermal energy extractions, and purifications of metal from non-metal enclosures, polymer technology and metallurgy. Various industrial heat transfer processes involved the hydromagnetic flows and thermophoresis such as in MHD energy systems, many numerical studies on magnetohydrodynamic heat and mass transfer. Some examples of investigations dealing with hydromagnatic flows over a surface can be found throughout the work of Watanabe and Pop (1993), Chandran et al. (1996), Yih (1999) and Muhaimin et al. (2013). In all these studies, the thermo-physical properties of the fluid, especially the thermal conductivities were assumed to be constant. However, it is well known that the thermal conductivity of fluid may change with temperature [see Chiam (1996, 1998)]. Prasad and Vajravelu (2009) performed the effect of variable thermal conductivity in a non-isothermal sheet stretching through power law fluids. Abel et al. (2009) investigated the combined effects of thermal buoyancy and variable thermal conductivity on a magnetohydrodynamic flow and the associated heat transfer through a power-law fluid past a vertical stretching sheet in the presence

of a non-uniform heat source. Both studies revealed that the variable thermal studied the unsteady convective boundary-layer flow of a viscous fluid at a vertical surface with variable fluid properties.

The thickness of the thermal boundary layer relative to the velocity boundary layer depends upon the Prandtl number which by its definition varies inversely with the thermal conductivity of the fluid. As the thermal conductivity varies with temperature so does the Prandtl number. Despite this fact, all the afore-mentioned studies treated the Prandtl number as a constant. The use of a constant Prandtl number within the boundary layer when the thermal conductivities of fluid are temperature dependent, introduces errors in the computed results. Recently, Rahman and Eltayeb (2011) initiated the effect of variable thermal conductivity and variable Prandtl number on convective slip flow of rarefied fluids over a wedge with thermal jump. Both studies confirmed that in modeling, the thermal boundary-layer flow when the thermal conductivities of fluid are temperature dependent, the Prandtl number must be treated as a variable to obtain realistic results.

Therefore, the aim of the present study is to investigate the thermophoresis particle deposition on an unsteady two-dimensional forced convective heat and mass transfer flow along a permeable wedge taking into account the variable thermal conductivity. Thus, one of the main focuses behind this study is also to investigate how the Prandtl number varies within the boundary layer when the thermal conductivities are linearly dependent on temperature and in addition, there is a mass transfer (suction or injection) at the wedge surface. The governing non-linear partial differential equations have been reduced to locally similar ordinary differential equations, which are solved numerically using Nachtsheim-Swigert shooting iteration procedure. Graphs and table are presented to show the important features of the solution.

5.2. Prandtl boundary layer equations

Mathematical formulation of the present problem has been discussed in section 2.4.3 as case III of chapter 2. The dimensionless concentration equation is same as equation (2.28). On the other hand, there are some changes in the momentum equation, energy equation and boundary conditions due to magnatohydrodynamic, temperature dependent thermal conductivity, variable Prandtl number and suction/injection. The modified dimensionless momentum equation, energy equation and boundary conditions are given in equations (2.61), (2.62) and (2.63). Thus the modified equations governing present problem and the boundary conditions are:

$$f''' + ff'' + \beta(1 - f'^2) - \lambda(2 - 2f' - \eta f'') - \frac{2}{m+1} Ha^2 (f' - 1) = 0,$$

$$\theta'' + \frac{\gamma}{1+\gamma\theta}\theta'^2 + \frac{\mathrm{Pr}_\infty}{1+\gamma\theta} f\theta' + \frac{\mathrm{Pr}_\infty}{1+\gamma\theta}\lambda\eta\theta' = 0,$$

with the transformed boundary conditions:

$$f = f_w, f' = 0, \theta = 1, \phi = 1 \quad at \quad \eta = 0,$$

$$f' = 1, \quad \theta = 0, \quad \phi = 0 \quad as \quad \eta \to \infty,$$

where $\mathrm{Pr}_\infty = \frac{\mu c_p}{\kappa_\infty}$ is the ambient Prandtl number, $Ha = B_0\sqrt{\frac{\sigma x}{\rho U}}$ is the Hartmann number, $f_w = -v_w(x,t)\left(\frac{2}{m+1}\right)^{\frac{1}{2}} \frac{\delta^{\frac{m+1}{2}}}{\upsilon x^{\frac{m-1}{2}}}$ is the wall mass transfer coefficient which is positive ($f_w > 0$) for suction and negative ($f_w < 0$) for injection.

The rate of heat transfer in terms of the local Nusselt number within the boundary-layer has been modified as equation (2.64) due to temperature dependent thermal conductivity.

$$Nu_x\sqrt{2-\beta} = -\mathrm{Re}^{\frac{1}{2}}\left(\frac{1}{1+\gamma\theta}\right)\theta'(0).$$

5.3 Code verification

To check the validity of the present code, the values of stream function $f(0)$, velocity $f'(0)$ and local skin friction coefficient $f''(0)$ for the Falkner-Skan boundary-layer equation for the case $\gamma = 0$ (for constant fluid thermal conductivity), $\beta = 0$, *Ha = 0,* $f_w = 0$ (impermeable wedge) and $\lambda = 0$ (for steady flow) for different values of η are presented in Table 5.2. This Table shows that the present result is a close agreement with White (2006).

5.4 Findings and analysis

Numerical values of velocity, temperature, concentration and thermophoretic velocity are presented graphically for different values of the mass transfer coefficient f_w = - 0.5 to 1.0, Hartmann number *Ha* = 0.0 (non magnetic field) to 4, thermal conductivity variation parameter γ = 0.0 (constant thermal conductivity) to 7.0, Schmidt number *Sc* = 0.22 to 2, thermophoresis parameter N_t = 2 to 50, concentration ratio N_c = 2 to 9, wedge angle parameter β = 0 (flat plate) to 4, thermophoretic coefficient κ = 0.2 to 1.2. When thermal conductivity does not depend on the temperature, the values of the ambient Prandtl number, $\Pr_\infty$ = 0.71, 1, 2.97, 4.24, and 7.0 correspond to air, electrolyte solution such as salt water, methylchloride, sulfur dioxide and water at 20^0. When thermal conductivity depends on the temperature, these values at the surface of the wedge ($\eta = 0$) and for $\gamma = 0.5$ correspond to 0.47, 0.66, 1.98, 2.83, and 4.66, respectively. The values of Schmidt number *Sc* are taken for hydrogen (*Sc* = 0.22), helium (*Sc* = 0.30) and water-vapor (*Sc* = 0.60).

Figures 5.1 (a)-(c) depict the influence of the suction/injection parameter f_w on the dimensionless velocity, temperature and concentration profiles within the boundary layer, respectively. It is to be mentioned that $f_w > 0$ represents fluid suction, whereas $f_w < 0$ represents fluid injection. Figure 5.1 (a) shows that the velocity within the boundary layer enhances with the increase of the suction parameter f_w. It is also noticeable that the thickness of the velocity

boundary layer decreases with the increase of the suction parameter f_w. The physical explanation for such a behavior that removal of the decelerated fluid particles through the porous surface reduce the growth of the boundary layer. Variation of both the temperature and the concentration profiles against η for different values of the parameter $f_w = -0.5,\ 0,\ 0.5$ and 1.0 are shown in Figures 5.1 (b)-(c), respectively. It is found that the temperature and concentration of the fluid within the boundary layer decreases with the increase of the values of f_w for suction $f_w > 0$, whereas for injection $f_w < 0$ reverse trend is observed. Suction therefore acts as a powerful mechanism for cooling the flow and such features are important in high temperature energy systems such as magnetohydrodynamic power generators, nuclear energy processes etc. These Figures also show that velocity, thermal and concentration boundary layer thickness decrease with the increase of the suction velocity even in the presence of thermophoresis.

Figures 5.2 (a)-(c) show that dimensionless velocity, temperature and concentration profiles against η for various values of Hartman number Ha, respectively. Figure 5.2 (a) presents significant impact of the applied magnetic field on the flow field. The velocity increases hence thickness of the hydrodynamic boundary layer decreases with the increase of Hartman number *Ha*. This is due to the fact that the application of a magnetic field moving with the free stream has the tendency to induce a motive force, which increases the motion of the fluid. On the other hand the temperature and concentration of the fluid within the boundary layer decrease with the increase of Hartman number *Ha.* It can further be noted that the thickness of the thermal and concentration boundary layers decrease with the increase of the strength of the applied magnetic field. This work is consistent throughout the work of Ishak et al. (2008).

The effects of the unsteadiness parameter λ on the dimensionless velocity within the boundary layer are shown in Figure 5.3 (a). From this Figures it is observed that for large values of the parameter λ that is for higher unsteadiness, separation occurs even in the case of accelerated flow or of adverse pressure

gradient $(m > 0, \beta > 0)$. Velocity here is also found to decrease with the increase of the parameter λ within some domain $\eta \le \eta_{critical}$ and then for $\eta > \eta_{critical}$ the tendency is reversed in the upper portion of the boundary layer. Similar behavior has been observed by Sattar (2011). Figures 5.3 (b)-(c), depict the non-dimensional temperature and concentration profiles for different values of the unsteadiness parametersλ. From these figures, it is observed that both the temperature and concentration of the fluid within the boundary layer decrease with the increasing values of the unsteadiness parameter λ.

The effects of the thermal conductivity variation parameter γ on the non-dimensional temperature profiles have been displayed in Figure 5.4 (a). From this Figure, we observe that the non-dimensional temperature of the fluid increases with the increase of the thermal conductivity variation parameter as expected. The value of $\gamma = 0$ corresponds to the constant conductivity of the fluid. Thus for the constant conductivity of the fluid the surface temperature is found to be low compared that of the variable conductivity. This can be explained as; when γ increases i. e. thermal conductivity of the fluid increases, the value of the Prandtl number decreases (see equation (2.65) which then increases the temperature of the fluid. That is temperature of the fluid increases, if the Prandtl number decreases. On the other hand, from Figure 5.4 (b), we see that the dimensionless concentration of the fluid particles within the boundary layer decreases with the increase of the thermal conductivity variation parameter. Figure 5.4 (c) presents variation of variable Prandtl number Pr_v within the boundary layer for different values of γ for fixed values of ambient Prandtl number $\mathrm{Pr}_\infty = 0.71$. From this Figure it is found that variable Prandtl number Pr_v within the boundary layer decreases with the increase of the thermal conductivity variation parameter γ. For constant thermal conductivity it is found that variable Prandtl number at the surface of the wedge is lower than the ambient Prandtl number $\mathrm{Pr}_\infty = 0.71$. The results also show that the values of variable Prandtl number Pr_v within the boundary layer asymptotically converge to the value of Pr_∞ far away from the surface of the wedge (i.e. $\eta \to \infty$). This figure clearly establishes that the Prandtl

number varies significantly within the boundary layer when the fluid thermal conductivity varies with temperature.

The variation of dimensionless concentration inside the boundary layer for various values of Schmidt number *Sc*, thermophoresis parameter N_t and concentration ratio N_c are displayed in Figures 5.5 (a)-(c), respectively. From these Figures, It is observed that concentration of the fluid particles within the boundary layer increases with the increasing values of the concentration ratio whereas it decreases with the increasing values of both Sc and N_t. It has been detailed in chapter 3.

Figure 5.6 (a) presents dimensionless velocity profiles for different values of wedge angle parameter β due to the temperature dependent thermal conductivity. It is clearly shown that the velocity of the fluid increases whereas the temperature and concentration of the fluid are not significant with increase of the wedge angle parameter β. The results also show that the velocity profiles become steeper for larger values of the wedge angle parameter β. The wedge angle parameter is a measure of the pressure gradient and so positive values of β indicate a negative (or favorable) pressure g*r*adient. For accelerated flows, i. e. positive values of β, velocity profiles squeeze closer and closer to the surface of the wedge and overshoot or backflow phenomenon does not occur. The influence of variable Prandtl number Pr_v on the temperature within the boundary layer is depicted in Figure 5.6 (b). It is well known that Prandtl number is the ratio of viscous force and thermal force. So increasing values of variable Prandtl number Pr_v decreases thermal action of the fluid, for this reason it can be observed from Figure 5.6 (b) that the temperature of the fluid decreases with the increasing values of variable Prandtl number Pr_v. Figure 5.6 (c) shows that the concentration of the fluid particles increases with the increasing values of thermophoretic coefficient. This is because when the values of thermophoretic coefficient increases, the thermophoretic force increases and also mass transfer enhance as a result concentration of the fluid increases.

The combined effects of γ and N_t, κ and N_t on thermophoretic velocity ($V_{Tw}\,\mathrm{Re}^{-1/2}$) are shown in Figures 5.7 (a)–(b), respectively. From these Figures, it is seen that the thermophoretic velocity increases with the increasing values of κ while it decreases with the increasing values of the thermal conductivity variation parameter γ and the thermophoresis parameter N_t. This behavior is expected since thermophoretic velocity is proportional to κ and inversely proportional to N_t [see equation (2.42)].

Table 5.1 shows the variation of the Prandtl number at the surface of the wedge for several values of γ for a fixed value of the ambient Prandtl number Pr_∞ = 0.71. From this Table, it is observed that Prandtl number at the surface of the wedge Pr_w decreases as γ increases. As the value of thermal conductivity variation parameter γ is increased from 0.0 to 7.0 the Prandtl number decrease by 87.46%.

Table 5.3 presents the variations of the thermophoretic particle deposition velocity ($V_d^*\,\mathrm{Re}^{-1/2}$) at the wedge surface for various values of Schmidt number for both suction $f_w > 0$ as well as injection $f_w < 0$ cases. From this Table, It is seen that the thermophoretic particle deposition velocity decreases with the increase of the Schmidt number for both suction as well as injection. For experimental interest, the thermophoretic particle deposition velocity decreases by 50.95% and 64.93% with the increase in the Schmidt number from 0.22 to 0.94 for both suction as well as injection.

The significance of the thermal conductivity variation parameter γ on the local rate of heat transfer for both variable Prandtl number Pr_v and constant Prandtl number Pr_c is displayed in Table 5.4 for both suction $f_w > 0$ as well as injection $f_w < 0$ cases. From this Table, it is found that in both cases, the local rate of heat transfer $-\theta'(0)$ for the variable Prandtl number Pr_v case is higher than the constant Prandtl number Pr_c case, and the variation between them increases significantly with the increases of γ. Therefore, consideration of Prandtl number as constant

within the boundary layer for variable thermal conductivity is unrealistic. It is also found that the heat transfer rate decreases by 45.18% when the thermal conductivity variation parameter γ varies from 0 to 9 for variable Prandtl number, whereas the corresponding decreases by 76.56% for constant Prandtl number in case of suction.

Table 5.1: Values of Pr_w versus thermal conductivity variation parameter γ for ambient Prandtl number Pr_∞ = 0.71 at η = 0.

γ	0.0	0.50	1.0	3.0	5.0	7.0
Pr_w	0.71	0.473	0.355	0.177	0.118	0.089

Table 5.2: Comparison of the present numerical results of stream function, velocity and local skin friction coefficient with White (2006) for case of $\beta = 0, \gamma = 0$, $Ha = 0$, $f_w = 0$ and $\lambda = 0$.

η	$f(\eta)$		$f'(\eta)$		$f''(\eta)$	
	Present work	White (2006)	Present work	White (2006)	Present work	White (2000)
0.0	0.00000000	0.00000	0.00000000	0.00000	0.47027089	0.46960
0.5	0.05872926	0.05864	0.23456114	0.23423	0.46568757	0.46503
1.0	0.23332581	0.23299	0.46127690	0.46063	0.43494906	0.43438
1.5	0.51575598	0.51503	0.66235843	0.66147	0.36218408	0.36180
2.0	0.88800281	0.88680	0.81770859	0.81669	0.25581418	0.25567
3.0	1.79780496	1.79557	0.97006212	0.96905	0.06763291	0.06771
4.0	2.78709815	2.78388	0.99872084	0.99777	0.00684790	0.00687
5.0	3.78738993	3.78323	1.00087632	0.99994	0.00025589	0.00026

Table 5.3: Variations of thermophoretic particle deposition velocity at the wedge surface for several values of Schmidt number *Sc*.

f_w	*Sc*	$V_d^* \, \mathrm{Re}^{-1/2}$
0.5 (suction)	0.22	1.464883
	0.30	1.251766
	0.60	0.890707
	0.94	0.718497
- 0.5 (injection)	0.22	1.116588
	0.30	0.906355
	0.60	0.556096
	0.94	0.391592

Table 5.4: Numerical values of rate of heat transfer $-\theta'(0)$ for various values of thermal conductivity variation parameter γ.

f_w	$-\theta'(0)$			Variation
	γ	Pr_v	Pr_c	
0.5 (suction)	0.0	0.902102	0.902102	0.00%
	1.0	0.675392	0.551469	18.35%
	2.0	0.599989	0.423934	29.34%
	3.0	0.562266	0.355324	36.08%
	5.0	0.524614	0.280500	46.53%
	7.0	0.505784	0.238762	52.79%
	9.0	0.494490	0.211389	57.25%
-0.5 (injection)	0.0	0.426180	0.426180	0.00%
	1.0	0.318993	0.313947	1.58%
	2.0	0.283352	0.264757	6.56%
	3.0	0.265515	0.235251	11.40%
	5.0	0.247676	0.199283	19.54%
	7.0	0.238789	0.177172	25.80%
	9.0	0.223472	0.161631	30.77%

(a)

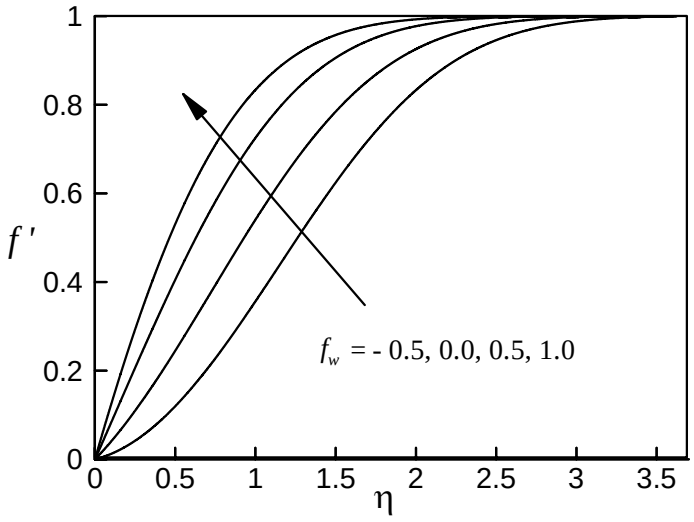

(b)

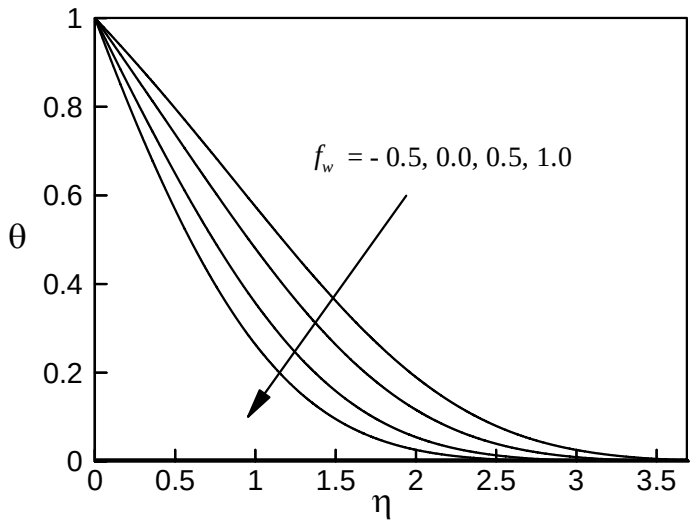

(c)

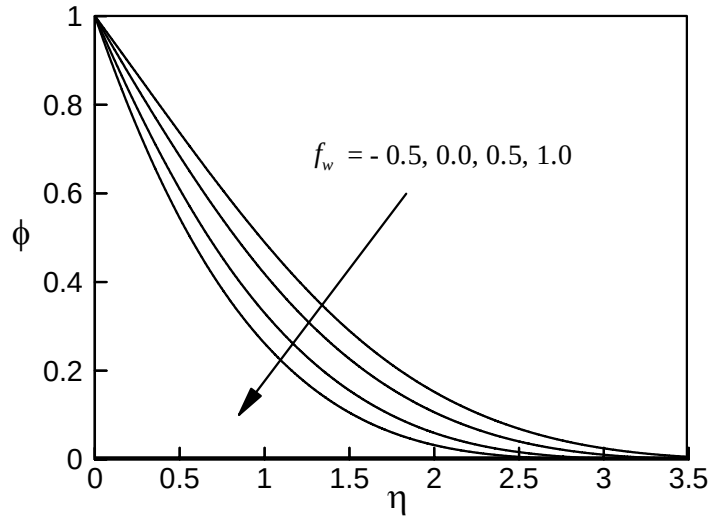

Figure 5.1: Variation of dimensionless (a) velocity, (b) temperature and (c) concentration for several values of f_w

(a)

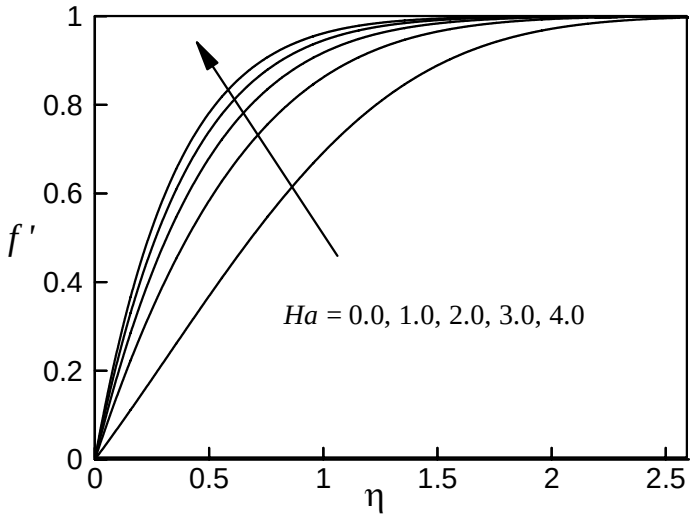

(b)

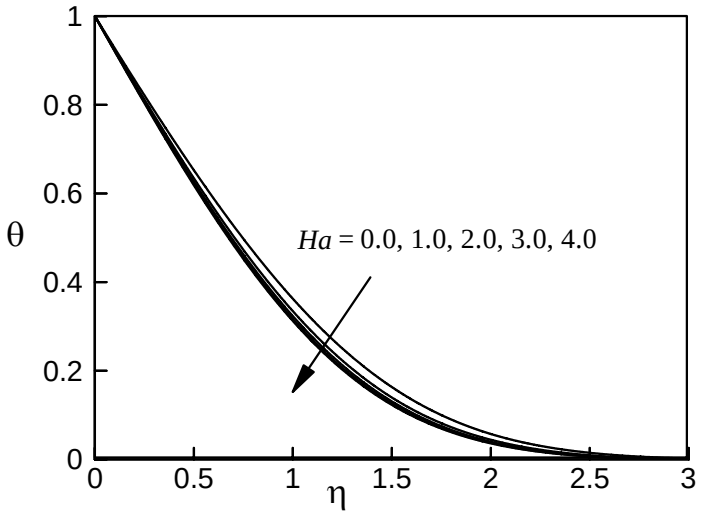

(c)

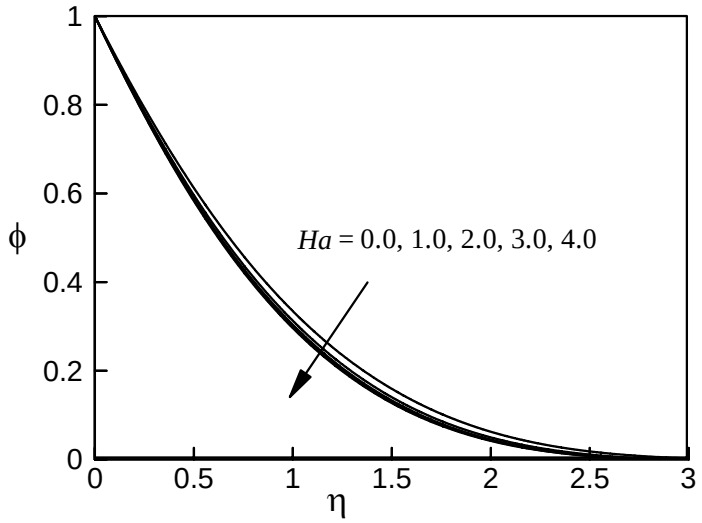

Figure 5.2: Variation of dimensionless (a) velocity, (b) temperature and (c) concentration for several values of *Ha*

(a)

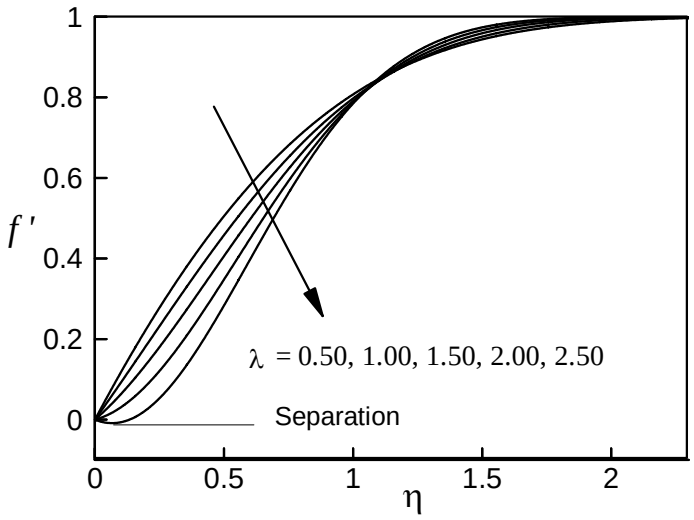

(b)

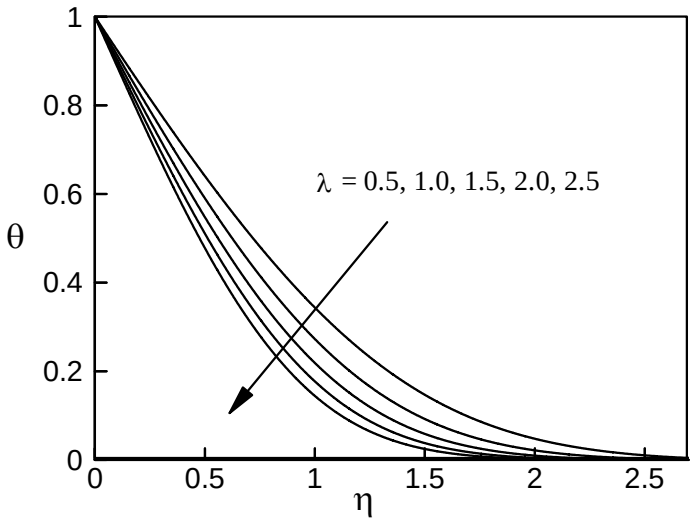

(c)

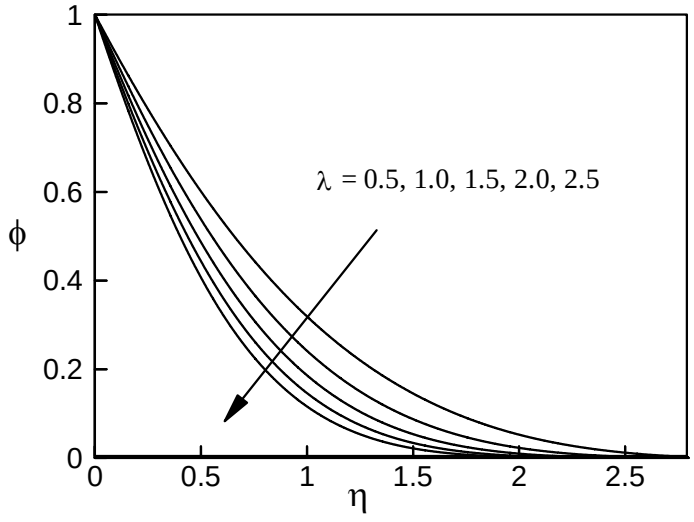

Figure 5.3: Variation of dimensionless (a) velocity, (b) temperature and (c) concentration for several values of λ

(a)

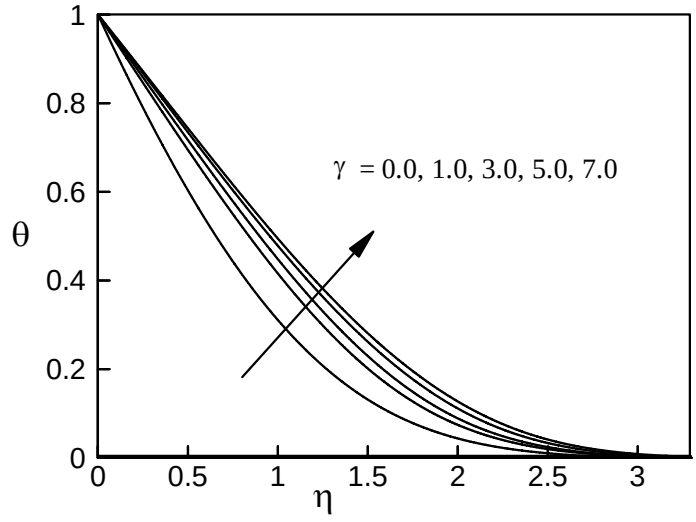

(b)

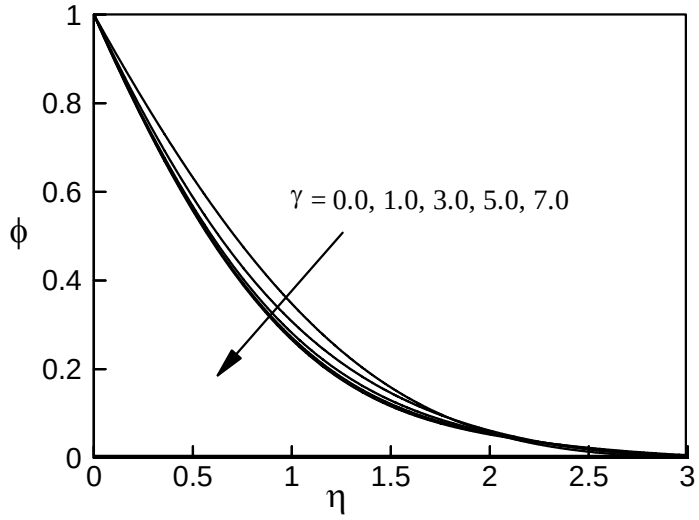

(c)

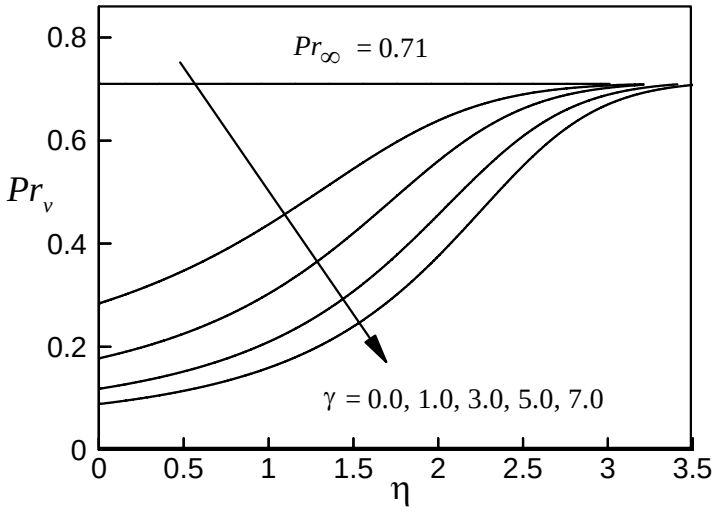

Figure 5.4: Dimensionless (a) temperature, (b) concentration and (c) variable Prandtl number Pr_v for several values of γ

(a)

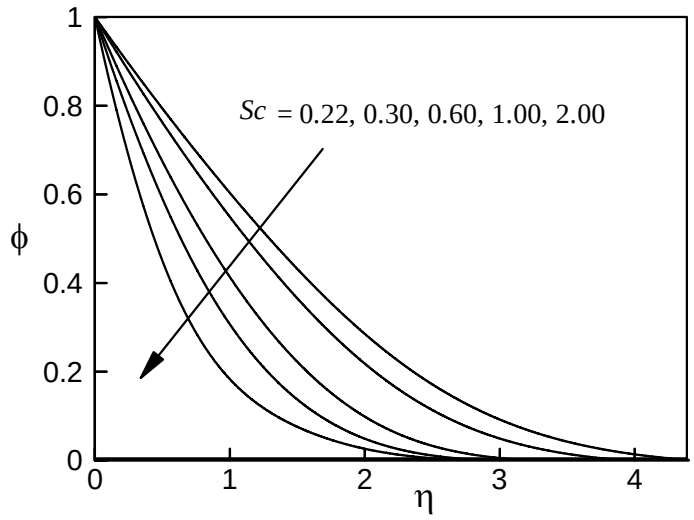

(b)

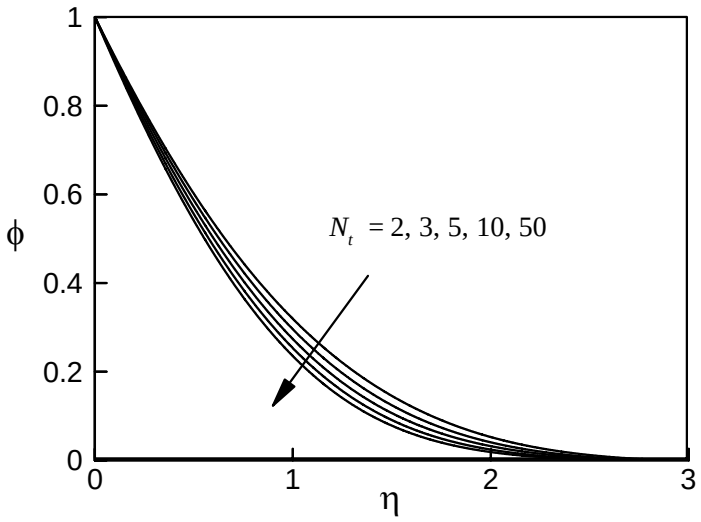

(c)

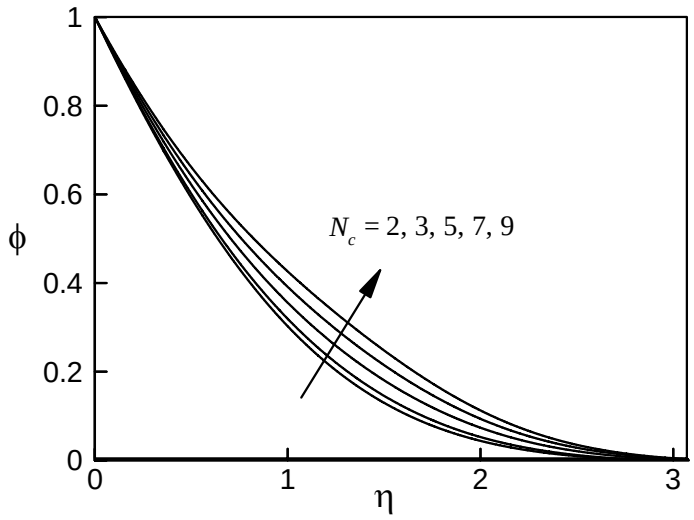

Figure 5.5: Variation of dimensionless concentration profiles for various values of (a) *Sc*, (b) N_t and (c) N_c

(a)

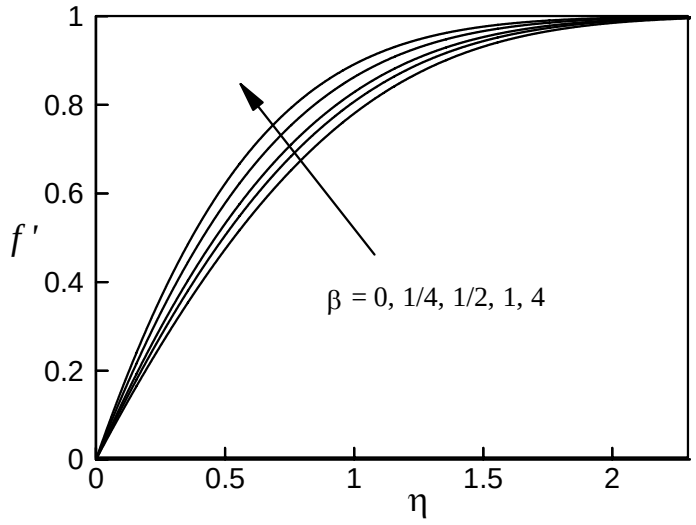

(b)

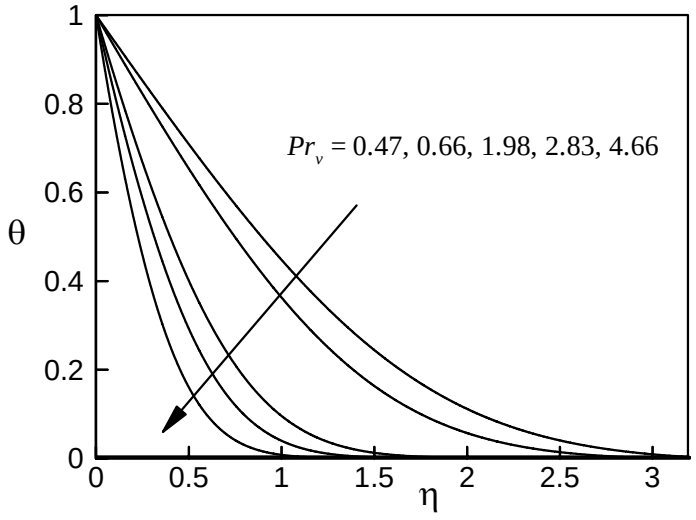

(c)

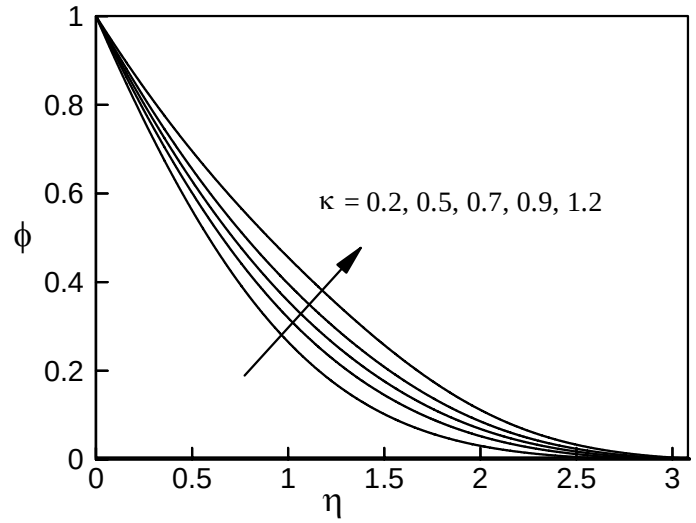

Figure 5.6 Variation of dimensionless concentration profiles for various values of (a) β, (b) Pr_v and (c) κ

(a)

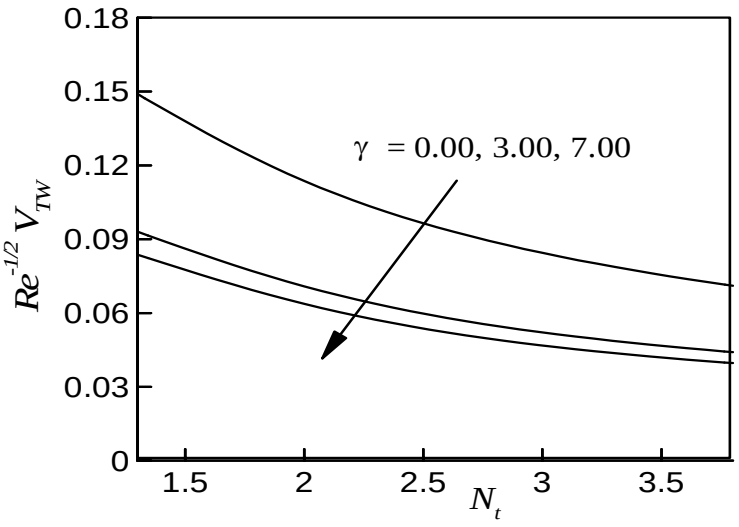

(b)

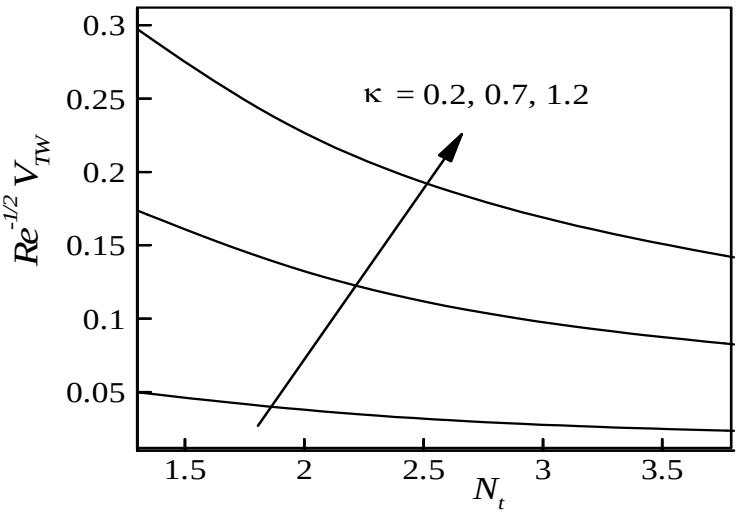

Figure 5.7: Variation of termophoretic velocity for various values of (a) γ and N_t and (b) κ and N_t

5.5 Conclusions

Thermophoresis particle deposition on unsteady MHD forced convective flow along a porous wedge with variable thermal conductivity, and variable Prandtl number has been analyzed. A set of similarity equations governing the fluid velocity, temperature and the particle mass concentration are obtained by using similarity transform. A comparison with previously published work was performed, and the results were found to be in excellent agreement. From the present numerical computations, the following major conclusions may be listed:

i. Suction or injection strongly controls the boundary-layer growth.

ii. Velocity within the boundary layer enhance with the increase of the suction parameter f_w. On the other hand, the thickness of the velocity boundary layer reduces with the increase of the suction parameter f_w.

iii. Velocity increases hence thickness of the hydrodynamic boundary layer decreases with the increase of Hartman number *Ha*. Moreover, the temperature and concentration of the fluid within the boundary layer decrease with the increase of Hartman number.

iv. Concentration of the fluid particles within the boundary layer decreases with the increase of the thermal conductivity variation parameter γ.

v. Thermophoretic particle deposition velocity ($V_d^* \, \mathrm{Re}^{-1/2}$) increases with the increase of Schmidt number *Sc*.

vi. Thermophoretic velocity V_{Tw} increases with the increasing values of thermophoretic coefficient κ.

vii. Heat transfer rate decreases by 45.18% when the thermal conductivity variation parameter varies from 0 to 9 for variable Prandtl number, whereas the corresponding decreases by 76.56% for constant Prandtl numbe*r* in case of suction.

Chapter 6

Thermophoretic Particle Deposition on Unsteady Convective Slip Flow over a Wedge with Variable Fluid Properties and Prandtl Number

6.1 Introduction

Slip velocity is a function of the velocity gradient near the wall. It is known that for gaseous flow there always exists a non–zero velocity near the wall and based on a momentum balance at the wall. In certain situations, the assumption of no slip boundary condition does no longer apply. When fluid flows in micro electro mechanical systems (MEMS), the no-slip condition at the solid fluid interface is no longer applicable. A slip flow model more accurately describes the non-equilibrium near the interface. A partial slip may occur on a stationary and moving boundary when the fluid is particulate such as emulsions, suspensions, foams, and polymer solutions. The slip flows under various flow configurations for Newtonian and non-Newtonian fluids have been studied widely in the literature on a stationary flat plate, moving plate as well as on a stretching surface (see for examples, Hasimoto (1958), Vedantam (2006), Martin and Boyd (2010)). Therefore the present study is to investigate the effects of thermophoresis particle deposition on unsteady convective slip flow over a wedge with variable fluid properties and variable Prandtl number. The governing non-linear partial differential equations are reduced to locally similar ordinary differential equations, which are solved numerically by applying shooting method and the results are discussed from the physical point of view.

6.2 Governing equations

Formulation of the governing equations has been discussed in section 2.4.4 as case IV of chapter 2. The dimensionless concentration equation is same as equation (2.28), however there are some modifications in the momentum equation, energy equation and boundary conditions due to variable viscosity, variable thermal conductivity, variable Prandtl number and slip flow. The modified dimensionless momentum equation, energy equation and boundary conditions are given in equations (2.73), (2.77) and (2.75).

6.3 Numerical results and explanation

In order to investigate the effects of pertinent parameters on the flow fields, there are ten parameters in the governing equations which are very important to analyse the flow, heat and mass transfer behaviour for the current problem. Three parameters in momentum equation and they are wedge angle parameter, unsteadiness parameter and temperature dependent viscosity variation parameter, two parameters in the energy equation namely Prandtl number and thermal conductivity variation parameter, four parameters in the concentration equation like as Schmidt number, concentration ratio, thermophoretic coefficient parameter and thermophoresis parameter and one in the boundary condition which is slip parameter.

When the viscosity and the thermal conductivity does not depend on the temperature the value of the ambient Prandtl number, $\mathrm{Pr}_{\infty} = 0.71$, 2.97 and 7.0 corresponds to air, methyl chloride and water. When the viscosity and the thermal conductivity depend on the temperature the value of the variable Prandtl number at the surface of the wedge ($\eta = 0$) correspond to 1.18, 4.95 and 11.66, respectively when $\theta_r = 2.00$ and $\gamma = 0.2$. Therefore, in the simulation the value of the variable Prandtl number Pr_v is chosen as 1.18.

The governing momentum equation (2.73), energy equation (2.77) and concentration equation (2.28) have been solved numerically based on the

boundary condition (2.75) for different values of the above parameters numerically by applying Nachtsheim-Swigert shooting iteration technique along with sixth order Runge-Kutta integration scheme which is elaborately discussed in Appendix.

The values of Schmidt number *Sc* = 0.60, 0.78, 0.94 represents water-vapour, ammonia and Carbon-Dioxide, respectively. The remaining parameters are taken as follows: unsteadiness parameter $\lambda = 0.10\text{-}0.20$; temperature dependent viscosity variation parameter $\theta_r = 2-100$; thermal conductivity variation parameter $\gamma = 0.0-0.90$, thermophoresis parameter $N_t = 2-15$ and concentration ratio $N_c = 3-7$. The default values of the parameters throughout the simulation are considered as θ_r = 2.0, γ = 0.2, ε = 0.5, λ = 0.10, $\beta = 1/3$ (i. e. $\Omega = 60^0$), κ = 0.5, N_c = 2.0, N_t = 2.0 and Pr_∞ = 0.71 unless otherwise specified.

6.3.1 Effects of the wedge angle parameter β

Figures 6.1 (a)-(c), present dimensionless velocity, temperature and concentration profiles within the boundary layer for both no-slip $(\varepsilon = 0)$ and slip $(\varepsilon \neq 0)$ flows for various values of wedge angle parameter β. The dashed lines represent when there is no-slip at the boundary and the solid lines represent when there is slip at the surface of the boundary. From Figure 6.1 (a) it is observed for both no-slip and slip cases velocity within the boundary-layer increases with the increasing values of wedge angle parameter β. The thickness of the velocity boundary layer also reduces with the increase of β. It is also mentionable that velocity is lower for the case of no-slip than the presence of slip which is expected. For experimental interest at $\eta = 0$, the velocity increases by approximately 40.09% and 62.88% (for $\varepsilon \neq 0$) when wedge angle parameter β increases from 1/6 to 1/3 and 1, respectively. From Figures 6.1(b)-(c) it is seen that both the temperature and concentration of the fluid within the boundary-layer decrease with the increasing value of β. It is also noticeable that thickness of the thermal and concentration boundary layer decrease with the increasing values of β.

6.3.2. Effects of the unsteadiness parameter λ

The variation of dimensionless velocity, temperature and concentration profiles for different values of unsteadiness parameter λ for both no-slip $(\varepsilon = 0)$ and slip $(\varepsilon \neq 0)$ flows at the boundary are displayed in Figures 6. 2 (a)-(c), respectively. The increasing values of unsteadiness parameter reduce fluid motion within the boundary layer which is illustrated in Figure 6.2 (a). This is due to the fact that the viscosity is higher at the surface of the wedge. At $\eta = 0$, the velocity decreases by approximately 15.92% and 27.65% (for $\varepsilon \neq 0$) with the increase in the unsteadiness parameter λ from 0.10, 0.15 and 0.20, respectively. From Figures 6.2 (b)-(c) it can be seen that both the temperature and concentration of fluid increase with the increasing values of the unsteadiness parameter λ. It is also observed that both the temperature and concentration are higher for the case of no-slip than the presence of slip flows.

6.3.3 Effects of the variable viscosity parameter θ_r

The effect of the variable viscosity parameter θ_r (for $\theta_r > 0$ and $\theta_r < 0$) on the dimensionless velocity, temperature, concentration for both slip and no- slip flows are depicted in Figures 6.3 (a)-(c) and Figures 6.4 (a)-(c), respectively . Figure 6.3 (a) shows that the velocity within the boundary-layer increases, i.e. thickness of the velocity boundary layer decreases with the increasing values of variable viscosity parameter θ_r when it is positive. An opposite effect of variable viscosity parameter θ_r on the velocity and on the boundary layer thickness is observed when it is negative which is displayed in Figure 6.4 (a). Both the Figure 6.3 (a) and Figure 6.4 (a) reveal that for very large variable viscosity parameter θ_r change in $f'(\eta)$ is negligible. This is due to the fact that $|\theta_r| \to \infty$, the dynamic viscosity of the fluid (μ) equals viscosity of the fluid at the ambient temperature (μ_∞). For $\theta_r > 0$ (Figures 6.3 (b)-(c)) both the temperature and concentration decrease with the increasing values of variable viscosity parameter θ_r but for $\theta_r < 0$ (Figures 6.4 (b)-(c)) both the temperature and concentration increase with

the increasing values of $|\theta_r|$. In both the case of slip ($\varepsilon \neq 0$) and no-slip ($\varepsilon = 0$), the thickness of the thermal and concentration boundary layer decrease when $\theta_r > 0$ and increase when $\theta_r < 0$. However, the values of the velocity are 0.17162, 0.23762, 0.25564 and 0.27050 for $\varepsilon = 0.5$ which occurs at the surface of the wedge. It is also seen that the velocity increases by approximately 57.62% as variable viscosity parameter θ_r increases from 2 to 100. On the other hand, the values of the velocity are 0.33667, 0.30095, 0.28716 and 0.27362 for $\varepsilon = 0.5$ which occurs at the surface of the wedge. It is also seen that the velocity decreases by approximately 18.73% as variable viscosity parameter θ_r increases from -2 to -100.

6.3.4. Effects of the thermal conductivity variation parameter γ and variable Prandtl number Pr_v

The temperature profiles against η for different values of variable Prandtl number are presented graphically in Figure 6.5 (a). The temperature of the fluid within the boundary layer decreases for the increasing values of the variable Prandtl number which is observed from Figure 6.5 (a). Moreover, it is observed that the thickness of the thermal boundary layer become thinner for increasing values of the variable Prandtl number. The above are the predictable physical significance of the Prandtl number as it is known that the Prandtl number is the ratio of viscous force and thermal action. Thus the increasing value of the Prandtl number represents a fluid with increasing viscosity or decreasing thermal conductivity. Therefore the increasing viscosity reduces the flow of the fluid and lower thermal conductivity decreases temperature within the boundary layer.

The variation of temperature and thermophoretic velocity profiles for different values of thermal conductivity variation parameter for both no-slip and slip flows at the boundary are presented in Figures 6.5 (b)-(c), respectively. From Figure 6.5 (b), it is seen that the non-dimensional temperature increases with the increase of the thermal conductivity variation parameter γ as expected. It is also found that temperature of the fluid is lower for the case of a constant conductivity

than the variable conductivity, which is true for both the case of no-slip $(\varepsilon = 0)$ and slip $(\varepsilon \neq 0)$. It is known that thermophoresis parameter is inversely proportional to the thermophoretic velocity as a result thermophoretic velocity decreases with the increase of thermophoresis parameter N_t, which is depicted from Figure 6.5(c).

6.3.5. Effects of the Schmidt number *Sc*, thermophoresis parameter N_t and concentration ratio N_c

The concentration profiles against η for different values of Schmidt number, thermophoresis parameter and concentration ratio are displayed graphically in Figures 6.6 (a)-(c), respectively. Figure 6.6 (a) shows typical concentration profiles for various values of the Schmidt number *Sc*. It is clear from this figure that the concentration of the fluid particles within the boundary layer thickness reduces as the Schmidt number *Sc* increases and this is the analogous to the effect of increasing the Prandtl number on the thickness of a thermal boundary layer. From Figure 6.6 (b) it is readily seen that the concentration of the fluid particles within the boundary-layer decreases with the increasing values of N_t. Physical significance of the values of the thermophoretic parameter used here: when the wall is warm, bearing in mind the definition of thermophoresis parameter, $N_t T_w = (1 + N_t) T_\infty$, so that $N_t = 1$ means a wall twice warmer than the ambient fluid, i. e. $T_w = 2T_\infty$, while $N_t = 1000$ describes a very cold wall. From these Figure it is noticeable that thickness of the thermal boundary layer is higher for the slip no-slip $(\varepsilon = 0)$ case than the slip $(\varepsilon \neq 0)$ case. From Figure 6.6 (c) it is seen that the concentration of the fluid particles within the boundary-layer increases with the increasing values of N_c.

6.3.6 Effects of the ambient Prandtl number Pr_∞

The effect on ambient Prandtl number Pr_∞ for different values of $\theta_r > 0$ and $\theta_r < 0$ are displayed in Figure 6.7(a) and Figure 6.7(b). The ambient Prandtl number Pr_∞ at the surface of the wedge increases with the increasing positive values of θ_r, which is presented in Figure 6.7(a). The results also show that the values of ambient Prandtl number Pr_∞ within the boundary layer asymptotically converge to the value of variable Prandtl number Pr_v as $\eta \to \infty$. Figure 6.7 (b) shows that the ambient Prandtl number decreases for increasing values of $|\theta_r|$. It is observed that the ambient Prandtl number asymptotically converge to the value of Pr_v as $\eta \to \infty$. On the other hand from equation (2.76) it can be seen that for large negative value of θ_r, the ambient Prandtl number, at the surface of the wedge approaches the value $1+\gamma$. It is also seen that for large θ_r, i.e. $\theta_r \to \infty$ and constant conductivity, i.e. $\gamma = 0$, the variable Prandtl number Pr_v equals to the ambient Prandtl number Pr_∞. This means that consideration of prandtl number as a constant within the boundary layer except for very large $|\theta_r|$ produce unrealistic result.

Figure 6.7 (c) illustrates variation of ambient Prandtl number Pr_∞ within the boundary layer for different values of thermal conductivity variation parameter γ. The ambient Prandtl number, at the surface of the wedge increases for the increasing values of the thermal conductivity variation parameter γ. From this Figure it is also observed that values of ambient Prandtl number Pr_∞ within the boundary layer converge asymptotically to the value of variable Prandtl number Pr_v far away from the surface of the wedge.

Table 6.1 presents the comparison of the stream function $f(0)$, velocity $f'(0)$ and the local skin friction $f''(0)$ obtained in the present work with $\theta_r \to \infty$, wedge angle parameter $\beta = 0$, thermal conductivity variation parameter $\gamma = 0$, no slip parameter $\varepsilon = 0$ and $\lambda = 0$ (for steady flow) for different values of η. Thus from

Table 6.1 it is observed that the data produced by the present code and those of White (2006) are in excellent agreement, which gives us confidence to use the present numerical code.

Table 6.2 shows the fluid velocity and the thermophoretic particle deposition velocity for different values of variable viscosity parameter θ_r and wedge angle parameter β. From Table 6.2 it can be concluded that the correlation coefficient *r* between fluid velocity f' and thermophoretic particle deposition velocity $V_d^*(\mathrm{Re})^{-1/2}$. From this Table, the values of *r* show that fluid velocity and thermophoretic particle deposition velocity are highly correlated for all values of θ_r. From this table it is clearly observed that when the fluid velocity increases, the thermophoretic particle deposition velocity also increases which is expected.

Table 6.3 shows the variation of thermophoretic particle deposition velocity for different values of Schmidt number *Sc* and slip parameter ε. The Table shows that thermophoretic particle deposition velocity decreases with the increase of Schmidt number for both no-slip $(\varepsilon = 0)$ and slip $(\varepsilon \neq 0)$ flows. From Table 6.4 it is observed that the local skin friction coefficient and the local rate of heat transfer in a fluid of constant Prandtl number Pr_c is lower than in a fluid of variable Prandtl number Pr_v when no slip flows while the opposite result is found for slip flows**.** From this Table, it is also seen that the variation between the produced results differ by less than 1% when the negative values of variable viscosity parameter θ_r are very large. The variation between the produced results is more than 2.98% when $\theta_r = -0.5$ (for local skin friction and no slip flow) but these variations become 25.87% at $\theta_r = -0.5$ (for local skin friction and slip flow). On the other hand, the variation in $-\theta'(0)$ is 50.57% at $\theta_r = -0.5$ when slip flow is applied at the surface of the wedge.

Table 6.5 shows values of $f''(0)$, $-\theta'(0)$ and $-\phi'(0)$ which are respectively proportional to local skin friction coefficient, local rate of heat transfer and local rate of mass transfer for different values of variable viscosity parameter θ_r,

wedge angle parameter β and unsteadiness parameter λ for variable Prandtl number Pr_v = 1.18. From this Table it is seen that local skin friction coefficient, the local rate of heat transfer and local rate of mass transfer increase with the increasing values of variable viscosity parameter θ_r and wedge angle parameter β. These behaviors depict the nature of the profiles shown in Figures 6.3 (a)-(c), Figures 6.1 (a)-(c) and Figures 6.2 (a)-(c), respectively. It is also observed that for slip flow ($\varepsilon \neq 0$) the values of local skin friction coefficient are lower than the corresponding values of no-slip ($\varepsilon = 0$). On the other hand, for slip flow ($\varepsilon \neq 0$) local rate of heat transfer and local rate of mass transfer are higher than the corresponding values of no-slip ($\varepsilon = 0$) case.

Table 6.1: Comparison of the present numerical results of stream function, velocity and local skin friction coefficient with White (2006) for different values of η when $\beta = \gamma = \varepsilon = \lambda = 0$ and $\theta_r \to \infty$.

η	$f(\eta)$		$f'(\eta)$		$f''(\eta)$	
	Present work	White (2006)	Present work	White (2006)	Present work	White (2000)
0.0	0.00000000	0.00000	0.00000000	0.00000	0.47027089	0.46960
0.5	0.05872926	0.05864	0.23456114	0.23423	0.46568757	0.46503
1.0	0.23332581	0.23299	0.46127690	0.46063	0.43494906	0.43438
1.5	0.51575598	0.51503	0.66235843	0.66147	0.36218408	0.36180
2.0	0.88800281	0.88680	0.81770859	0.81669	0.25581418	0.25567
3.0	1.79780496	1.79557	0.97006212	0.96905	0.06763291	0.06771
4.0	2.78709815	2.78388	0.99872084	0.99777	0.00684790	0.00687
5.0	3.78738993	3.78323	1.00087632	0.99994	0.00025589	0.00026

Table 6.2: Effects of variable viscosity parameter θ_r and wedge angle parameter β on the fluid velocity and thermophoretic particle deposition velocity.

θ_r	β	f'	$V_d^*(\mathrm{Re})^{-\frac{1}{2}}$	$r = \frac{COV(X,Y)}{\sqrt{V(X)V(Y)}}$
2	1/3	0.172790	0.607769	0.998761
5	1/3	0.238197	0.641280	
10	1/3	0.255921	0.648418	
2	1	0.280901	0.561996	0.985634
5	1	0.356388	0.577122	
10	1	0.375487	0.580865	

Table 6.3: Variation of thermophoretic particle deposition velocity for different values of Schmidt number *Sc*.

Parameters	$\varepsilon = 0$				$\varepsilon = 0.5$			
Sc	0.22	0.30	0.60	0.94	0.22	0.30	0.60	0.94
$\mathrm{Re}^{-\frac{1}{2}} V_d^*$	0.915	0.744	0.470	0.334	0.986	0.809	0.525	0.384

Table 6.4: Values of local skin friction coefficient $f''0)$ and local rate of heat transfer $-\theta'(0)$ for different values of slip parameter ε and variable viscosity parameter θ_r.

Parameters		(i) Constant Prandtl number Pr_c		(ii) Variable Prandtl number Pr_v		Variation in $f''0)$	Variation in $-\theta'(0)$
ε	θ_r	$f''0)$	$-\theta'(0)$	$f''(0)$	$-\theta'(0)$		
0	-100	0.626462	0.487600	0.626477	0.499818	<1%	2.50%
	-10	0.665711	0.492882	0.666026	0.510886	<1%	3.65%
	-5	0.707475	0.498546	0.708079	0.522764	<1%	4.85%
	-2	0.820679	0.512554	0.823687	0.555938	<1%	8.46%
	-1	0.979338	0.530394	0.990346	0.605700	1.12%	14.19%
	-0.5	1.225401	0.553306	1.262082	0.691934	2.98%	25.05%
0.5	-100	0.622368	0.589572	0.547269	0.498215	12.06%	18.34%
	-10	0.660767	0.604805	0.573659	0.503896	13.18%	20.03%
	-5	0.701292	0.621413	0.601069	0.509726	14.29%	21.91%
	-2	0.811729	0.667154	0.671292	0.525057	17.30%	27.06%
	-1	0.964188	0.735753	0.762221	0.543540	20.95%	35.36%
	-0.5	1.199220	0.854953	0.888958	0.567824	25.87%	50.57%

Table 6.5: Values of local skin friction coefficient $f''(0)$, local rate of heat transfer $-\theta'(0)$ and local rate of mass transfer $-\phi'(0)$ for different values of θ_r, wedge angle parameter β and unsteadiness parameter λ.

Parameters			$\varepsilon = 0$			$\varepsilon = 0.5$		
θ_r	β	λ	$f''(0)$	$-\theta'(0)$	$-\phi'(0)$	$f''(0)$	$-\theta'(0)$	$-\phi'(0)$
2	$1/3$	0.10	0.362133	0.427890	0.411904	0.345581	0.486456	0.466470
2	$1/3$	0.15	0.280273	0.426332	0.410684	0.270822	0.485501	0.464907
2	$1/3$	0.20	0.223084	0.417398	0.400549	0.210691	0.472746	0.452444
2	$1/2$	0.10	0.464185	0.447128	0.430217	0.416003	0.508721	0.487193
2	$1/2$	0.15	0.401204	0.454672	0.436708	0.377269	0.514558	0.492178
2	$1/2$	0.20	0.328025	0.459173	0.440621	0.310314	0.517128	0.494311
2	1	0.10	0.700149	0.483080	0.468643	0.561801	0.549186	0.528277
2	1	0.15	0.657524	0.494517	0.476003	0.540310	0.559565	0.535475
2	1	0.20	0.612561	0.506012	0.485252	0.516981	0.570734	0.544830
5	1	0.10	0.972205	0.527592	0.477773	0.712776	0.611039	0.542495
5	1	0.15	0.919019	0.540978	0.487309	0.691689	0.623865	0.552039
5	1	0.20	0.862710	0.553746	0.497197	0.668690	0.635933	0.561031
10	1	0.10	1.050410	0.541239	0.480204	0.750975	0.629501	0.546014
10	1	0.15	0.994431	0.555063	0.490240	0.730157	0.642700	0.555172
10	1	0.20	0.935130	0.568148	0.499729	0.707466	0.655137	0.563758

(a)

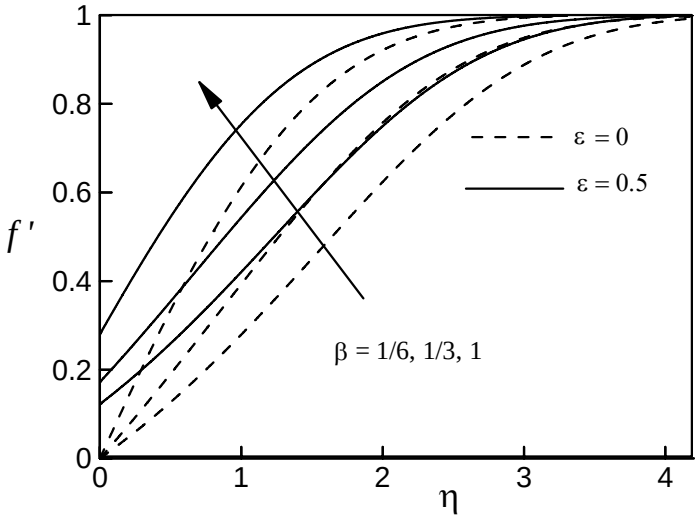

(b)

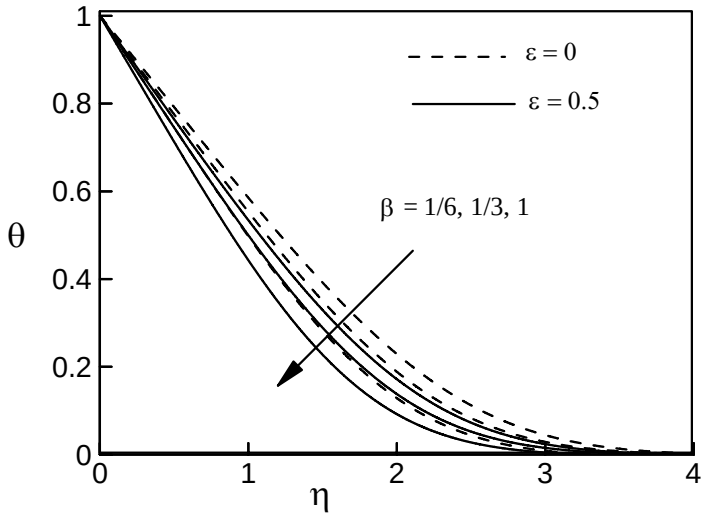

(c)

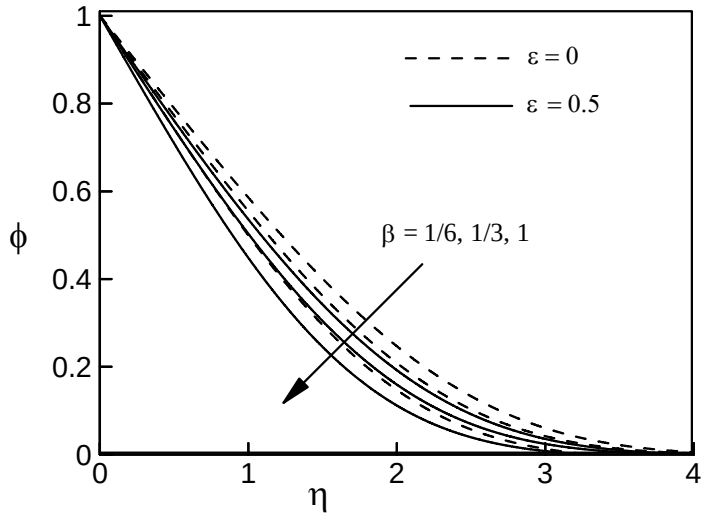

Figure 6.1: Variation of dimensionless (a) velocity, (b) temperature and(c) concentration for several values of β and ε

(a)

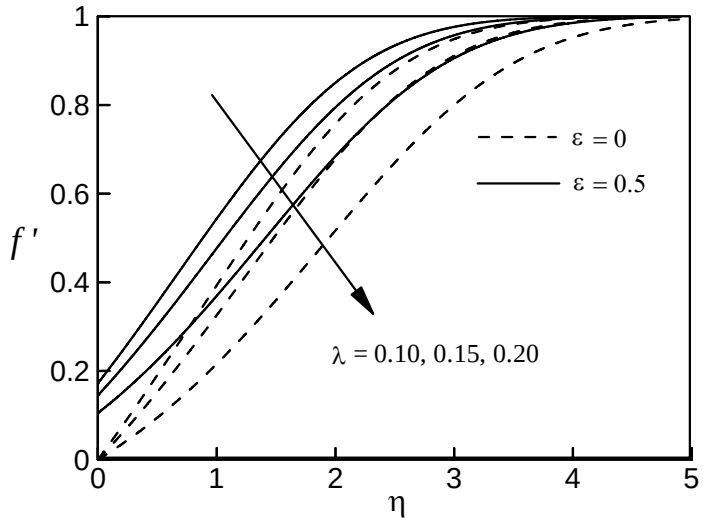

(b)

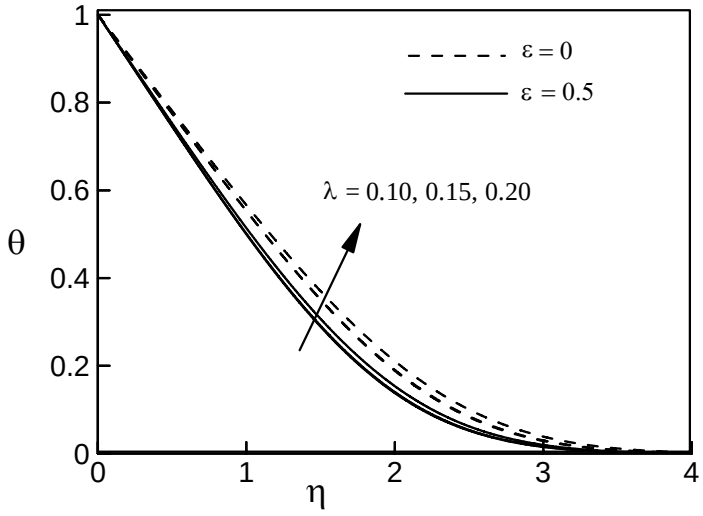

(c)

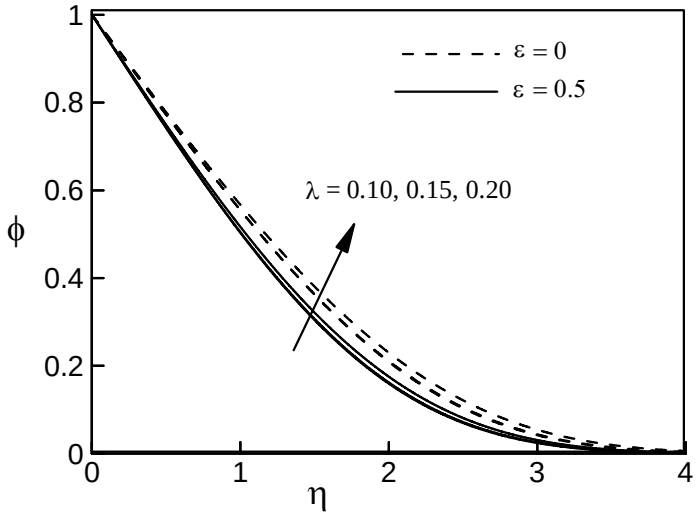

Figure 6. 2: Variation of dimensionless (a) velocity, (b) temperature and(c) concentration for several values of λ and ε

(a)

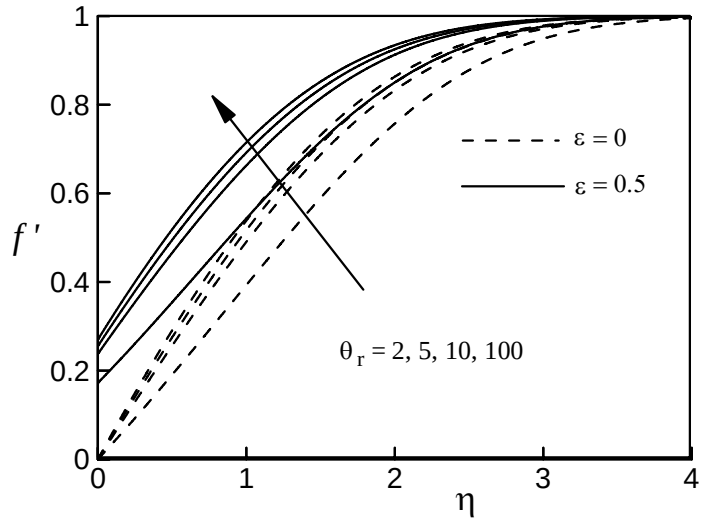

(b)

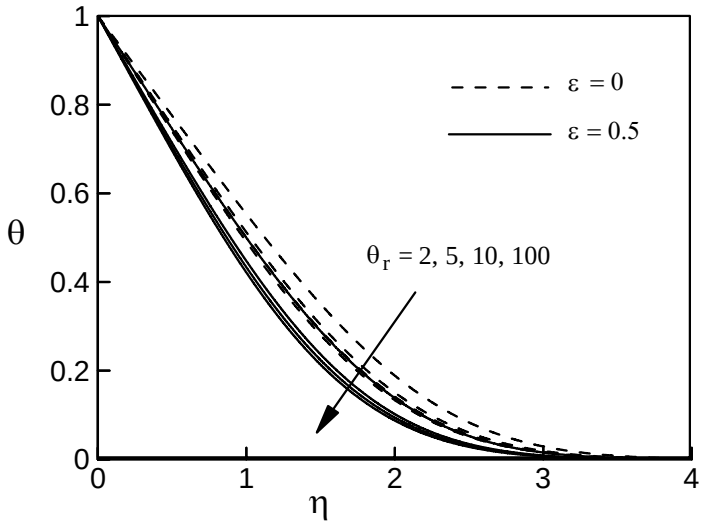

(c)

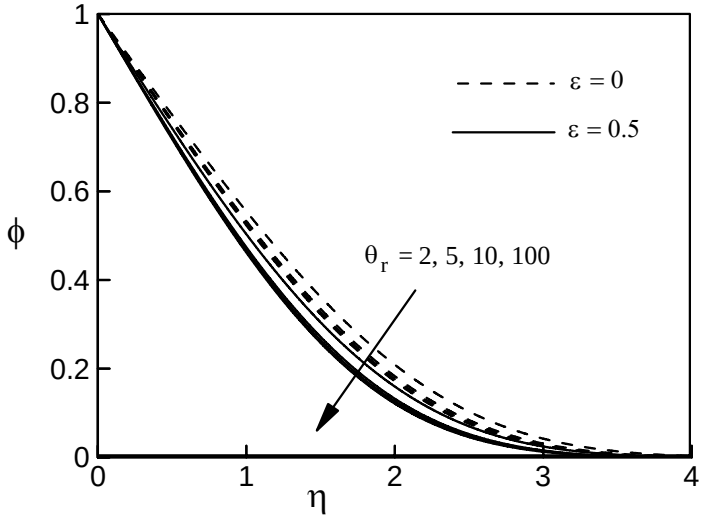

Figure 6.3: Variation of dimensionless (a) velocity, (b) temperature and (c) concentration for several values of $\theta_r > 0$ and ε

(a)

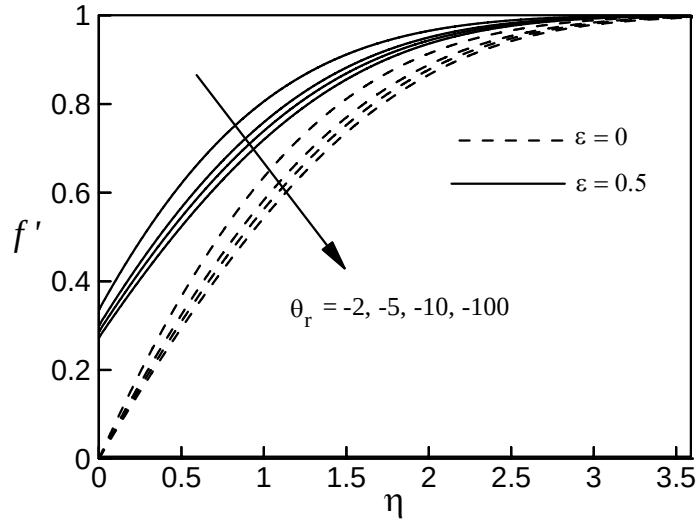

(b)

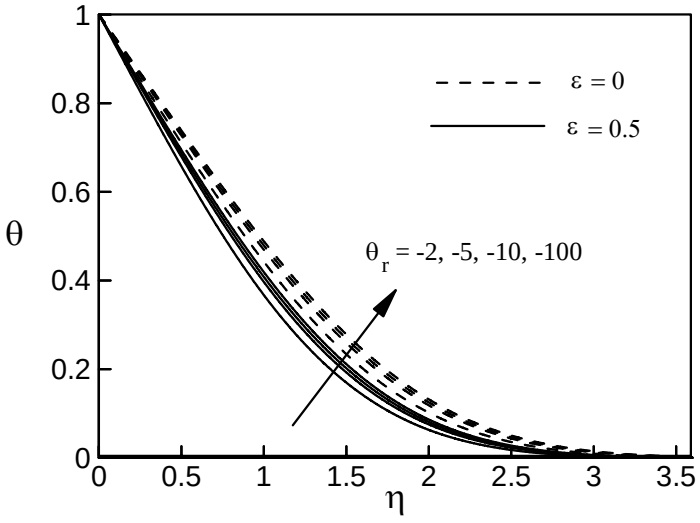

(c)

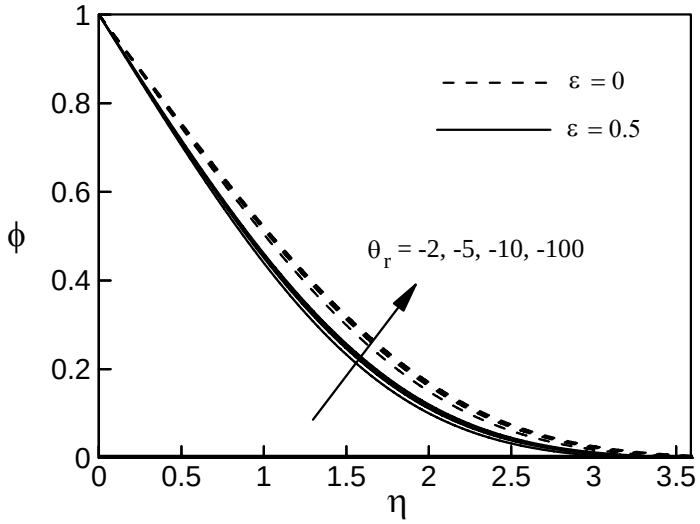

Figure 6.4: Variation of dimensionless (a) velocity, (b) temperature and (c) concentration for several values of $\theta_r < 0$ and ε

(a)

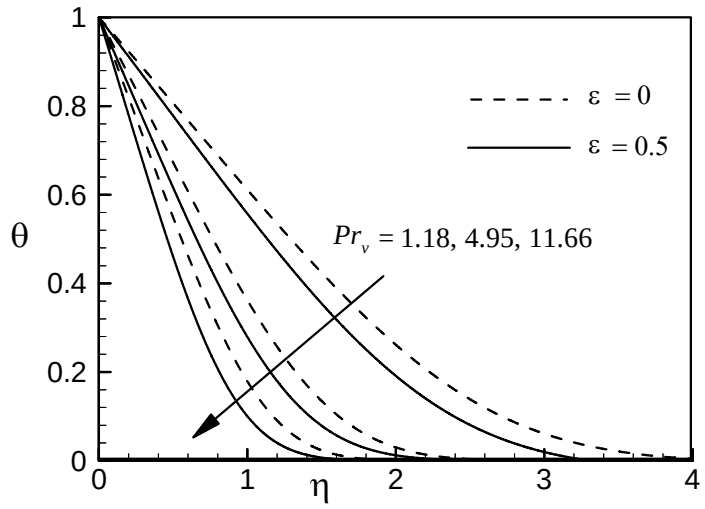

(b)

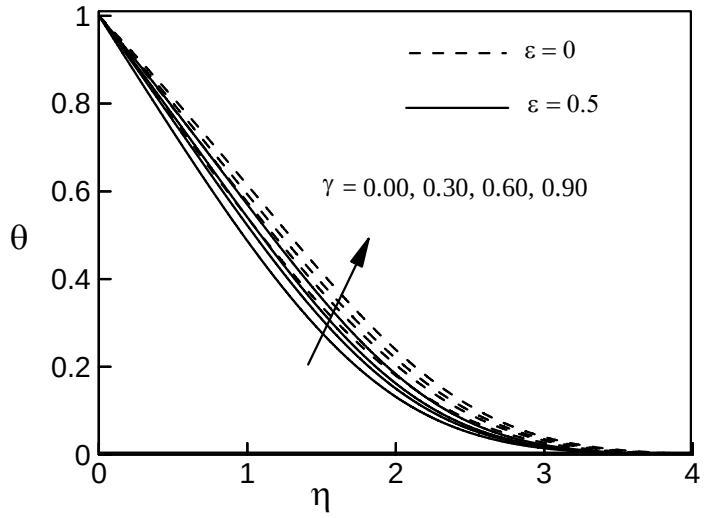

(c)

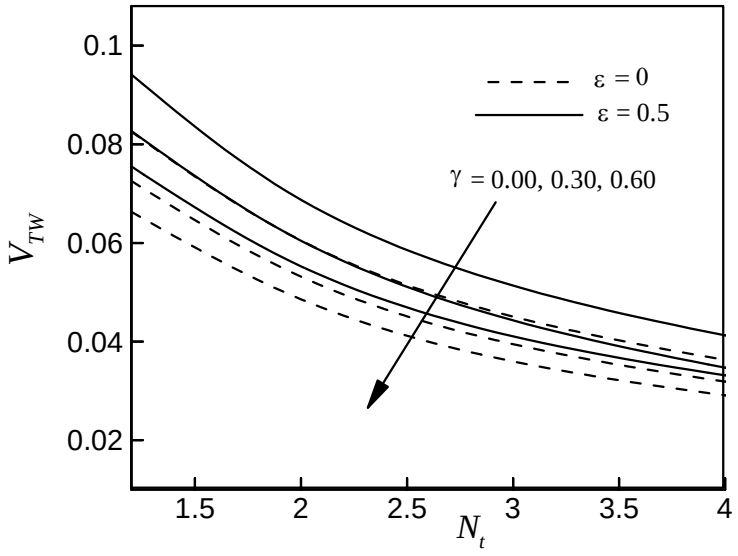

Figure 6.5: Variation of dimensionless temperature for several values of (a) Pr_v and ε, (b) γ and ε and (c) thermophoretic velocity for several values of γ and ε

(a)

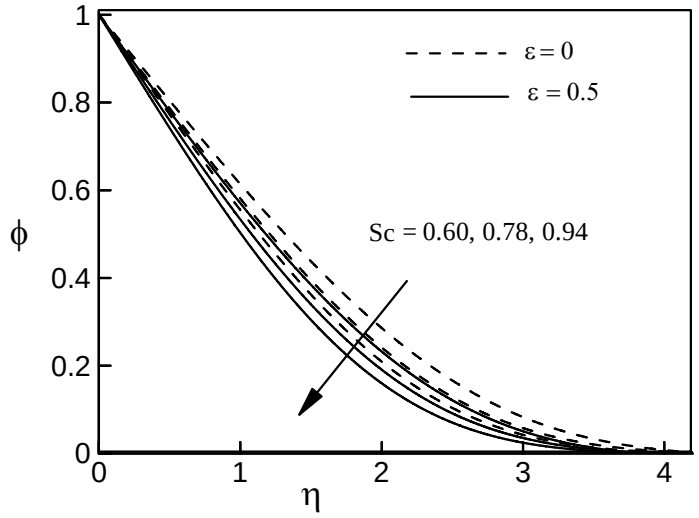

(b)

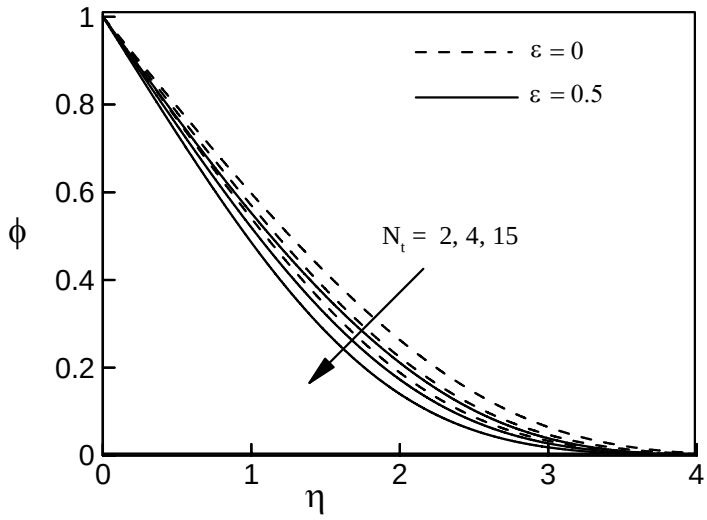

(c)

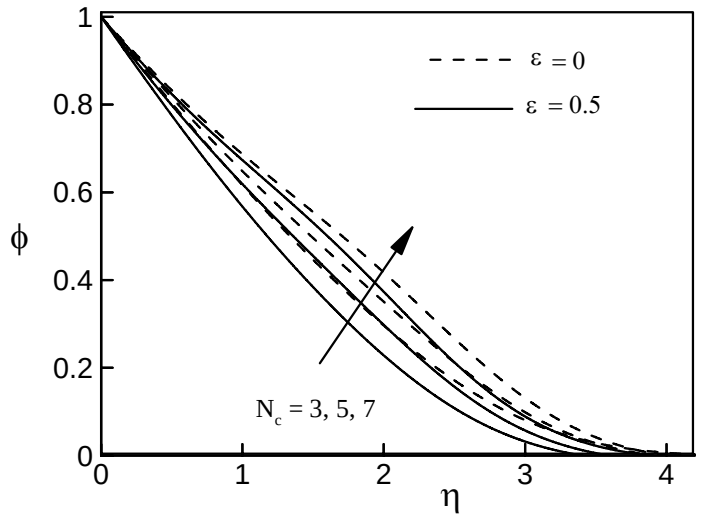

Figure 6.6: Variation of dimensionless concentration for several values of ε and (a) *Sc*, (b) N_t and (c) N_c

(a)

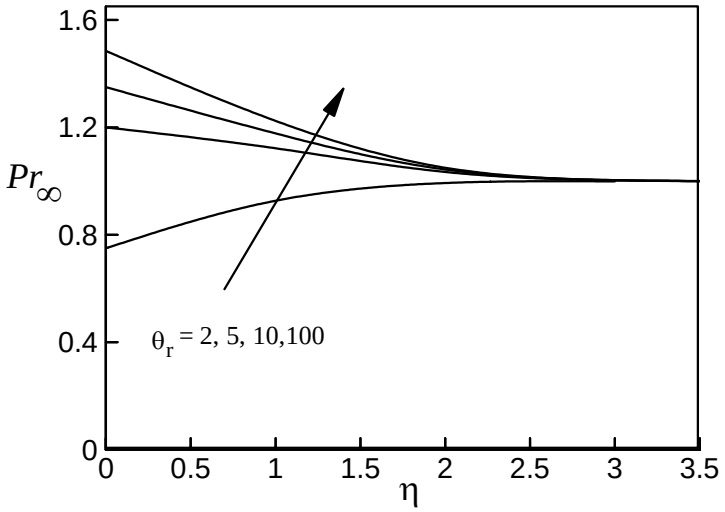

(b)

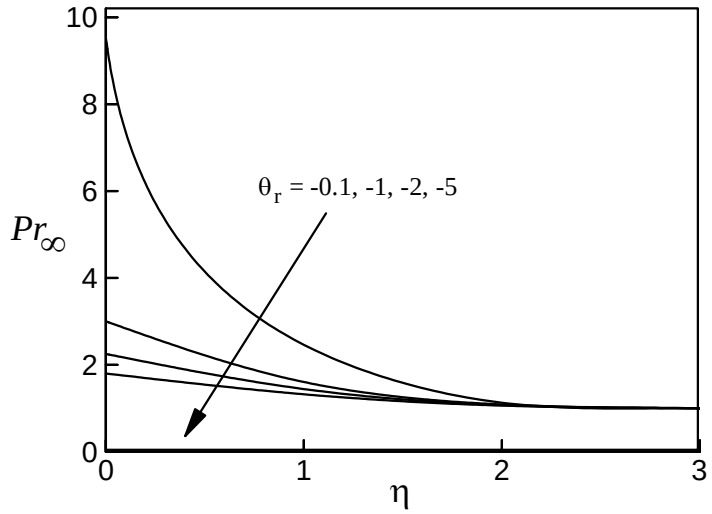

(c)

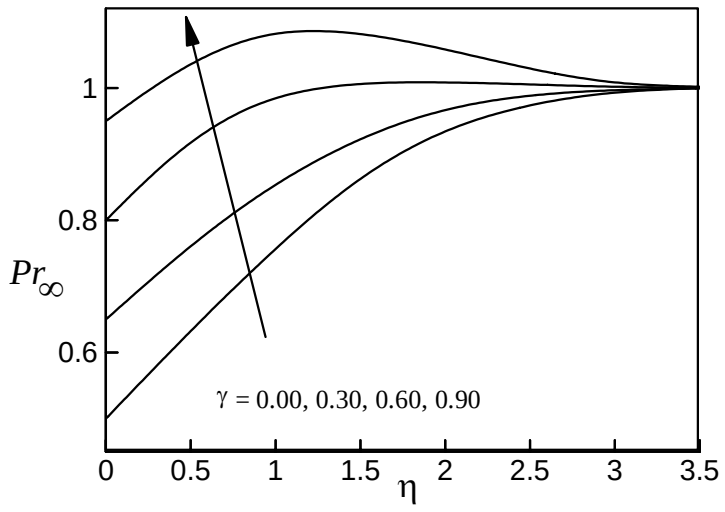

Figure 6.7: Variation of dimensionless ambient Prandtl number Pr_∞ for different values of (a) $\theta_r > 0$, (b) $\theta_r < 0$ and (c) γ

6. 4 Conclusions

In this work, the effects of thermophoretic particle deposition on unsteady convective slip flows over a wedge with variable fluid properties and variable Prandtl number have been studied numerically. The fluid properties such as viscosity and thermal conductivity are considered to be temperature dependent. From the present numerical investigations, the following major conclusions can be drawn:

i. Velocity within the boundary-layer increases with the increasing values of wedge angle parameter β for both no-slip and slip cases. The thickness of the velocity boundary layer also decreases with the increase of β. It is also mentionable that velocity is lower for the case of no-slip than the presence of slip which is expected. At $\eta = 0$, the velocity increases by approximately 40.09% and 62.88% (for $\varepsilon \neq 0$) when wedge angle parameter β increases from 1/6, 1/3 and 1, respectively.

ii. The increasing values of unsteadiness parameter reduce fluid motion within the boundary layer. This is due to the fact that the viscosity is higher at the surface of the wedge. On the other hand, both the temperature and concentration of fluid increase with the increasing values of the unsteadiness parameter λ.

iii. The ambient Prandtl number Pr_∞ at the surface of the wedge increases with the increasing positive values of variable viscosity parameter θ_r.

iv. The local skin friction and the local rate of heat transfer in a fluid of constant Prandtl number is lower than in a fluid of variable Prandtl number when no slip flows while the opposite result is found for slip flows**.**

v. Thermophoretic particle deposition velocity decreases ($\mathrm{Re}^{-\frac{1}{2}} V_d^*$**)** with the increase of Schmidt number *Sc.*

Chapter 7

Final Clarification and Future Works

7.1 Conclusions

Thermophoresis is an important phenomenon in several scientific and engineering applications, and can be the dominant mechanism of transport of sun-micron particles. In the current study, the author has developed a physical model of unsteady Magnetohydrodynamic (MHD) convective heat and mass transfer flow of Newtonian, viscous incompressible and electrically conducting fluid along a wedge with thermophoresis considering boundary layer approximation. Various flow conditions such as temperature dependent viscosity, thermal conductivity and slip flow have been considered in different models. The potential flow velocity has been taken as a function of the distance x and time t. The governing time dependent non-linear partial differential equations are reduced to a set of non-linear ordinary differential equations by introducing a new class of similarity transformations. The resulting local similarity equations for unsteady flow have been solved numerically by applying Nachtsheim-Swigert shooting iteration technique along with sixth order Runge-Kutta integration scheme. Steady solutions are compared with previously published works which show excellent agreement. There are twelve parameters obtained throughout the thesis, seven parameters in chapter 3 and those are wedge angle parameter β, unsteadiness parameter λ, Prandtl number Pr, thermophoresis parameter N_t, thermophoretic coefficient κ, Schmidt number Sc, and concentration ratio N_c.; two new parameters in chapter 4 and those are viscosity variation parameter θ_r, and variable Prandtl number Pr_v; three new parameters in chapter 5 and those are suction/injection parameter f_w, Hartman number Ha ,thermal conductivity variation parameter γ and one new parameter in chapter 6 and that is slip parameter ε. A representative set of numerical results for the velocity, temperature and concentration profiles, the local skin friction coefficients as well

as the local rate of heat and mass transfer, thermophoretic velocity and thermophoretic particle deposition velocity are presented graphically and discussed in the respective chapters for the above parameters. However, overall discussions on the works are presented below in brief:

The effects of wedge angle parameter β on the dimensionless velocity, temperature and concentration profiles as well as on the local skin-friction coefficient, the local Nusselt number and the local Sherwood number are discussed in chapter 3, chapter 4, chapter 5 and chapter 6. For accelerated flows, i.e. positive values of wedge angle parameter β, velocity profiles squeeze closer and closer to the surface of the wedge. Both the temperature and concentration of the fluid within the boundary layer decrease with the increasing values of the wedge angle parameter β. But separation is found to occur for very small non-negative values of wedge angle parameter β in chapter 3.

The velocity of the fluid within the boundary layer decreases whereas both the temperature and concentration of the fluid within the boundary layer increase with the increasing values of the unsteadiness parameter λ. Both the local Nusselt number and local Sherwood number increase whereas the local skin-friction coefficient decreases with increasing values of the unsteadiness parameter as discussed in chapter 4, chapter 5 and chapter 6.

In chapter 4 and chapter 6, the effect of variable viscosity parameter θ_r on the dimensionless velocity, temperature and concentration profiles are discussed for various parametric conditions. Hydrodynamic boundary-layer thickness decreases with the increasing values of a variable viscosity parameter θ_r when it is positive while it increases for increasing values of a variable viscosity parameter when it is negative. The local rate of heat transfer in a fluid of constant Prandtl number is lower than in a fluid of variable Prandtl number when variable viscosity parameter θ_r is negative while the opposite result is found positive values of variable viscosity parameter θ_r.

The non-dimensional temperature of the fluid increases with the increase of the thermal conductivity parameter γ. Variable Prandtl number within the boundary layer Pr_v decreases with the increase of the thermal conductivity parameter γ. The results also show that the values of Pr_v within the boundary layer asymptotically converge to the value of Pr_∞ far away from the surface of the wedge (i.e. $\eta \to \infty$). It is clearly established that the Prandtl number varies significantly within the boundary layer when the fluid thermal conductivity varies with temperature as discussed in chapter 5 and chapter 6.

In chapter 5, it is exposed that the thickness of the hydrodynamic, thermal and concentration boundary layer decrease with the increasing values of the suction parameter. Magnetic field moving with the free stream has the tendency to induce a motive force which increases the motion of the fluid and decreases its boundary layer.

The dimensionless concentration of the fluid particles within the boundary-layer increases with the increasing values of the thermophoretic coefficient κ whereas it decreases with the increasing values of both Sc and N_t. Thermophoretic velocity decreases for increasing thermophoresis parameter N_t whereas it increases with the increasing values of κ and β. Thermophoretic particle deposition velocity decreases with the increase of the thermophoretic coefficient κ while it increases with the increase of the unsteadiness parameter λ which is found in chapter 3, chapter 4, chapter 5 and chapter 6.

The combined effect of the temperature dependent variable viscosity and thermal conductivity with slip flow has been discussed in chapter 6. It is found that the fluid velocity within the boundary-layer is found lower whereas both the temperature and concentration are higher for the case of no slip flows than the slip flows. It is also found that for slip flow ($\varepsilon \neq 0$) the values of local skin friction coefficient are lower than the corresponding values for no-slip ($\varepsilon = 0$). On the other hand, for slip flow ($\varepsilon \neq 0$) local Nusselt number and the local Sherwood number are higher than the corresponding values for no-slip ($\varepsilon = 0$) case.

Since no experimental results of the corresponding studies are available, the obtained numerical results have been compared with that of the established numerical results. As for example, qualitative agreement of our results with those of White (2006) is excellent.

Finally, it is expected that the presented numerical works can be used as a vehicle for understanding the thermophoresis particle deposition on MHD heat and mass transfer produced unsteady laminar convective boundary-layer flows along a permeable wedge in the presence of a magnetic field and heat source.

7.2 Recommendations for future works based on the thesis

The study on this thesis may be extended considering following cases:

i. The effect of thermophoresis particle deposition with thermal radiation has not been considered throughout the thesis; this mode of heat transfer may be considered with the present model.
ii. The study can be extended considering porous medium.
iii. The author has considered an unsteady two-dimensional laminar flow in this thesis. One can consider unsteady three dimensional flows.
iv. The effect of temperature dependent viscosity may be extended considering Joule heating, heat generation, stress work and viscous dissipation.
v. This study may be extended with considering these fluid properties with different geometry.

References

Abel M. S., Siddheshwar and Mahesha N., (2009): Effects of thermal buoyancy and variable thermal conductivity on the MHD flow and heat transfer in a power-law fluid past a vertical stretching sheet in the presence of a non-uniform heat source, Int. J. Non-Linear Mech., Vol. 44, pp. 1-12.

Aitken J., (1884): On the formation of small clear spaces in dusty air, Trans. R. Soc. Edinb., Vol. 32, pp. 239-272.

Al-Khawaja M. J., Agarwal R. K. and Gardner R. A., (1999): Numerical study of magneto-fluid mechanics combined free and forced convection heat transfer, Int. J. Heat Mass Transfer, Vol. 42, pp. 467-475.

Anderson H. I., (2002): Slip flow past a stretching surface, Acta Mech., Vol. 158, pp. 121-125.

Alam M. S., Rahman M. M. and Samad M. A., (2006): Numerical study of the combined free-forced convection and mass transfer flow past a vertical porous plate in a porous medium with heat generation and thermal diffusion, Non-linear Analysis; Modeling and control, Vol. 11(3), pp. 331-343.

Ali E., (2006): The effect of variable viscosity on mixed convection heat transfer along a vertical moving surface, Int. J. Thermal Sci., Vol. 45, pp. 60-69.

Alam M. S., Rahman M. M. and Sattar M. A., (2008): Effects of variable suction and thermophoresis on steady MHD combined free-forced convective heat and mass transfer flow over a semi-infinite permeable inclined flat plate in the presence of thermal radiation, Int. J. Thermal Sci., Vol. 47, pp.758-765.

Alam M. S., Rahman M. M. and Sattar M. A., (2009): Transient magnetohydrodynamic free convective heat and mass transfer flow with thermophoresis past a radiative inclined permeable plate in the presence of variable chemical reaction and temperature dependent viscosity, Non-linear Anal. Model. Control, Vol. 14, pp. 3-20.

Aziz A., (2010): Hydrodynamic and thermal slip flow boundary layer over a flat plate with constant heat flux boundary condition. Commun Numer Simul., Vol. 15, pp. 573-580.

Batchelor G. K. and Shen C., (1985): Thermophoretic deposition of particles in gas flowing over cold surface, J. Colloid Interface Sci., Vol. 107, pp. 21-37.

Bakier A. Y. and Mansour M. A., (2007): Combined of magnetic field and thermophoresis particle deposition in free convection boundary layer from a vertical flat plate embedded in a porous medium, Thermal Science, Vol. 11, No.1, pp. 65-74.

Chiam T. C., (1996): Heat transfer with variable conductivity in a stagnation-point flow towards a stretching sheet, Int. Communications in Heat and Mass Transfer, Vol. 23, pp. 239-248.

Chiam T. C., (1998): Heat transfer in a fluid with variable thermal conductivity over a linearly stretching sheet, Acta Mech., Vol. 129, pp. 63-72.

Chandran P., Sacheti N. C. and Singh A. K., (1996): Hydromegnetic flow and heat transfer past a continuously moving porous boundary, Int. Communications in Heat and Mass Transfer, Vol. 23, pp. 889-898.

Chiou M. C. and Cleaver J. W., (1996): Effect of thermophoresis on sub-micron particle deposition from a laminar forced convection boundary layer flow on to an isothermal cylinder, J. Aerosol Science, Vol. 27, pp. 1155-1167.

Chiou M. C., (1998): Effect of thermophoresis on sub-micron particle deposition from a forced laminar boundary layer flow on to an isothermal moving plate, Acta Mechanica, Vol. 129, pp. 219-229.

Chamkha A. J. and Issa C., (2000): Effects of heat generation/absorption and thermophoresis on hydromagnetic flow with heat and mass transfer over a flat surface, Int. J. Numer. Methods Heat Fluid Flow, Vol. 10(4), pp. 432-448.

Chamkha A. J., Jaradat M. and Pop I., (2004): Thermophoresis free convection from a vertical cylinder embedded in a porous medium, Int. J. Applied Mechanics and Engineering, Vol. 9, pp. 471-481.

Cobble M. A., (1977): Magneto fluid dynamic flow with a pressure gradient and fluid suction, J. Engineering Math., Vol. 11(3), pp. 249-261.

Cramer K. R., (1963): Several magnetohydrodynamic free convection solutions, ASME J. Heat Transfer, Vol. 85, pp. 35-40.

Damesh R. A., Tahat M. S. and Benim A. C., (2009): Non-similar solutions of magnetohydrodynamic and thermophoresis particle deposition on mixed convection problem in porous media along a vertical surface with variable wall temperature, Progress in Comput. Fluid Dynamics, Vol. 9(1), pp. 58-65.

Derjaguin B. V., Rabinovich Ya. I., Storozhilova A. I. and Shcherbina G. I., (1976): Measurement of the coefficient of thermal slip of gases and the thermophoresis velocity of large-size aerosol particles, J. Colloid Interface Science, Vol. 57, pp. 451-461.

Duwairi H. M. and Damesh R. A., (2008): Effects of thermophoresis particle deposition on mixed convection from vertical surfaces embedded in saturated porous medium, Int. J. Numer. Meth. Heat Fluid Flow, Vol. 18(2), pp. 202-216.

Elbashbeshy E. M. A. and Bazid M. A. A., (2000): The effect of temperature dependent viscosity on heat transfer over a continuous moving surface, J. Phys: D. Appl. Phys., Vol. 33, pp. 2716-2721.

Epstein M., Hauser G. M. and Henry R. E., (1985): Thermophoretic deposition of particles in natural convection flow from vertical plate, ASME J. Heat Transfer, Vol. 107, pp. 272-276.

Gardner G. and Stokes G., (1856): On the effect of internal friction of fluids on the motion of pendulums, Trans Cambr. Phil. Soc., Vol. 9, No. 2, pp. 8-106.

Garg V. K. and Jayaraj S., (1988): Thermophoresis of aerosol particles in laminar flow over inclined plates, Int. J. Heat Mass Transfer, Vol. 31, pp. 875-890.

Garg V. K. and Jayaraj S., (1990): Thermophoretic deposition over a cylinder, Int. J. Engrg. Fluid Mech., Vol. 3, pp. 175-196.

Goldsmith P. and May F. G., (1966): Diffusiophoresis and thermophoresis in water vapour systems, in: C. N. Davies (Ed.), Aerosol Science, Academic Press, London, pp. 163-194.

Goren S. L., (1977): Thermophoresis of aerosol particles in the laminar boundary layer on a flat plate, J. Colloid Interface Science, Vol. 61, pp. 77-85.

Grardner R. A. and Lo, Y. T., (1975): Combined free and forced convection heat transfer in magneto fluid mechanic pipe flow, AICHE, Vol. 73 (164), pp. 133-144.

Gupta A. S., Misra J. C. and Reza M., (2003): Effects of suction or blowing on the velocity and temperature distribution in the flow past a porous flat plate of a power-law fluid, Fluid Dynamics Research, Vol. 32, pp. 283-294.

Hasimoto H., (1957): Boundary layer growth on a flat plate with suction or injection, J. Phys. Soc. Japan, Vol. 12, pp. 68-72.

Hasimoto H., (1958): Boundary layers slip solutions for a flat plate, J Aeronaut Sci., Vol. 25, pp. 68-69.

Hales J. M., Schwendiman L. C. and Horst T. W., (1972): Aerosol transport in a natural-convection boundary layer, Int. J. Heat Mass Transfer, Vol. 15, pp. 1837-1849.

Haldavneker D. D. and Soundalgeker V. M., (1977): Effects of mass transfer on free convection flow of an electrically conducting, viscous fluid past an infinite porous plate with constant suction and transversely applied magnetic field, Acta Phys. Acad. Sci. Hung, Vol. 43(3-4), p. 243

Homsy G. M., Geyling F. T. and Walker K. L., (1981): Blasius series for thermophoretic deposition of small particles, J. Colloid Interface Science, Vol. 83, pp. 495-501.

Hossain M. A. and Ahmed M., (1990): MHD forced and free convection boundary layer flow near the leading edge, Int. J. Heat Mass Transfer, Vol. 33, pp. 571-375.

Hossain M. A., Munir M. S. and Rees D. A. S., (2000): Flow of viscous incompressible fluid with temperature dependent viscosity and thermal conductivity past a permeable wedge with uniform surface heat flux, Int. J. Therm. Sci., Vol. 39, pp. 635-644.

Hossain M. A., Bhowmick S. and Goral R. S. R., (2006): Unsteady mixed-convection boundary layer flow along a symmetric wedge with variable surface temperature, Int. J. of Engineering Science, Vol. 44, pp. 607-620.

Hunt R. and Wilks G., (1980): On the behaviour of the laminar boundary layer equations of mixed convection near a point of zero skin friction, J. Fluid Mechanics, Vol. 101, p. 377.

Ishak A., Nazar R. and Pop I., (2008): MHD boundary layer flow of a micropolar fluid past a wedge with variable wall temperature, Acta Mechanica, Vol. 196, pp.75-86.

Jayaraj S., Dinesh K. K. and Pillai K. L., (1999): Thermophoresis in natural convection with variable properties, Heat and Mass Transfer, Vol. 34, pp. 469-475.

Jha B. K., (1991): MHD unsteady mixed convection flow through a porous medium, Astrophys, Space Science, Vol. 175, p. 101.

Jia G., Cipolla J. W. and Yener Y., (1992): Thermophoresis of a radiating aerosol in laminar boundary-layer flow, J. Thermophys. Heat Transfer, Vol. 6, pp. 476-482.

Jha B. K. and Prasad R., (1989): Effect of magnetic field on the free convection and mass transfer flow through a porous medium, Astrophys Space Science, Vol. 161, pp. 195-200.

Jha B. K. and Prasad R. and Rai, S., (1994): MHD free convection and mass transfer flow past an exponentially accelerated vertical plate through a porous medium, J. Energy, Heat and Mass Transfer, Vol. 16, p.173.

Kafoussias N. G. and Williams E. W., (1995): Thermal diffusion and diffusion thermo effects on mixed free-forced convective and mass transfer flow with temperature dependent viscosity, Int. J. Eng. Sci., Vol. 33, pp. 1369-1384.

Ling J. X. and Dybbs A., (1987): Forced convection over a flat plate submersed in a porous medium: variable viscosity case, ASME, paper 87-WA/HT-23, ASME winter annual meeting, Boston, Massachusetts, pp. 13-18.

Martin M. J. and Boyd I. D., (2000): Blasius boundary layer with slip flow conditions, In Bartel TJ, Gallis MA (eds) 22nd Rarefied gas dynamics symposium, Sydney, Australia.

Martin M. J. and Boyd I. D., (2006): Momentum and heat transfer in laminar boundary layer with slip flow, J. Thermophys Heat Transf., Vol. 20, pp. 710-719.

Martin M. J. and Boyd I. D., (2010): Falkner-Skan flow over a wedge with slip boundary conditions, J. Thermophys Heat Transf., Vol. 24, pp. 263-270.

Mia M. M., Sattar M A., and Alam M. S., (2011): A local similarity solution for unsteady two- dimensional hydrodynamic boundary layer flow in a convergent channel, Int. J. Energy and Technology, Vol. 3, pp.1-4.

Muhaimin I., Kandasamy R., Khamis A. B. and Rozaini R., (2013): Influence of thermophoresis particle deposition and chemical reaction on unsteady non-Darcy MHD mixed convective flow over a porous wedge in the presence of temperature dependent viscosity, J. Mechanical Science and Technology, Vol. 27, No.5, pp.1545-1555.

Nachtsheim P. R. and Swigert P., (1965): Satisfaction of the asymptotic boundary conditions in numerical solution of the system of non-linear equations of boundary layer type, NASA TND-3004.

Nanbu K., (1971): Vortex flow over a flat surface for large suction, AIAA J., Vol. 9, p. 1642.

Noor N. F. M., Abbasbandy S. and Hashim I., (2013): Heat and mass transfer of thermophoretic MHD flow over an inclined radiate isothermal permeable surface in the presence of heat source/sink,

Pantokratoras A., (2005): Forced and mixed convection boundary layer flow along a flat plate with variable viscosity and variable Prandtl number, new results, Heat Mass Transfer, Vol. 41, pp. 1085-1094.

Pantokratoras A., (2007): Non-Darcian forced convection heat transfer over a flat plate in a porous medium with variable viscosity and variable Prandtl number, J. Porous Media, Vol. 10, pp. 201-208.

Postelnicu A., (2007): Effects of thermophoresis particle deposition in free convection boundary layer from a horizontal flat plate embedded in a porous medium, Int. J. Heat Mass Transfer, Vol. 50, pp.2981-2985.

Postelnicu A., (2012): Thermophersis particle deposition in natural convection over inclined surfaces in porous media, Int. J. Heat and Mass Transfer, Vol. 55, pp. 2087-2094.

Prasad K. V., Vajravelu K., (2009): Heat transfer in the MHD flow of a power law fluid over a non-isothermal stretching sheet, Int. J. Heat and Mass Transfer, Vol. 152 pp. 4956-4965.

Rahman M. M., Rahman M. A., Samad M. A. and Alam M. S., (2009): Heat transfer in micropolar fluid along a non-linear stretching sheet with temperature dependent viscosity and variable wall temperature, Int. J. Thermophys., Vol. 30, pp.1649-1670.

Rahman M. M. and Postelnicu A., (2010): Effects of thermophoresis on the forced convective laminar flow of a viscous incompressible fluid over a rotating disk, Mech. Res. Cumm., Vol. 37, 598-603.

Rahman M. M. and Eltayeb I. A., (2011): Convective slip flow of rarefied fluids over a wedge with thermal jump and variable transport properties, Int. J. Thermal Sci., Vol. 50, pp. 468-379.

Rahmana M. M., Rosca A. V. and Pop I., (2014): Boundary layer flow of a nanofluid past a permeable exponentially shrinking/stretching surface with second order slip using Buongiorno's model, Int. J. Heat Mass Transfer, Vol. 77, pp.1133–1143.

Raptis A. and Kafoussias N. G., (1982): Magnetohydrodynamic free convective flow and mass transfer through porous medium bounded by an infinite vertical porous plate with constant heat flux, Can. J. Phys., Vol. 60, pp. 1725-1729.

Sattar M. A. and Hossain M. M., (1992): Unsteady hydromagnetic free convection flow with Hall current and mass transfer along an accelerated porous plate with time dependent temperature and concentration, Can. J. Physics, Vol.70, pp. 369-374.

Sattar M. A., Samad M. A. and Kalim M. H., (1997): Unsteady MHD forced and free convection flow through a porous medium with constant heat source and a variable suction, Dhaka Univ. J. Sci., Vol. 45(2), p. 205.

Savvas TA, Markatos NC, Papaspyrides CD, (1994): On the flow of non-Newtonian polymer solutions, Appl. Math. Model, Vol. 18, pp. 14-22.

Sattar M. A., (2011): A local similarity transformation for the unsteady two-dimensional hydrodynamic boundary layer equations of a flow past a wedge, Int. J. Appl. Math. and Mech., Vol. 7, pp.15-28.

Schlichting H., (1958): Boundary layer theory, McGraw Hill, Sixth Edition.

Schneider W., (1979): A similarity solution for combined forced and free convection flow over a horizontal plate, Int. J. Heat Mass Transfer, Vol. 22, pp. 1401-1406.

Schlichting H. and Gersten K., (2000): Boundary Layer Theory, 8th Edition, Springer-Verlag, Berlin/Heidelberg.

Seddeek M. A., (2000): The effect of variable viscosity on hydrodynamic flow and heat transfer past a continuously moving porous boundary with radiation, Int. Communications in Heat and Mass Transfer, Vol. 27, pp. 1037-1047.

Seddeek M. A., (2006): Influence of viscous dissipation and thermophoresis on Darcy-Forchheimer mixed convection in a fluid saturated porous media, J. Colloid Interface Science, Vol. 293(1), pp. 137-142.

Selim A., Hossain M. A. and Rees D. A. S., (2003): The effect of surface mass transfer on mixed convection flow past heated vertical flat permeable plate with thermophoresis, Int. J. Thermal Sciences, Vol. 42, pp. 973-982.

Singh P. J., Roy S. and Ravindran, R., (2009): Unsteady mixed convection flow over a vertical wedge, Int. J. Heat Mass Transfer, Vol. 52, pp. 415-421.

Soundalgeker V. M. and Ramanamurthy T. U., (1980): Heat transfer in MHD flow with pressure gradient suction and injection, J. Engineering Math., Vol. 14, No. 2, p. 155.

Sohn Y. M., Beak S. W. and Kim D. Y., (2002): Thermophoresis of particles in gas-particle two-phase flow with radiation effect, Numer. Heat Transfer, Part A, Vol. 41, pp. 165-181.

Sparrow E. M. and Cess R. D., (1961): The effect of magnetic field on free convection heat transfer, Int. J. Heat Mass Transfer, Vol. 3, pp. 267-274.

Stokes G. G., (1856): On the effect of internal friction of fluids on the motion of pendulums, Trans Cambr. Phil. Soc., Vol. 9, No. 2, pp. 8-106.

Talbot L., Chenge R. K., Schefer A. W. and Willis D. R., (1980): Thermophoresis of particles in a heated boundary layer, J. Fluid Mechanics, Vol. 101, pp. 737-758.

Tyndall J., (1870): On dust and disease, Proc. R. Inst., Vol. 6, pp. l1-14.

Vajravelu K., Prasad K.V. and Chiu-On Ng, (2013): Unsteady convective boundary layer flow of a viscous fluid at a vertical surface with variable fluid properties, Nonlinear Analysis: Real World Applications, Vol. 14, pp. 455-464.

Vedantam N. K., (2006): Effect of slip on the flow characteristics of a laminar flat plate boundary layer. In: Proceeding of ASME fluids engineering summer meeting, Miami, Florida, July 17-20, pp. 1551-1560.

Walker K. L., Homsy G. M. and Geying F. T., (1979): Thermophoretic deposition of small particles in laminar tube, J. Colloid Interface Science, Vol. 69, pp. 138-147.

Watanabe T. and Pop I., (1993): Magnetohydrodynamic free convection flow over a wedge in the presence of a transverse magnetic field, Int. Communications in Heat and Mass Transfer, Vol. 20, pp. 871-881.

Wang C.Y., (2006): Stagnation slip flow and heat transfer a moving plate, Chem. Eng. Sci., Vol. 61, pp. 7668-7672.

Wang C. C. and Chen C. K., (2006): Thermophoretic deposition of particles from a boundary layer flow onto a continuously moving wavy surface, Acta Mechanica, Vol. 181, pp. 139-151.

Wang C.Y., (2009): Analysis of viscous flow due to a stretching sheet with surface slip and suction. Nonlinear Anal Real World Appl., Vol.10, pp. 375-380.

Weast R. C., (1990): CRC Handbook of Chemistry and Physics, 71st edn. CRC Press, Boca Raton, Florida.

White F. M., (2006): Viscous Fluid Flows, Third ed. McGraw-Hill, New York.

Yih K. A., (1999): MHD forced convection flow adjacent to a non-isothermal wedge, Int. Communications in Heat and Mass Transfer, Vol. 26, pp. 819-827.

Yu C. P., (1965): Combined forced and free convection channel flows in Magnetohydrodynamic, AIAA. J., Vol. 3, pp. 1184-1186.

Appendix

Nachtsheim-Swigert shooting technique

In a shooting method, the missing (unspecified) initial condition at the initial point of the interval is assumed, and the differential equation is then integrated numerically as an initial value problem to the terminal point. The accuracy of the assumed missing initial condition is then checked by comparing the calculated value of the dependent variable at the terminal point with its given value there. If a difference exists, another value of the missing initial condition must be assumed and the process is repeated. This process is continued until the agreement between the calculated and the given condition at the terminal point is within the specified degree of accuracy. For this type of iterative approach, one naturally inquires whether or not there is a systematic way of finding each succeeding (assumed) value of the missing initial condition.

The Nachtsheim-Swigert iteration technique thus needs to be discussed elaborately. The boundary condition (2.24) associated with the non-linear ordinary differential equations (2.21)-(2.23) [in chapter 2] are the two-point asymptotic class. Two-point boundary conditions have values of the dependent variable specified at two different values of independent variable. Specification of an asymptotic boundary condition implies that the first derivative (and higher derivatives of the boundary layer equations, if exist) of the dependent variable approaches zero as the outer specified value of the independent variable is approached.

The method of numerically integrating a two-point asymptotic boundary-value problem of the boundary-layer type, the initial-value method is similar to an initial-value problem. Thus it is necessary to estimate as many boundary conditions at the surface as were (previously) given at infinity. The governing differential equations are then integrated with these assumed surface boundary

conditions. If the required outer boundary condition is satisfied, a solution has been achieved. However, this is not generally the case. Hence, a method must be devised to estimate logically the new surface boundary conditions for the next trial integration. Asymptotic boundary value problems such as those governing the boundary-layer equations are further complicated by the fact that the outer boundary condition is specified at infinity. In the trial integration infinity is numerically approximated by some large value of the independent variable. There is no a priori general method of estimating these values. Selecting too small a maximum value for the independent variable may not allow the solution to asymptotically converge to the required accuracy. Selecting large a value may result in divergence of the trial integration or in slow convergence of surface boundary conditions. Selecting too large a value of the independent variable is expensive in terms of computer time.

Nachtsheim-Swigert (1965) developed an iteration method to overcome these difficulties. Extension of the Nachtsheim-Swigert iteration scheme to the system of equation (2.21)-(2.23) and the boundary conditions (2.24) [in chapter 2] is straightforward. In equation (2.24) [in chapter 2] there are three asymptotic boundary conditions and hence three unknown surface conditions $f''(0)$, $\theta'(0)$ and $\phi'(0)$.

Within the context of the initial-value method and Nachtsheim-Swigert iteration technique the outer boundary conditions may be functionally represented as

$$f'(\eta_{\max}) = f'(f''(0), \theta'(0), \phi'(0)) = \delta_1, \tag{A.1}$$

$$\theta(\eta_{\max}) = \theta(f''(0), \theta'(0), \phi'(0)) = \delta_2, \tag{A.2}$$

$$\phi(\eta_{\max}) = \phi(f''(0), \theta'(0), \phi'(0)) = \delta_3, \tag{A.3}$$

with the asymptotic convergence criteria given by

$$f''(\eta_{\max}) = f''(f''(0), \theta'(0), \phi'(0)) = \delta_4, \tag{A.4}$$

$$\theta'(\eta_{\max}) = \theta'(f''(0), \theta'(0), \phi'(0)) = \delta_5, \tag{A.5}$$

$$\phi'(\eta_{\max}) = \phi'(f''(0), \theta'(0), \phi'(0)) = \delta_6. \tag{A.6}$$

Choosing $f''(0) = g_1, \theta'(0) = g_2$ and $\phi'(0) = g_3$ and expanding in a first-order Taylor's series after using equations (A.1)-(A.6) yields

$$f'(\eta_{\max}) = f'_C(\eta_{\max}) + \frac{\partial f'}{\partial g_1}\Delta g_1 + \frac{\partial f'}{\partial g_2}\Delta g_2 + \frac{\partial f'}{\partial g_3}\Delta g_3 = \delta_1, \tag{A.7}$$

$$\theta(\eta_{\max}) = \theta_C(\eta_{\max}) + \frac{\partial \theta}{\partial g_1}\Delta g_1 + \frac{\partial \theta}{\partial g_2}\Delta g_2 + \frac{\partial \theta}{\partial g_3}\Delta g_3 = \delta_2, \tag{A.8}$$

$$\phi(\eta_{\max}) = \phi_C(\eta_{\max}) + \frac{\partial \phi}{\partial g_1}\Delta g_1 + \frac{\partial \phi}{\partial g_2}\Delta g_2 + \frac{\partial \phi}{\partial g_3}\Delta g_3 = \delta_3, \tag{A.9}$$

$$f''(\eta_{\max}) = f''_C(\eta_{\max}) + \frac{\partial f''}{\partial g_1}\Delta g_1 + \frac{\partial f''}{\partial g_2}\Delta g_2 + \frac{\partial f''}{\partial g_3}\Delta g_3 = \delta_4, \tag{A.10}$$

$$\theta'(\eta_{\max}) = \theta'_C(\eta_{\max}) + \frac{\partial \theta'}{\partial g_1}\Delta g_1 + \frac{\partial \theta'}{\partial g_2}\Delta g_2 + \frac{\partial \theta'}{\partial g_3}\Delta g_3 = \delta_5, \tag{A.11}$$

$$\phi'(\eta_{\max}) = \phi'_C(\eta_{\max}) + \frac{\partial \phi'}{\partial g_1}\Delta g_1 + \frac{\partial \phi'}{\partial g_2}\Delta g_2 + \frac{\partial \phi'}{\partial g_3}\Delta g_3 = \delta_6, \tag{A.12}$$

where subscript '*C*' indicates the value of the function at $\eta_{\max}$ determined from the trial integration.

Solution of these equations in a least-squares sense requires determining the minimum value of

$$E = \delta_1^2 + \delta_2^2 + \delta_3^2 + \delta_4^2 + \delta_5^2 + \delta_6^2 \tag{A.13}$$

with respect to g_1, g_2 and g_3.

Now differentiating *E* with respect to g_1 yields

$$\delta_1 \frac{\partial \delta_1}{\partial g_1} + \delta_2 \frac{\partial \delta_2}{\partial g_1} + \delta_3 \frac{\partial \delta_3}{\partial g_1} + \delta_4 \frac{\partial \delta_4}{\partial g_1} + \delta_5 \frac{\partial \delta_5}{\partial g_1} + \delta_6 \frac{\partial \delta_6}{\partial g_1} = 0$$

or,

$$\left(f'_C + \frac{\partial f'}{\partial g_1}\Delta g_1 + \frac{\partial f'}{\partial g_2}\Delta g_2 + \frac{\partial f'}{\partial g_3}\Delta g_3 \right)\frac{\partial f'}{\partial g_1} + \left(\theta_C + \frac{\partial \theta}{\partial g_1}\Delta g_1 + \frac{\partial \theta}{\partial g_2}\Delta g_2 + \frac{\partial \theta}{\partial g_3}\Delta g_3 \right)\frac{\partial \theta}{\partial g_1}$$

$$+\left(\phi_C+\frac{\partial\phi}{\partial g_1}\Delta g_1+\frac{\partial\phi}{\partial g_2}\Delta g_2+\frac{\partial\phi}{\partial g_3}\Delta g_3\right)\frac{\partial\phi}{\partial g_1}+\left(f_C''+\frac{\partial f''}{\partial g_1}\Delta g_1+\frac{\partial f''}{\partial g_2}\Delta g_2+\frac{\partial f''}{\partial g_3}\Delta g_3\right)\frac{\partial f''}{\partial g_1}$$

$$+\left(\theta_C'+\frac{\partial\theta'}{\partial g_1}\Delta g_1+\frac{\partial\theta'}{\partial g_2}\Delta g_2+\frac{\partial\theta'}{\partial g_3}\Delta g_3\right)\frac{\partial\theta'}{\partial g_1}+\left(\phi_C'+\frac{\partial\phi'}{\partial g_1}\Delta g_1+\frac{\partial\phi'}{\partial g_2}\Delta g_2+\frac{\partial\phi'}{\partial g_3}\Delta g_3\right)\frac{\partial\phi'}{\partial g_1}=0$$

$$\text{or, }\left[\left(\frac{\partial f'}{\partial g_1}\right)^2+\left(\frac{\partial\theta}{\partial g_1}\right)^2+\left(\frac{\partial\phi}{\partial g_1}\right)^2+\left(\frac{\partial f''}{\partial g_1}\right)^2+\left(\frac{\partial\theta'}{\partial g_1}\right)^2+\left(\frac{\partial\phi'}{\partial g_1}\right)^2\right]\Delta g_1$$

$$+\left[\frac{\partial f'}{\partial g_2}\frac{\partial f'}{\partial g_1}+\frac{\partial\theta}{\partial g_2}\frac{\partial\theta}{\partial g_1}+\frac{\partial\phi}{\partial g_2}\frac{\partial\phi}{\partial g_1}+\frac{\partial f''}{\partial g_2}\frac{\partial f''}{\partial g_1}+\frac{\partial\theta'}{\partial g_2}\frac{\partial\theta'}{\partial g_1}+\frac{\partial\phi'}{\partial g_2}\frac{\partial\phi'}{\partial g_1}\right]\Delta g_2$$

$$+\left[\frac{\partial f'}{\partial g_3}\frac{\partial f'}{\partial g_1}+\frac{\partial\theta}{\partial g_3}\frac{\partial\theta}{\partial g_1}+\frac{\partial\phi}{\partial g_3}\frac{\partial\phi}{\partial g_1}+\frac{\partial f''}{\partial g_3}\frac{\partial f''}{\partial g_1}+\frac{\partial\theta'}{\partial g_3}\frac{\partial\theta'}{\partial g_1}+\frac{\partial\phi'}{\partial g_3}\frac{\partial\phi'}{\partial g_1}\right]\Delta g_3$$

$$=-\left[f_C'\frac{\partial f'}{\partial g_1}+\theta_C\frac{\partial\theta}{\partial g_1}+\phi_C\frac{\partial\phi}{\partial g_1}+f_C''\frac{\partial f''}{\partial g_1}+\theta_C''\frac{\partial\theta'}{\partial g_1}+\phi_C'\frac{\partial\phi'}{\partial g_1}\right] \qquad \text{(A.14)}$$

Similarly differentiating E with respect to g_2 and g_3, we obtain respectively

$$\delta_1\frac{\partial\delta_1}{\partial g_2}+\delta_2\frac{\partial\delta_2}{\partial g_2}+\delta_3\frac{\partial\delta_3}{\partial g_2}+\delta_4\frac{\partial\delta_4}{\partial g_2}+\delta_5\frac{\partial\delta_5}{\partial g_2}+\delta_6\frac{\partial\delta_6}{\partial g_2}=0$$

$$\text{or, }\left[\left(\frac{\partial f'}{\partial g_2}\right)^2+\left(\frac{\partial\theta}{\partial g_2}\right)^2+\left(\frac{\partial\phi}{\partial g_2}\right)^2+\left(\frac{\partial f''}{\partial g_2}\right)^2+\left(\frac{\partial\theta'}{\partial g_2}\right)^2+\left(\frac{\partial\phi'}{\partial g_2}\right)^2\right]\Delta g_2$$

$$+\left[\frac{\partial f'}{\partial g_1}\frac{\partial f'}{\partial g_2}+\frac{\partial\theta}{\partial g_1}\frac{\partial\theta}{\partial g_2}+\frac{\partial\phi}{\partial g_1}\frac{\partial\phi}{\partial g_{22}}+\frac{\partial f''}{\partial g_1}\frac{\partial f''}{\partial g_2}+\frac{\partial\theta'}{\partial g_1}\frac{\partial\theta'}{\partial g_2}+\frac{\partial\phi'}{\partial g_1}\frac{\partial\phi'}{\partial g_2}\right]\Delta g_1$$

$$+\left[\frac{\partial f'}{\partial g_3}\frac{\partial f'}{\partial g_2}+\frac{\partial\theta}{\partial g_3}\frac{\partial\theta}{\partial g_2}+\frac{\partial\phi}{\partial g_3}\frac{\partial\phi}{\partial g_2}+\frac{\partial f''}{\partial g_3}\frac{\partial f''}{\partial g_2}+\frac{\partial\theta'}{\partial g_3}\frac{\partial\theta'}{\partial g_2}+\frac{\partial\phi'}{\partial g_3}\frac{\partial\phi'}{\partial g_2}\right]\Delta g_3$$

$$=-\left[f_C'\frac{\partial f'}{\partial g_2}+\theta_C\frac{\partial\theta}{\partial g_2}+\phi_C\frac{\partial\phi}{\partial g_2}+f_C''\frac{\partial f''}{\partial g_2}+\theta_C''\frac{\partial\theta'}{\partial g_2}+\phi_C'\frac{\partial\phi'}{\partial g_2}\right]. \qquad \text{(A.15)}$$

and

$$\delta_1 \frac{\partial \delta_1}{\partial g_3} + \delta_2 \frac{\partial \delta_2}{\partial g_3} + \delta_3 \frac{\partial \delta_3}{\partial g_3} + \delta_4 \frac{\partial \delta_4}{\partial g_3} + \delta_5 \frac{\partial \delta_5}{\partial g_3} + \delta_6 \frac{\partial \delta_6}{\partial g_3} = 0$$

or, $$\left[\left(\frac{\partial f'}{\partial g_3} \right)^2 + \left(\frac{\partial \theta}{\partial g_3} \right)^2 + \left(\frac{\partial \phi}{\partial g_3} \right)^2 + \left(\frac{\partial f''}{\partial g_3} \right)^2 + \left(\frac{\partial \theta'}{\partial g_3} \right)^2 + \left(\frac{\partial \phi'}{\partial g_3} \right)^2 \right] \Delta g_3$$

$$+ \left[\frac{\partial f'}{\partial g_1}\frac{\partial f'}{\partial g_3} + \frac{\partial \theta}{\partial g_1}\frac{\partial \theta}{\partial g_3} + \frac{\partial \phi}{\partial g_1}\frac{\partial \phi}{\partial g_3} + \frac{\partial f''}{\partial g_1}\frac{\partial f''}{\partial g_3} + \frac{\partial \theta'}{\partial g_1}\frac{\partial \theta'}{\partial g_3} + \frac{\partial \phi'}{\partial g_1}\frac{\partial \phi'}{\partial g_3} \right] \Delta g_1$$

$$+ \left[\frac{\partial f'}{\partial g_2}\frac{\partial f'}{\partial g_3} + \frac{\partial \theta}{\partial g_2}\frac{\partial \theta}{\partial g_3} + \frac{\partial \phi}{\partial g_2}\frac{\partial \phi}{\partial g_3} + \frac{\partial f''}{\partial g_2}\frac{\partial f''}{\partial g_3} + \frac{\partial \theta'}{\partial g_2}\frac{\partial \theta'}{\partial g_3} + \frac{\partial \phi'}{\partial g_2}\frac{\partial \phi'}{\partial g_3} \right] \Delta g_2$$

$$= -\left[f'_C \frac{\partial f'}{\partial g_3} + \theta_C \frac{\partial \theta}{\partial g_3} + \phi_C \frac{\partial \phi}{\partial g_3} + f''_C \frac{\partial f''}{\partial g_3} + \theta''_C \frac{\partial \theta'}{\partial g_3} + \phi'_C \frac{\partial \phi'}{\partial g_3} \right]. \qquad \text{(A.16)}$$

We can write equations (A.14)-(A.16) in a system of linear equations as follows:

$$a_{11}\Delta g_1 + a_{12}\Delta g_2 + a_{13}\Delta g_3 = b_1, \qquad \text{(A.17)}$$

$$a_{21}\Delta g_1 + a_{22}\Delta g_2 + a_{23}\Delta g_3 = b_2, \qquad \text{(A.18)}$$

$$a_{31}\Delta g_1 + a_{32}\Delta g_2 + a_{33}\Delta g_3 = b_3. \qquad \text{(A.19)}$$

Here

$$a_{11} = \left[\left(\frac{\partial f'}{\partial g_1} \right)^2 + \left(\frac{\partial \theta}{\partial g_1} \right)^2 + \left(\frac{\partial \phi}{\partial g_1} \right)^2 + \left(\frac{\partial f''}{\partial g_1} \right)^2 + \left(\frac{\partial \theta'}{\partial g_1} \right)^2 + \left(\frac{\partial \phi'}{\partial g_1} \right)^2 \right],$$

$$a_{12} = \frac{\partial f'}{\partial g_2}\frac{\partial f'}{\partial g_1} + \frac{\partial \theta}{\partial g_2}\frac{\partial \theta}{\partial g_1} + \frac{\partial \phi}{\partial g_2}\frac{\partial \phi}{\partial g_1} + \frac{\partial f''}{\partial g_2}\frac{\partial f''}{\partial g_1} + \frac{\partial \theta'}{\partial g_2}\frac{\partial \theta'}{\partial g_1} + \frac{\partial \phi'}{\partial g_2}\frac{\partial \phi'}{\partial g_1},$$

$$a_{13} = \frac{\partial f'}{\partial g_3}\frac{\partial f'}{\partial g_1} + \frac{\partial \theta}{\partial g_3}\frac{\partial \theta}{\partial g_1} + \frac{\partial \phi}{\partial g_3}\frac{\partial \phi}{\partial g_1} + \frac{\partial f''}{\partial g_3}\frac{\partial f''}{\partial g_1} + \frac{\partial \theta'}{\partial g_3}\frac{\partial \theta'}{\partial g_1} + \frac{\partial \phi'}{\partial g_3}\frac{\partial \phi'}{\partial g_1},$$

$$a_{21} = \frac{\partial f'}{\partial g_2}\frac{\partial f'}{\partial g_1} + \frac{\partial \theta}{\partial g_2}\frac{\partial \theta}{\partial g_1} + \frac{\partial \phi}{\partial g_2}\frac{\partial \phi}{\partial g_1} + \frac{\partial f''}{\partial g_2}\frac{\partial f''}{\partial g_1} + \frac{\partial \theta'}{\partial g_2}\frac{\partial \theta'}{\partial g_1} + \frac{\partial \phi'}{\partial g_2}\frac{\partial \phi'}{\partial g_1},$$

$$a_{22} = \left[\left(\frac{\partial f'}{\partial g_2} \right)^2 + \left(\frac{\partial \theta}{\partial g_2} \right)^2 + \left(\frac{\partial \phi}{\partial g_2} \right)^2 + \left(\frac{\partial f''}{\partial g_2} \right)^2 + \left(\frac{\partial \theta'}{\partial g_2} \right)^2 + \left(\frac{\partial \phi'}{\partial g_2} \right)^2 \right],$$

$$a_{23} = \frac{\partial f'}{\partial g_3}\frac{\partial f'}{\partial g_2} + \frac{\partial \theta}{\partial g_3}\frac{\partial \theta}{\partial g_2} + \frac{\partial \phi}{\partial g_3}\frac{\partial \phi}{\partial g_2} + \frac{\partial f''}{\partial g_3}\frac{\partial f''}{\partial g_2} + \frac{\partial \theta'}{\partial g_3}\frac{\partial \theta'}{\partial g_2} + \frac{\partial \phi'}{\partial g_3}\frac{\partial \phi'}{\partial g_2},$$

$$a_{31} = \frac{\partial f'}{\partial g_3}\frac{\partial f'}{\partial g_1} + \frac{\partial \theta}{\partial g_3}\frac{\partial \theta}{\partial g_1} + \frac{\partial \phi}{\partial g_3}\frac{\partial \phi}{\partial g_1} + \frac{\partial f''}{\partial g_3}\frac{\partial f''}{\partial g_1} + \frac{\partial \theta'}{\partial g_3}\frac{\partial \theta'}{\partial g_1} + \frac{\partial \phi'}{\partial g_3}\frac{\partial \phi'}{\partial g_1},$$

$$a_{32} = \frac{\partial f'}{\partial g_3}\frac{\partial f'}{\partial g_2} + \frac{\partial \theta}{\partial g_3}\frac{\partial \theta}{\partial g_2} + \frac{\partial \phi}{\partial g_3}\frac{\partial \phi}{\partial g_2} + \frac{\partial f''}{\partial g_3}\frac{\partial f''}{\partial g_2} + \frac{\partial \theta'}{\partial g_3}\frac{\partial \theta'}{\partial g_2} + \frac{\partial \phi'}{\partial g_3}\frac{\partial \phi'}{\partial g_2},$$

$$a_{33} = \left[\left(\frac{\partial f'}{\partial g_3}\right)^2 + \left(\frac{\partial \theta}{\partial g_3}\right)^2 + \left(\frac{\partial \phi}{\partial g_3}\right)^2 + \left(\frac{\partial f''}{\partial g_3}\right)^2 + \left(\frac{\partial \theta'}{\partial g_3}\right)^2 + \left(\frac{\partial \phi'}{\partial g_3}\right)^2\right],$$

$$b_1 = -\left[f_C' \frac{\partial f'}{\partial g_1} + \theta_C \frac{\partial \theta}{\partial g_1} + \phi_C \frac{\partial \phi}{\partial g_1} + f_C'' \frac{\partial f''}{\partial g_1} + \theta_C'' \frac{\partial \theta'}{\partial g_1} + \phi_C' \frac{\partial \phi'}{\partial g_1}\right],$$

$$b_2 = -\left[f_C' \frac{\partial f'}{\partial g_2} + \theta_C \frac{\partial \theta}{\partial g_2} + \phi_C \frac{\partial \phi}{\partial g_2} + f_C'' \frac{\partial f''}{\partial g_2} + \theta_C'' \frac{\partial \theta'}{\partial g_2} + \phi_C' \frac{\partial \phi'}{\partial g_2}\right],$$

and

$$b_3 == -\left[f_C' \frac{\partial f'}{\partial g_3} + \theta_C \frac{\partial \theta}{\partial g_3} + \phi_C \frac{\partial \phi}{\partial g_3} + f_C'' \frac{\partial f''}{\partial g_3} + \theta_C'' \frac{\partial \theta'}{\partial g_3} + \phi_C' \frac{\partial \phi'}{\partial g_3}\right].$$

Now solving the equations (A.17)-(A.19) by using Cramer's rule, we have

$$\Delta g_1 = \frac{\det A_1}{\det A},\ \Delta g_2 = \frac{\det A_2}{\det A} \text{ and } \quad \Delta g_3 = \frac{\det A_3}{\det A}$$

where

$$\det A_1 = \begin{vmatrix} b_1 & a_{12} & a_{13} \\ b_2 & a_{22} & a_{23} \\ b_3 & a_{32} & a_{33} \end{vmatrix} = b_1\left(a_{22}a_{33} - a_{32}a_{23}\right) + b_2\left(a_{32}a_{13} - a_{12}a_{33}\right) + b_3\left(a_{12}a_{23} - a_{22}a_{13}\right)$$

,

$$\det A_2 = \begin{vmatrix} a_{11} & b_1 & a_{13} \\ a_{21} & b_2 & a_{23} \\ a_{31} & b_3 & a_{33} \end{vmatrix} = b_1\left(a_{31}a_{23} - a_{21}a_{33}\right) + b_2\left(a_{11}a_{33} - a_{31}a_{13}\right) + b_3\left(a_{21}a_{13} - a_{11}a_{23}\right)$$

,

$$\det A_3 = \begin{vmatrix} a_{11} & a_{12} & b_1 \\ a_{21} & a_{22} & b_2 \\ a_{31} & a_{32} & b_3 \end{vmatrix} = b_1\left(a_{21}a_{32} - a_{31}a_{22}\right) + b_2\left(a_{31}a_{12} - a_{11}a_{32}\right) + b_3\left(a_{11}a_{22} - a_{21}a_{12}\right)$$

,

$$\det A = \begin{vmatrix} a_{11} & a_{12} & a_{13} \\ a_{21} & a_{22} & a_{23} \\ a_{31} & a_{32} & a_{33} \end{vmatrix} = a_{11}\left(a_{22}a_{33} - a_{23}a_{32}\right) + a_{21}\left(a_{32}a_{13} - a_{12}a_{33}\right) + a_{31}\left(a_{12}a_{23} - a_{22}a_{13}\right)$$

.

Then we obtain the missing (unspecified) values g_1, g_2 and g_3 as

$g_1 \approx g_1 + \Delta g_1$,

$g_2 \approx g_2 + \Delta g_2$,

$g_3 \approx g_3 + \Delta g_3$

Thus adopting the numerical technique aforementioned, the solution of the equations (2.21)-(2.23) with boundary conditions (2.24) [in chapter 2] is obtained together with sixth-order implicit Runge-Kutta initial value solver.